Techniques for Probing the Processes by Which Microwaves Interact with Chemical and Biological Systems

Philip E. Kay

PhD, The University of Edinburgh

2006

Declaration

I hereby declare that this thesis is of my own composition. It is all my own work, unless otherwise stated, carried out at the University of Edinburgh between October 2002 and September 2006. It has not been submitted for any other degree or professional qualification.

Philip Kay

Abstract

Microwave heating is a relatively mature field and is theoretically well understood. However, recently there has been debate as to whether microwaves can interact with chemical and biological systems by means other than heating alone. There is some theoretical justification for such interactions but experimental evidence is often unreliable due to poor or non-existent measurement of heating and/or poor control experiments. Therefore improved techniques for probing these systems are required.

One of the reasons why microwave-assisted chemistry is poorly understood is that there is little available dielectric property data even for common solvents. A simple method for the measurement of the dielectric spectra of liquids was verified and used to probe a room temperature ionic liquid and a chemical mixture used in a stage of a microwave-heated industrial process. The temperature and frequency dependence of the dielectric properties explained the observed rapid microwave heating of the ionic liquid and the relative failure of the process as a result of changing the irradiation conditions in order to scale it up.

Temperature measurement during microwave-assisted chemistry, whilst crucial to the elucidation of non-thermal effects, is problematic. A method of component specific or spatially-resolved thermometry during microwave heating of solid-phase organic synthesis (SPOS) suspensions has been developed. Measurements of the temperature-dependent lifetime of a fluorophore covalently attached to SPOS resin beads yield temperature values accurate to within around 0.5°C. Selective microwave heating of the resin was not observed, even for a system artificially designed to have significant dielectric inhomogeneity.

Techniques for the *in situ* and *in vitro* probing of model biological systems offer significant improvements over previous methods used to determine the possibility of microwaves effecting living things by non-thermal means. Thermally induced changes in the structures of a lipid and a globular protein were followed by small angel neutron scattering and circular dichroism respectively during microwave exposure. No evidence for non-thermal effects was obtained.

Contents

Acknowledgements

First and foremost I have to thank my supervisors, Andrew Harrison and Gavin Whittaker, for giving me the opportunity to undertake this study. Andrew was always willing to give whatever time he had to patiently help me with any problem and throughout my 3+ years he never failed to be encouraging and inspiring. Gavin's enthusiasm and expert knowledge were crucial to the work presented here and I am particularly grateful for his assistance in programming the vector network analyser interface and his input in the design of the bespoke applicators.

None of the work reported in chapter 2 would have been possible without the dielectric measurement method devised by Adrian Porch of the University of Cardiff. He was also extremely helpful in demystifying the workings of network analysers and the strange language they speak in. I must also thank Naomi Mack who spent part of an honours year project trying to apply the dielectric measurement method to solids but also aided me in verifying the method for liquids. Brian Flynn of the School of Electrical Engineering generously allowed me occasional use of his precious network analyser calibration kit and for some reason was also very keen to help me to create my own. I am also grateful to Andy Mount and Colin Pulham for supplying me with the ionic liquid.

The fluorescence measurement equipment described in chapter 3 was incredibly complicated so I am grateful for the time that Steven Magennis and Rob Neely spent adjusting lasers, mirrors and lenses and whatever else it was that was required for me to obtain the measurements I needed. Rob was a great help in fitting the data and the positive criticism and ideas of Steven and Anita Jones were crucial in the success of this project. I also thank Cara Humphrey for getting me started on fluorescence labelling of SPOS beads.

Jeremy Bradshaw was instrumental in choosing the DOPE-Me system for the *in situ* neutron diffraction experiments and Richard Heenan's support during and after our time at ISIS was particularly valued. In carrying out the BLG work I was in the very fortunate position of having Lindsay Sawyer as a collaborator. His unrivalled knowledge regarding the protein and his endless supply of anecdotes were priceless. I am also grateful for the work done by two project students under my supervision, John Rowe and Georgia McCulloch, in this project area.

Bespoke probes and applicators were crucial to this thesis therefore I am extremely grateful to Davy Paden and Stuart Mains of the mechanical workshop in The School of Chemistry for putting up with the constant demands for modifications. I must also thank Donald Palin in the electronic workshop for his soldering skills and for equipment loan.

I thank the School of Chemistry and CEM for jointly funding my PhD. I particularly thank Dave Lofty of CEM for his part in organising this funding and for arranging for my expenses to be paid for a conference visit.

I am grateful for the support and friendship of those around me including Fiona, Marcela, Gaetan, Mark and all the others who have been in and around lab 79 during my time there. However, I probably owe the biggest debt of gratitude to my wife Hannah, who has been especially supportive during the writing of this thesis despite having had a much more important and exciting ‘burden’ to be dealing with.

Introduction

Despite having been utilised in heating and telecommunications for more than half a century the ways in which microwaves might interact with chemical and biological systems are still debated. Microwave heating has a sound theoretical foundation but its application to chemical reactions has been observed to produce results that cannot be explained by thermal effects alone. Similarly, though conventional understanding suggests that the radiation that humans are exposed to as a result of mobile telecommunications is of insufficient power to be harmful, there is some theoretical and experimental support for the potential of microwaves to act detrimentally upon biologically systems by means other than heating. The aim of the work reported in this thesis was to develop improved experimental techniques for probing these interactions.

Descriptions of the various mechanisms of interaction, both accepted and contested, are included in chapter 1 along with an introduction to the practical application of microwaves in heating and mobile telecommunication. More specifically, the practical aspects of microwave-assisted chemical synthesis are discussed. These methods are increasingly popular in the laboratory but the paucity of data on the microwave susceptibility of common reaction components means that the theoretical understanding of the heating of these systems is generally poor. Subsequently scale-up to industrial processes is not common.

Chapter 2 is a description of the use of a relatively simple method for measuring the dielectric spectra of materials. From knowledge of the temperature dependence of these properties it is possible to determine other parameters relevant to understanding the way in which a material is heated by microwaves. The usefulness of this approach is demonstrated by the determination of the temperature dependent dielectric spectra of a room temperature ionic liquid and the probing of a microwave-heated industrial process.

Determining the reliability of experimental observations of *non-thermal* microwave effects is often complicated because the extent of the *thermal* effect is poorly measured or because conventionally heated control experiments are poor mimics. Accurate and representative measurement of temperature and well characterised exposure conditions are therefore crucial. Chapters 3 and 4 detail techniques for improved experimental probing of model chemical and biological systems during microwave heating.

In chapter 3 a novel thermometry method is described. Solid-phase organic synthesis resin beads were labelled with a fluorophore with a temperature-dependent fluorescence lifetime. Using time-resolved fluorescence measurement techniques it was possible to determine the temperature of the resin during microwave heating. Chapter 4 is a report of the first *in situ* and *in vitro* determinations of the effect of microwave irradiation on thermally induced structural transitions in model biological systems.

1 Interactions of microwaves with chemical and biological systems: theory and practice

1.1 Introduction

The purpose of this chapter is to give an overview of the mechanisms by which microwaves are thought to interact with chemical and biological systems and the practical issues associated with their application in heating and in telecommunication. Some of these mechanisms are relatively well understood, however, others are more contentious and are at the centre of arguments as to whether microwaves can interact with chemical and biological entities by means other than heating.

The theoretical and practical aspects of the application of microwave heating will be introduced first. The implications of microwave heating when applied to chemical synthesis will then be described, focussing on the unique thermal profiles than can be attained and the problems of measuring temperature in these situations. The chapter will conclude with a critical appraisal of specific and non-thermal mechanisms of interaction with biological systems, with reference to the extent to which they can justify concerns over the safety of exposure to low power microwaves such as those emitted by mobile communications technology.[1]

1.2 Microwaves and microwave heating

1.2.1 Theory of microwave heating

Microwaves lie between the infrared and radio frequency regions of the electromagnetic spectrum, at wavelengths of between 1 cm and 1 m (30 GHz $\geq \nu \geq$ 300 MHz). It is a legal constraint that microwave heaters are only permitted to operate at either 2.45 GHz or 900 MHz, leaving the rest of the spectrum free from interference for radar and telecommunications. The mechanism of microwave heating is a classical phenomenon and not related to microwave spectroscopy, in which gas phase molecules absorb photons at sharp bands in the frequency range 3-60 GHz due to transitions between quantised rotational energy levels.

In liquids and solids, where rotation is damped, incident microwave radiation can be converted to thermal energy. The electric field component of microwaves can exert a force on polar molecules and charge carriers. In conductors, where charge carriers (usually electrons) are free to move, microwaves can induce a current in the material. Where charges are bound to regions on a molecule (e.g. dipolar molecules such as water), the electric field will force a movement of the charge so that it is in alignment with the field. Both of these phenomena are termed dielectric polarisation, α, which manifests itself in four specific polarisation effects. Electronic polarisation, α_e, is the displacement of electrons from their equilibrium positions relative to the nucleus. Atomic polarisation, α_a, is induced when the electric field displaces atoms relative to one another. The interfacial polarisation, α_i, is due to charges at interfaces in inhomogeneous materials. Dipole polarisation, α_d, arises when the permanent dipole of a molecule aligns to the electrical field direction.

The dielectric properties of a material are described by its complex dielectric constant, ε^*. It is the sum of two further terms that quantify the polarisibility of a material by an external electric field and the efficiency of a material to transform applied electromagnetic (EM) energy into thermal energy. These are expressed, respectively, as the real dielectric constant, ε', and the imaginary dielectric constant, ε'', according to

$$\varepsilon^* = \varepsilon' - i\varepsilon'' . \qquad \textbf{1.1}$$

The electric field in an EM wave is by nature alternating. When the polarity of the field reverses, any dielectric polarisation relaxes. At microwave frequencies the time taken for the change in field direction is much greater than the time taken for realignment of electronic and atomic polarisation. However, in substances where dipoles have some freedom to rotate, such as liquids of dipolar molecules, the relaxation time of the dipole polarisation, τ, is similar to the time scale of electric field reversal. From Stokes theorem, τ for a spherical dipole of radius, r, in a medium of viscosity, η, will be

$$\tau = \frac{4\pi r^3 \eta}{k_b T}. \qquad \textbf{1.2}$$

The reorientation of the dipole lags behind the change in field giving rise to a polarisation current. The result is that a form of resistive heating will occur in the material. The phase lag between the field and the dielectric polarisation, δ, is related to ε' and ε'' as

$$\tan\delta = \varepsilon''/\varepsilon' . \qquad \textbf{1.3}$$

$\tan\delta$ is termed the loss tangent of the system. Where there is no conversion to thermal energy, e.g. at frequencies well above or well below the resonant frequency of dipole relaxation, the imaginary term approaches zero and, therefore, so does tan δ. However, at frequencies where dielectric heating occurs, ε'' and, by extension, $\tan\delta$ are no longer zero.

The dielectric constants are thus dependent upon the frequency, ω, of the applied field and the relaxation time of the dipole, τ, as denoted by the Debye equations,

$$\varepsilon' = \frac{\varepsilon_\infty + (\varepsilon_s - \varepsilon_\infty)}{(1+\omega^2\tau^2)} \qquad \textbf{1.4}$$

and

$$\varepsilon'' = \frac{(\varepsilon_s - \varepsilon_\infty)\omega\tau}{(1+\omega^2\tau^2)}, \qquad \textbf{1.5}$$

where ε_∞ and ε_s are the dielectric constants at infinite frequency and zero frequency (static), respectively.

From equation 1.5, it can be seen that ε'' has a maximum where $\omega = 1/\tau$ (applied frequency is equal to 'relaxation frequency'). For water at 20 °C the maximum is at around 18 GHz (figure 1.1). However, at this frequency the heating is so effective that the penetration of microwaves is poor. For this reason commercial microwave ovens operate at 2.45 GHz. The approximate penetration depth, D_p, is the depth at which the incident power is reduced to half of its original value and can be predicted for microwaves of wavelength λ_0 using the following equation:

$$D_p \propto \frac{3\lambda_0}{8.686\pi \tan\delta\sqrt{\varepsilon'}} \qquad \textbf{1.6}$$

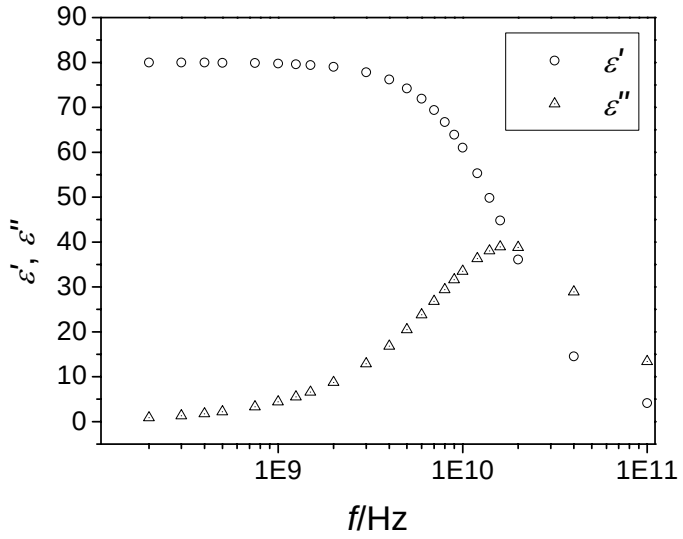

Figure 1.1: A plot of the real, ε', and imaginary, ε'', dielectric constants as a function of frequency (the *dielectric* spectrum) for water at 293 K.

There is also a conductive mechanism of interaction between microwaves and matter. The magnetic field component of an applied EM wave can generate currents in conductive material, which leads to losses by electrical resistance. By adding this term to the complex dielectric constant we arrive at the expression,

$$\varepsilon^* = \varepsilon'_\infty + \frac{\varepsilon'_0 - \varepsilon''_\infty}{1 + i\omega\tau} - \frac{i\sigma}{\omega\varepsilon'_s}, \qquad \textbf{1.7}$$

where σ is the conductivity of the material. In most solids conductive heating dominates the dielectric properties. However, in bulk metals, which are generally good reflectors of microwaves, the penetration is poor. The skin depth (also given the symbol δ) - the depth at which the applied field has decreased to 1/e of its original magnitude - is commonly used to describe the penetration:

$$\delta = \frac{1}{\sqrt{\sigma\omega\mu}} \qquad \textbf{1.8}$$

where μ is the magnetic permeability of the conducting material. Thus heating of large samples of metals by microwaves is ineffective, resulting in large field gradients in the microwave cavity and, ultimately, electrical discharges or *arcing* such as is observed from the gold rim of a tea-cup placed in a microwave oven. Free charges excited by the microwave fields in the surface of the metal have a tendency to accumulate at sharp edges, causing a concentration of electric field. This leads to a dielectric breakdown of the air in the immediate vicinity, which is observed as arcing. In contrast, metal powders heat very effectively in microwave fields due to the increased proportion of 'skin' in the sample.

Interfacial polarisation, α_i, can be responsible for microwave heating in heterogeneous materials consisting of a conducting phase in a non-conducting medium. This is sometimes called Maxwell-Wagner heating. This effect comprises terms relating to the conducting and dielectric components of the material. The extent of Maxwell-Wagner loss is sensitive to many physical parameters that can not be easily controlled. It is therefore difficult to formulate such materials without variation in microwave heating properties between samples.

The efficiency with which a mass of material, the workload, can be heated by microwaves is dependent not only upon its dielectric and conductive properties, as discussed above, but also on the way in which microwaves are applied. For most purposes the domestic microwave oven offers sufficiently reliable and efficient heating. However, for more specialised applications, such as those described later in this thesis, it may be advantageous to be able to convey the microwaves over a distance and apply them to a workload in a more controlled, reproducible or focussed manner. We will therefore now move to discuss apparatus for the transmission and application of microwaves.

1.2.2 Transmission of microwaves

A transmission line is a device to guide electrical energy from one point to another. Various kinds of transmission line (figure 1.2) can be used to propagate microwaves from a generator to irradiate samples in different types of environment. The simplest of these is a parallel wire

transmission line in which the electromagnetic wave is transported as a current along two parallel wires, the polarities of which alternate at the microwave frequency. Each wire is radiating but at 180 degrees out of phase with respect to its neighbour, therefore as long as the separation of the two wires is much greater than the wavelength of the electromagnetic wave, net radiation is zero and the line guides the wave. As the electric and magnetic fields are transverse to the direction of propagation, the wave is said to be propagating in a transverse electromagnetic or TEM mode.

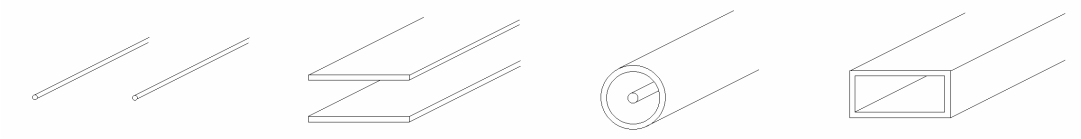

a) **b)** **c)** **d)**

Figure 1.2: Cross-section of common transmission lines and waveguides: a) parallel wire transmission line; b) parallel plate transmission line; c) co-axial line and; d) rectangular waveguide.

Lines where the wires are replaced with two plates (parallel plate), or with a wire held coaxially within a cylindrical conductor (coaxial line) have the advantage of being more shielded. Energy in the parallel plate configuration is largely reflected between the plates, although fringing fields can form at the edges. By effectively wrapping the plates around a 'co-axis' to form a tube the coaxial line negates this problem and offers complete shielding from loss. It has the additional advantage that the conductors and the dielectric used to separate them can be made of flexible materials, so it can be used in awkward spaces.

A defining parameter of a transmission line is its characteristic impedance, Z_0. This is the impedance at any point on a line of infinite length and is the ratio of the voltage across the line to the current along the line. The dimensions of the conductors and the properties of the dielectric determine Z_0. For an air-filled parallel plate line, the expression for Z_0,

$$Z_0 = \sqrt{\frac{\mu_0}{\varepsilon_0}}\frac{d}{w}, \qquad \textbf{1.9}$$

is a function of the width of the plates, w, and the separation of the plates, d. μ_0 and ε_0 are the permeability and permittivity of free space respectively. For air-filled coaxial lines, Z_0 is determined from the outer radius of the inner conductor, R_1, and the inner radius of the outer conductor, R_2, according to

$$Z_0 = \frac{1}{2\pi}\sqrt{\frac{\mu_0}{\varepsilon_0}}\frac{R_2}{R_1}. \qquad \textbf{1.10}$$

In lines where the conductors are separated, not by air, but by a dielectric material with a real dielectric constant, ε', the product, $\varepsilon_0\varepsilon'$, replaces ε_0 in equations 1.7 and 1.8. Where the dielectric is lossy, $\varepsilon_0\varepsilon^*$ replaces ε_0.

It is important to consider what happens when a load is placed at the end of the line. Figure 1.3 represents a transmission line (it resembles a parallel wire line but the same applies for parallel plate and coaxial lines) with characteristic impedance, Z_0, terminated by a load with impedance Z_L. A forward wave of voltage V^+ will be propagated from the source until incident upon Z_L, giving rise to a reflected wave of voltage V^-.

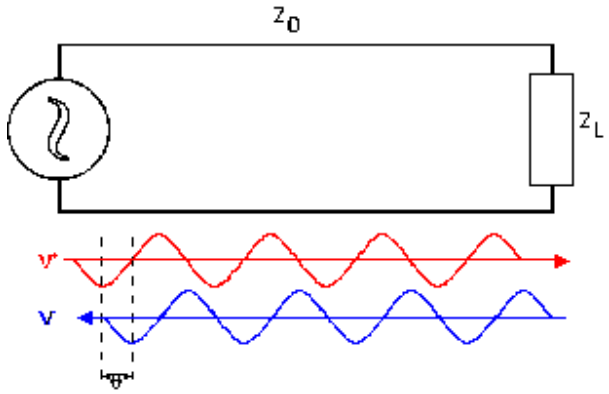

Figure 1.3: A representation of a transmission line with characteristic impedance, Z_0, terminated by a load with impedance, Z_L. Below the line are representations of the forward and reflected volatages, V^+ and V^-, at an instant in time showing the phase difference between them, θ.

The complex reflection coefficient, Γ, is defined as

$$\Gamma = |\Gamma| e^{i\theta}, \qquad \textbf{1.11}$$

where θ is the phase difference between the forward and reflected waves. Its magnitude $|\Gamma|$ is equal to the magnitude, $|V^-/V^+|$. Γ can also be described by

$$\Gamma = \frac{Z_L - Z_0}{Z_L + Z_0}. \qquad \textbf{1.12}$$

Therefore if Z_L and Z_0 are the same, or 'matched', Γ is 0, there is no reflected wave and all power is dissipated in the termination. If the impedances are mismatched ($Z_L \neq Z_0$), power will be reflected. The consequent phase change and degree of reflection at the extremes of load impedance are summarised in table 1.1.

Therefore for efficient transmission of energy all components of the circuit – source, line and load – should have the same impedance. Reflected microwave power can also be damaging to the generator. For these reasons, impedances in microwave circuits are commonly set to a standard impedance of 50 or 75 Ω. However, even when great care is taken, there will inevitably be mismatches along the line.

Table 1.1: Consequences of impedance matching and extreme mismatching for terminated transmission lines.

Load	Z_L	$\|\Gamma\|$	Degree of reflection	Phase change
'Matched' load	Z_0	0	0%	N/A
Open circuit	∞	1	100%	0 °
Short circuit (perfect conductor)	0	-1	100%	180 °

In the case of coaxial line, impedance will be non-standard where dust builds up at connections and where the line is deformed and the conductors fissured from repeated flexing. There will also be intrinsic losses due to resistive heating in the conductors. The high current densities in coaxial line, particularly at the centre conductor, mean that there is a limit to the power level that can be propagated before resistive heating and arcing cause breakdown of the materials.

Microwaves of higher power can be propagated along waveguides: hollow metal tubes of defined rectangular or circular cross-section. Wave theory requires that, in a waveguide made of a good conductor, the electric field be zero at the walls and that, away from them, it is parallel to them. These requirements are satisfied when the transmission of the electric component is by a plane wave reflecting back and forth off the sidewalls of the guide. The reflected wave has to be exactly 180 degrees out of phase with the incident wave. At the walls the field is zero. In the centre of the guide, points on the incident and reflected waves will add to give a transverse electric (TE) wave with the resultant energy flow in a straight line along the length of the guide. The expression for the length of the wave along the guide,

$$\lambda_g = \frac{\lambda}{\sqrt{1-\left(\frac{\lambda}{2a}\right)^2}}, \qquad \textbf{1.13}$$

determines that λ_g is greater than that of the original radiation. λ_g is therefore constant when λ and a (the width of the waveguide) are constant.

For a rectangular waveguide propagation is only possible when $\lambda < 2a$. Thus the dimensions of the guide can be chosen such that waves only propagate in one plane. Choice of dimension can also ensure that the waveguide is single-moded. When $\lambda/2 < a < \lambda$, only the lowest order TE mode can be propagated. TE modes are named in the form $TE_{m,n}$, where m and n are integers that indicate the number of half cycles of sinusoidal variation of intensity along the a and b directions respectively. If $a > b$, the lowest order TE mode is therefore TE_{10} (figure 1.4). Where the width is greater than λ, higher order modes (TE_{20}, TE_{30} *etc*.) will be present and will have one or more nodes across the width of the cavity.

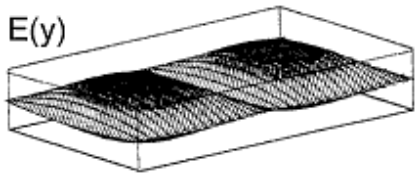

Figure 1.4: Variation in intensity of the electric field of for the TE_{10} mode in a rectangular waveguide

The only loss in a perfect waveguide is due to the conduction losses in the walls of the conductor, although these 'skin effects' are small. Therefore waveguides are the transmission line of choice where low loss is essential or where high power microwaves are to be used.

1.2.3 Application of microwaves for heating

The domestic microwave oven is possibly the simplest and certainly the most ubiquitous applicator for microwave heating. Microwaves are conveyed from a source, typically a magnetron, along waveguide and radiated into a cavity into which the workload is placed. The sides of the cavity, essentially a metal box, reflect the radiated microwaves back and forth thus certain resonant modes are sustained for a given frequency. For this reason, microwave ovens are termed multimode applicators. The field distribution is a sum of all the modes present and is therefore fundamentally non-uniform. As a result, a workload would be expected to heat differently depending upon where it is placed in the cavity. The uniformity of heating can be improved by movement of the workload (rotating turntable) or by inserting a metal fan (mode stirrer) into the cavity to continuously perturb the field distribution.

More reproducible heating is achieved with applicators designed to have better-defined field distributions. One such design is the single-mode cavity applicator. A microwave generator is connected to rectangular waveguide that is closed at the opposite end, creating a standing wave. The terminated end often has a plunger to allow the cavity to be tuned. Adjusting the position of the node of the standing wave by moving the plunger moves the entire wave along the length of the cavity. This moves the maximum of the field relative to the workload, providing a means to control the heating rate. Thin slits to allow sample introduction and measurements are also common features (figure 1.5).

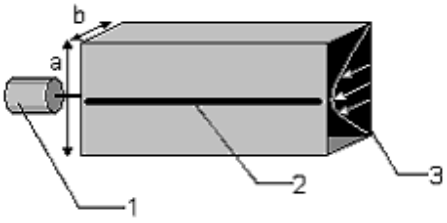

Figure 1.5: Schematic of a tunable single-mode cavity showing: dimensions *a* and *b*; 1) tuning plunger; 2) slit and; 3) diagram depicting the direction of the electric field for the TE_{10} mode and the variation of its magnitude in the direction of dimension *a*.

An obvious disadvantage of this design, when compared to the multi-mode cavity, is that choosing dimensions to selectively propagate certain modes also constrains the dimensions of the workload. In addition, although the field distribution is well defined it is not uniform. Inhomogeneous heating can therefore be expected for workloads with dimensions that are a significant fraction of a wavelength.

Parallel wire, parallel plate and co-axial transmission lines can also form the basis for microwave applicators. As with the waveguide applicator, the dimensions of the workload will be constrained by the dimensions of the transmission line required for propagation of microwaves of a given wavelength. Where a matched load terminates the transmission line, dissipating power not absorbed by the workload and ensuring efficient transmission of power from the generator, the applicator is known as a travelling wave applicator.

1.3 Microwaves in chemical synthesis

The popularity of microwaves in domestic culinary use is primarily due to their ability to efficiently heat water. At 2.45 GHz other dipolar liquids such as methanol, ethanol and dimethylformamide (DMF) – all commonly used solvents for organic synthesis – have high loss tangents and will therefore also be heated efficiently by microwaves. The susceptibility of a wide range of solvents to be heated by microwaves suggested that the technology, whose benefits have long been recognised in the kitchen, could also be useful in the laboratory.

A great deal of excitement followed initial experimentation in microwave chemistry when it was found that microwave heating appeared to significantly improve the rate of reactions.[2] It was thought that microwaves may have an effect on promoting reaction over and above simple

heating - a *specific* or *non-thermal microwave effect*. However, in the vast majority of cases the increased reaction rate can be rationalised by purely thermal effects: faster heating, and to higher temperatures.

1.3.1 Thermal effects of microwave heating in chemical synthesis

The steeper ramp of microwave heating is often termed *flash* heating and is due to the more direct nature of energy transfer. For a liquid with a high loss tangent, it is far more efficient to transform microwave energy to thermal energy *in situ* than it is to transfer thermal energy from a heat source to the reaction mass. Consider first the heating of a liquid mass using a conventional heat source such as an oil bath or a Bunsen burner. The source must first heat the vessel housing the reaction mixture; therefore there is a significant time lag before any heating of the contents can occur. The mass is then heated from the outside inwards primarily by a slow process of convection through the liquid. In contrast microwaves can couple directly with molecules. Thus, if penetration is good, the heating throughout the sample should be homogeneous and relatively rapid. Using microwave transparent material for the vessel, for instance silica glass or PTFE, eradicates the dead time associated with heating the container and ensures that energy is dissipated only in the reaction mixture.

The differences in the mechanism of energy transfer also account for the increased boiling points achievable by microwave heating. Boiling is seen to occur at the sides of the vessel where nucleation sites are present. In the case of a liquid heated to boiling from a conventional source (figure 1.6(a)) the temperature of the liquid in the centre of the vessel will be slightly lower due to the outside-inwards nature of its heating. However, a liquid mass heated to boiling by microwaves (figure 1.6(b)) will, because of conduction losses, have relatively lower temperature at the sides of the vessel where nucleation is most likely to occur. This can result in solvents *superheating* to temperatures 10-30 K above their normal boiling point.

A similar thermal inhomogeneity is observed in the heating of solid samples.[3] In a conventional oven or furnace, heating is from the outside inwards resulting in the surface being at a higher temperature. In the microwave heated case the sample heats volumetrically, with conduction losses and, at higher temperatures, radiation losses on the surface leading to higher temperatures in the centre. This is often called an *inverse temperature profile.*

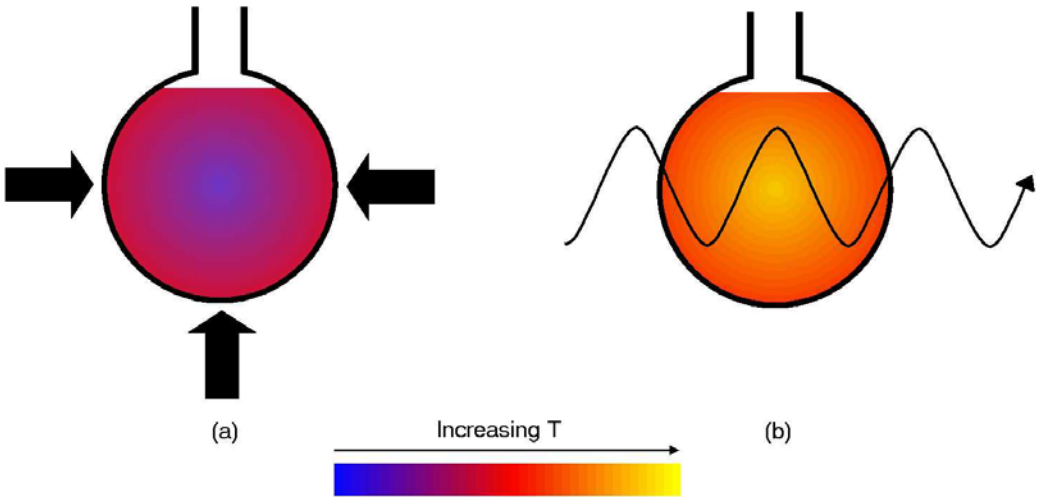

Figure 1.6: Superheating - heating of a liquid mass by conventional heating (a) and microwave heating (b).

Microwave heating in the solid state differs from that in the liquid phase. In most solids dipoles are locked in a rigid structure and are therefore not free to rotate. Not surprisingly, many inorganic oxides are virtually transparent to microwaves. However, where charged species such as electrons or ions are relatively free to move, as in semiconductors and ionic conductors, conduction losses are observed and the material will heat. Such materials are called *lossy* materials. The number and mobility of charged species often increases at higher temperatures as electrons start to populate conduction bands. Therefore an increase in temperature can increase microwave energy adsorption, which in turn results in a further temperature increase. If this process continues to feed back the temperature will increase rapidly and uncontrollably: this phenomenon is known as *thermal runaway*.

It has been shown that microwave heating can be used to drive many solid-state inorganic reactions if one or more of the component reagents is a lossy material. For example, $CuFe_2O_4$ can be prepared from CuO (lossy) and Fe_2O_3 (microwave transparent).[4] Product is often obtained more rapidly due to the increased mobility of ions in the coupling component and the rapid energy transfer to the sample.

1.3.2 Temperature in Microwave Heated Systems

Because microwave heating is often rapid and can be very selective, microwave heated systems are not necessarily in thermal equilibrium. It is therefore worth discussing what exactly is meant by temperature. Intuitively we have a sensory notion of temperature as a feeling of hot or cold. This is actually due to the energy flow between our bodies and objects with which we are in contact. We sense cold when heat is transferred from us to an object with less heat, and warmth when heat is transferred to us from an object with more heat. A thermodynamic definition that relates to this anthropocentric notion is that temperature is the property of an object that determines whether or not it is in thermal equilibrium with other objects. If two objects are in contact with one another there will be a transfer of heat between them if they are at different temperatures. The temperature tells us the direction of the flow of heat.

On a microscopic scale the temperature can be related to the population of quantum energy states of the system. For two systems, S_1 and S_2, in thermal contact to give the system S_3, probability arguments state that the overwhelmingly most likely distribution of energy is where N_3, the number of states in S_3, is greatest. This number is given by the product of the number of states, N_1 and N_2, accessible to S_1 and S_2 respectively:

$$N_3 = N_1 \times N_2 . \qquad \textbf{1.14}$$

The total energy of the system, E_3, is determined by,

$$E_3 = E_1 + E_2 . \qquad \textbf{1.15}$$

Therefore N_3 will be greatest when $N_1 \times N_2$ is stationary with respect to variations of E_1 and E_2. Therefore the equation,

$$\frac{d(\ln N_3)}{dE_1} = \frac{d(\ln N_1)}{dE_1} + \frac{d(\ln N_2)}{dE_1}, \qquad \textbf{1.16}$$

=is equal to 0 for a maximum in N_3.

However, $dE_1 = - dE_2$. Therefore at equilibrium, and as *ln N* is proportional to the entropy, σ,

$$\frac{d\sigma_1}{dE_1} = \frac{d\sigma_2}{dE_2}. \qquad \textbf{1.17}$$

The rate of change of σ with respect to the change in E increases as temperature decreases and T_1 must equal T_2. Therefore

$$\frac{1}{T} = \frac{d\sigma}{dE}. \qquad \textbf{1.18}$$

Although this is a rigorous definition of temperature it is perhaps most useful to think of temperature simply as a number that is proportional to the average energy of the molecules in a system in the form of heat.

In section 1.2.2 the inherent thermal inhomogeneities in microwave heated systems were discussed. These temperature gradients mean that it is very difficult to measure a representative temperature for a microwave heated system and therefore to deduce whether or not specific effects are acting. It is possible to reduce the inhomogeneity in a sample. In the case of a liquid, one can use vigorous stirring to reduce hot spots. For solids, insulation can be packed around the sample to minimise conduction losses from the surface. However, a more fundamental problem to be addressed is how to actually measure temperature in the presence of a microwave field. A mercury thermometer cannot be used as the microwaves will heat the mercury and at best provide an erroneous reading, but will more likely arc and heat up to the point of breaking. It is therefore necessary to use other kinds of thermometry.[5,6]

All thermometers exploit a property of a substance or system that changes regularly with temperature. In the case of the liquid-in-glass thermometer the property is the thermal expansion of a liquid, usually mercury or alcohol. If the liquid used is xylene, which has a low loss tangent and is a very poor conductor, the thermometer can be used in a microwave oven. Although this method is reasonably precise (~0.5 K), it is rarely used, as it does not lend itself readily to being incorporated into a computer-controlled heating system. The following thermometry techniques are preferred as they can output the temperature reading as some kind of electrical signal.

Thermocouples (figure 1.7) are made up of lengths of dissimilar conductors that are joined at two junctions to form a circuit. If one of these junctions is at a different temperature to the other, electrons will diffuse, generating an emf or *thermovoltage*. The magnitude of this emf will depend on the properties of each conductor, creating a measurable voltage difference between the conductors at the second (reference) junction. This voltage will also be dependent upon the temperature difference between the two junctions. Therefore, if the reference junction temperature can be maintained (either by immersion in an ice bath or electronically) thermocouples can be used to probe temperature.

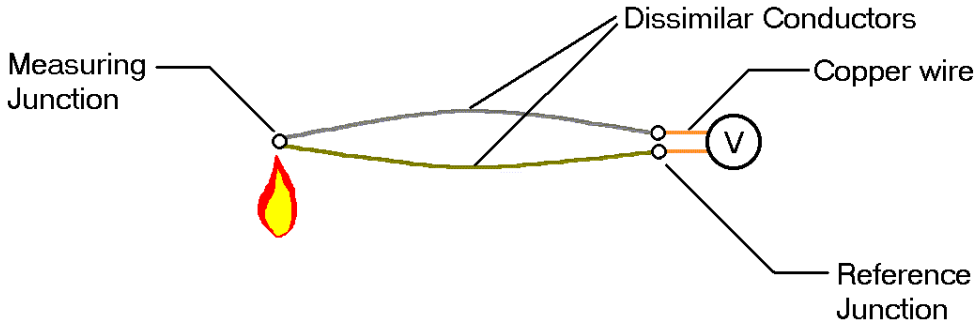

Figure 1.7: Schematic of a thermocouple with potentiometer across the reference junction.

The thermocouple probe can be shielded from the effects of microwave heating by a sheath of metal. Most of the incident microwave energy is reflected away by the metal cover but it is also necessary for it to be to grounded to the cavity wall to dissipate any currents induced.[7] When measuring solids the thermocouple will only measure the temperature where the tip touches the sample – not necessarily an accurate measure of the bulk temperature. The use of metal objects in a microwave field also introduces the risk of arcing and is likely to cause distortion of the electric field.

Infrared pyrometers side-step any problems associated with EM field interaction as the instrument can be used from outside the microwave cavity. The technique makes use of the temperature dependence of the intensity of the infrared radiation that all objects emit. Pyrometer devices focus the radiation on to a detector usually made of a semi-conductor such as silicon or lead sulphide. However, the technique will only measure the surface temperature.

A more accurate remote technique for microwave thermometry (particularly in the liquid phase) makes use of the temperature dependent fluorescence of rare earth-doped ceramic phosphors.[8] The phosphor can be introduced to the sample on the end of a fibre-optic cable that is used to simultaneously carry the excitation and emission pulses. From changes in either the fluorescence decay lifetime or the fluorescence yield the temperature can be obtained. The method is reasonably precise (~0.5 K) and is not affected by EM radiation.

Finally, a novel *post mortem* technique for measuring the temperature of microwave superheating has been reported.[9] A temperature dependent photochemical reaction was first carried out using conventional heating at a range of temperatures. The ratio of the different products obtained was plotted against the temperature to create a calibration curve. The product ratio obtained from the microwave heated reaction could then be used to determine the temperature of reaction and thus the superheating effect.

1.3.3 Apparatus for controlled microwave heating in chemical synthesis

Initial research on microwave chemistry was carried out using domestic microwave ovens. Modifications were made to these to allow the power and frequency to be varied. The addition of a port to introduce probes into the cavity or to allow safe refluxing of organic solvents[10] is also common. These ports rely on the fact that for a cylindrical waveguide of diameter a, it is not possible to propagate a wave effectively if $\lambda > 3.412a$. Thus at 2.45 GHz (λ = 12.2 cm) microwaves will not leak significantly through a copper tube of diameter 3.5 cm or less. Microwave ovens have multi-mode cavities and as such suffer from problems with control and reproducibilty due to non-uniform field distribution (section 1.1.2).

Recently, commercial microwave heaters specifically designed for applications in chemistry and the life sciences, such as the CEM Discover® have become available. These applicators offer greater control over reactions by simultaneously monitoring temperature and adjusting power levels to hold at desired set-points. In the CEM system temperature is monitored using an IR sensor beneath the reaction vial, in the bottom of the cavity. The cavity is circular and single mode thus the application of microwaves is focused and uniform throughout the sample. In the

unique design, microwaves are allowed to 'leak' into the self-tuning resonant cavity from the surrounding waveguide.

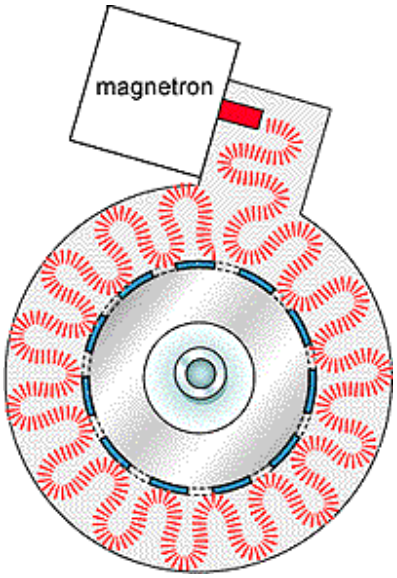

Figure 1.8: A schematic of the CEM Discover® microwave reactor displaying the unique circular cavity. Microwaves (red lines) are able to leak into the central resonant cavity containing the sample.

Most available systems are designed to allow safe use of pressurised conditions so even greater superheating is possible and reaction rates can be noticeably increased. The option for automated sample changeover has made these systems ideal for use in high-throughput synthesis. These and other features, such as *in situ* reaction monitoring, and simultaneous cooling to increase the power input for a given reaction temperature, have increased the breadth of possible applications and, at the same time, further exploited the unique advantages of microwaves for heating, making them 'the Bunsen burner for the twenty-first century.'

However, although these systems are increasingly popular they are still not commonplace, largely because they are expensive compared to conventional heating methods. In addition, industry has been slow to adopt the technology for applications much beyond the initial stages of target molecule discovery. Processes heated by microwaves do not scale-up in the same way as for conventional heating. To this end, flow-through cells are being incorporated into commercial laboratory scale systems. Continuous-flow methodology is more easily scaled-up than batch processing, where penetration depth limits the size of vessel that can be heated by microwaves.

However, a better understanding of key parameters for the microwave heating of chemical systems - including more comprehensive data on the dielectric properties of common solvents as a function of temperature - is required before scale-ups can be carried out as a matter of routine.

1.4 Microwaves and biological systems

1.4.1 Introduction

The interaction of microwaves with biological systems is currently of great interest due to public concerns over the health effects of exposure to the radiation used in mobile telecommunications.[1] Although mobile phones receive and emit microwaves at power levels well below currently accepted safety limits, the speed with which the technology has been adopted has led some to worry about the safety of long-term use. A number of epidemiological studies have been conducted to establish the validity or otherwise of these concerns but surprisingly little work has been done to elucidate possible mechanisms of interaction between low power microwave radiation and molecular components of biological systems.

In order to address this issue it is necessary to have an understanding of the exposure that humans can expect to be subject to due to mobile communications. Therefore a brief introduction to the technology of mobile phones will precede a discussion of the possible mechanisms by which biological matter could be affected by low power microwaves. This will be followed by a review of some of the more pertinent literature reports of experimental work to determine the effects of this radiation on biological systems.

1.4.2 Cellular mobile phone technology

This section is intended to give a sufficient overview of the technology to allow critical discussion of experimental reports of microwave effects upon biological systems with reference to whether or not they provide evidence of a risk to health from mobile phones. Much of the information was taken from a government commissioned report by The Independent Expert Group on Mobile Phones,[1] which was set-up to determine the health risk of using mobile phones.

Mobile phones send and receive information by radiocommunication. In the UK two frequency bands at the lower frequency end of the microwave range are used: 872-960 MHz and 1710-

1875 MHz. When a call is made (or text message/computer data sent) the signal from the handset is received by a base station linked to the main telephone network. Signals incoming to the handset are sent from the base station at a slightly different frequency. The maximum operational distance between phone and base station is approximately 35 km therefore a network of cells, each containing a base station at the centre, is used to give coverage over a large area.

The vast majority of mobile phones now convey information by a digital phone standard (Global System for Mobile communications or GSM) using phase modulation of the carrier wave. Each user requires one of more than five hundred 200 kHz bandwidth channels available in the two previously stated frequency bands. However, because neighbouring cells need to operate at different frequencies to prevent interference, the number of channels available to a user in a given cell is much reduced. A compression technique is therefore employed to allow more than one client to use each channel and hence increase then number of clients able to communicate with each base station. Time Division Multiple Access or TDMA, compresses each 4.6 ms to be transmitted into a pulse 0.58 ms long, effectively dividing each channel into eight.

The maximum permitted power levels of GSM phone transmission are 2 W at 900 MHz and 1 W at 1800 MHz. The average power level is never more than one-eighth of these values (0.25 W and 0.125 W respectively) due to TDMA and in fact, as one of the aims of mobile phones manufacturers is to increase battery life, the operational power levels are likely to be less than this. Adaptive power control, which reduces the power level according to proximity to the base station, can mean that peak power levels are reduced by a factor of as much as one thousand. The actual power incident on a user is less again as the field intensity falls off with distance according to the inverse square law. In free space, the maximum intensity at a distance of 2.2 cm from the antenna of a 2 W mobile phone is approximately 400 W m^{-2}. However, the maximum intensity within the head with the antenna 1.4 cm from the surface will be about a third of this.

Although base stations emit power at significantly higher power levels (typically 60 W) than handsets, the inverse square law means that the maximum possible intensity at ground level is of the order of 100 mW m^{-2}. As with handsets, and for similar reasons, the average power emission is normally much less. Measured intensities in buildings upon which base stations are mounted range from 0.01 to 10 mW m^{-2}. Therefore the intensity of exposure as a result of proximity to a

base station will always be much less than that experienced during handset use, but the total power absorbed may not be in the long term.

The intensity of exposure for biological systems is best quantified by the rate at which energy from an electric field of magnitude E, is absorbed by a given mass of tissue, m. This is known as the specific absorption rate, SAR, given by

$$SAR = \frac{m\sigma E^2}{\rho}, \qquad \textbf{1.19}$$

where σ and ρ are the conductivity and the density of the tissue respectively. Average values of conductivity at 900 MHz (1 S m^{-1}) and density (1000 kg m^{-3} = 1 kg $litre^{-1}$) for the body mean that a 30 V m^{-1} electric field is required to produce an SAR of 1 W kg^{-1}.

E can be determined from the intensity of the emitted power, I, according to

$$E = 19\sqrt{I}\,. \qquad \textbf{1.20}$$

The electric field 2.2 cm from the antenna of a mobile phone operating with a time-averaged output of 0.25 W would be around 50 V m^{-1}, resulting in an SAR of about 1.6 W kg^{-1}. Various models have been used to determine the expected increase in brain temperature for an SAR of this magnitude (see[1]), some including considerations of the effect of heat transfer due to blood flow. However, there is a general consensus that the maximum possible increase in brain temperature would be of the order of 0.1 °C. It can therefore be concluded that any damage caused by mobile phone radiation could not be as a result of heating.

1.4.3 Athermal microwave effects in biological systems

The ubiquity of water within biological systems means that high power microwave radiation can easily effect irreversible change upon biological matter by means of heating. This occurs whenever food is cooked in a microwave oven. However, since the radiation emitted by mobile phones is of insufficient power to cause significant heating, any damage to tissue would have to occur by means of an athermal effect.

It has been speculated that resonant coupling of microwaves with vibrational modes of biomolecules could facilitate such an effect.[11] Specific excitation in this way could significantly alter the conformation and therefore the function of biomolecules even for very low absorbed power levels. The majority of molecules in biological systems contain charged regions or dipoles and therefore couple with microwaves by a rotational relaxation mechanism, such as the one that accounts for the heating of polar liquids. This absorption generally occurs at frequencies below 100 MHz.[12] However, most molecular vibrational modes lie in the terahertz region of the spectrum and would therefore not be excited by microwaves.

It has been proposed that lower frequency modes could be manifested in biological systems as large-scale motions of portions of molecules such as DNA and proteins or as collective motions of a number of dipolar lipids in membranes. These modes could selectively absorb microwave energy and above a certain threshold of energy supply, S_0, molecules could be excited into a Bose-condensation like state.[11] Above S_0 the effect would therefore be independent of microwave power level.

However, the potential of these resonances to affect biological systems has been brought into doubt by considerations of the efficiency of coupling between biomolecules and electromagnetic fields oscillating at microwave frequencies. Calculations indicate that the energy absorbed would be small and furthermore, resonances would be severely over-damped in an aqueous medium as a result of energy loss to viscous friction with the surrounding water molecules.[13] The viscosity of the medium severely impairs radiative relaxation of the dipole element. Thus the resonant oscillator spends too long ($\sim 10^7$ s!) in the excited state to absorb sufficient energy from the electric field to effect the biological system. The excited elements can be expected to return to thermal equilibrium with the rest of the system by thermal conduction and dissipation of kinetic energy to the viscous medium over much shorter timescales ($\sim 10^{-11}$ s).[14]

Molecular ‘wring’ motions have also been posited as modes that could be resonantly excited by microwaves.[15] These modes are characterised by change in the local twist of circular chain molecules as a function of time with conservation of the total twist of the entire molecule. Biological chain molecules such as proteins are not closed, circular structures, rather they are linear and unconstrained. However, interaction with their environments slows the conformational change of these molecules to the extent that they are effectively topologically

constrained over the timescale of a wring mode cycle. Therefore these modes can, in theory, be sustained, resulting in conformational change. In the most extreme cases, variation in bending tendency along the length of a molecule could concentrate enough energy upon a small region to break chemical bonds.

Whilst there is some experimental evidence that appears to support this last theory[16] it is, in practice, very difficult to probe athermal effects. The relatively sparse literature on the probing of these interactions in model biological systems will be discussed in chapter 4, as a background to reports of two novel *in situ* techniques. However, there exists a great wealth of literature on the effects of microwave irradiation upon *in vivo* systems, some examples of which will be discussed in the following section.

1.4.4 *In vivo* experiments to determine the effect of low power microwaves on biological systems

Experimental studies that have measured the effect of microwave irradiation upon *in vivo* preparations are too numerous to be comprehensively reviewed here. An extensive review of the literature up to 2000 can be found in the report of the Independent Expert Group on Mobile Phones.[1] Throughout the literature a variety of irradiation conditions have been employed, many using power intensities that are orders of magnitude higher than those experienced during mobile phone use. In these cases, and particularly in those for which temperature monitoring was also poor or non-existent, it is virtually impossible to separate specific or non-thermal effects from the effects of heating.

A body of work on the effects of microwaves on growth and heat-shock gene expression in nematode worms[17-20] is notable for its more careful experimental design in comparison to other *in vivo* work. In initial studies[17] the heat-shock response for sham and exposed samples of model nematode worms were compared. Exposed samples were irradiated with low power microwaves (SAR = 4-40 mW kg^{-1}) in a copper TEM applicator. Sham and exposed samples were placed in the same incubator but sham samples were shielded in aluminium foil. An induction of reporter-gene expression equivalent to a temperature elevation of 3°C was seen for exposed worms relative to non-exposed. The possibility of such a temperature disparity was ruled out for several reasons but especially because the calculated SAR was too low to cause measurable heating.

Therefore the experiment appeared to provide strong evidence for athermal microwave effects. In another study reported by the same group, the accelerating effect of exposure on growth and maturation of the worms was also put down to athermal effects.[18]

Later experiments by the same group using two identical TEM applicators - one providing a more accurate sham exposure environment and one for the actual exposure as before - found much smaller, but still significant, differences due to exposure. However, the authors subsequently found that these differences could be attributed to heating of the applicator by microwaves.[19] In addition it was found that the heat response of the nematodes was not as predictable as previously thought. Exposure in an improved, silver-plated applicator gave the same results as for sham exposure in the copper applicator. The claims made for athermal effects have therefore been retracted.

Athermal effects have also been posited as the reason for increased incidence of lymphoma in microwave-exposed mice.[21] However, in a replication study[22,23] no such effect was observed. The authors suggest that the thermal effects could not be discounted in the earlier study but there were other changes to the experimental method that also complicate the comparison.

These examples highlight the problems encountered in probing of the effects of microwaves on biological systems *in vivo*. Namely, that exposing samples to microwaves without subjecting them to unquantifiable heating or other stresses not experienced by sham samples is difficult. Therefore *in vitro* methods may be preferable. However, accurate, representative thermometry and characterisation of the microwave exposure environment are still critical.

2 Dielectric measurement

2.1 Introduction

Dielectric properties are central to the theoretical understanding of microwave-heated processes. Knowledge of the dielectric properties of a substance as a function of temperature can be used to predict how microwave irradiation will heat the material: measures such as the extent to which microwaves will penetrate the material and the microwave power that the material will absorb per unit volume can be calculated. This level of understanding is crucial for microwave-assisted chemistry to be successfully transferred from the laboratory to larger scale processes.

However, the measurement of dielectric properties is not a trivial matter. The understanding of dielectric measurement techniques currently resides predominantly within the specialisation of electrical engineering. Consequently, for many common chemical substances there is no dielectric data and, even for common solvents, there is a paucity of data on how the dielectric properties change as a function of temperature.

This chapter contains a description of a simple novel technique for dielectric measurement developed elsewhere. The method uses a probe derived from a coaxial connector as the contact between the test substance and the vector network analyser that probes the substance with microwave test signals. The novelty of the technique lies in the measurement of a 'background' in air that can then be subtracted to remove the losses and reflections in the coaxial line between probe and analyser, thus complicated calibrations are not required.

The technique was used to obtain the first measurements of an ionic liquid as a function of temperature and to probe a microwave-heated industrial process. These systems provided useful demonstrations of the technique as well as highlighting the value of dielectric measurement. The results of these projects will be discussed after a description of the work done to validate the technique. However, the chapter will begin with a brief introduction to the different techniques that have been utilised previously.

2.2 Dielectric measurement techniques

This review will give a description of the practical aspects of various techniques for measuring dielectric properties. However, the theoretical basis of these techniques is beyond the scope of this thesis. Detailed description can be found in other reviews.[24,25]

2.2.1 Transmission techniques

In this method a transmission line, either coaxial or waveguide, is set up with part of the line filled with the test material. The material has to be shaped to either wholly fill the inside of a section of waveguide or to form the dielectric medium between the two conductors in a section of coaxial line. The complex dielectric constant of the material is then given by

$$\varepsilon_0 \, \varepsilon^* = \varepsilon_0 \left(\frac{Z_{01}}{Z_{02}} \right)^2 = \varepsilon_0 \left(\frac{\gamma_2}{\gamma_1} \right)^2 , \qquad \textbf{2.1}$$

where Z_{01} and Z_{02} are the characteristic impedances of the empty and sample-filled lines respectively and γ_1 and γ_2 are the propagation constants of the empty and sample-filled lines. However, it is not possible to directly measure these impedances or propagation constants.

In the original method of Roberts and von Hippel,[26] the transmission line is terminated by a short circuit and a signal generator sends a wave along the line to a dielectric sample of length, d. The voltage standing wave ratio (VSWR),

$$S = \frac{1 + |\Gamma|}{1 - |\Gamma|} , \qquad \textbf{2.2}$$

characteristic of the combination of the forward wave and reflected waves is measured at a distance, x_0, from the interface between the air-filled and sample-filled sections. ε^* can then be determined by solving the equation,

$$\frac{tanh(\gamma_2 d)}{\gamma_2 d} = \frac{S - i \cdot tan(\beta_1 x_0)}{1 - iS \cdot tan(\beta_1 x_0)} i\beta_1 d , \qquad \textbf{2.3}$$

(where β_1 is the phase constant of the wave in the empty line) and substituting into equation 2.1. The method has since been adapted and improved but the advantages and disadvantages remain

essentially the same: included in the former is the ability to measure over a range of frequencies only constrained by the cut-off of the coaxial line, in the latter is the problem of accurately shaping the sample to the dimensions of the line. This method is therefore best suited to the measurement of the dielectric properties of easily machinable solids.

2.2.2 Resonant cavity perturbation techniques

The dielectric properties of a material can be measured from the perturbing effect that it has upon the resonant properties of a tuned cavity. Measurement of the magnitude of the reflection coefficient, Γ, of a resonant cavity as a function of frequency will reveal a minimum (or a peak in $|1-\Gamma|$, i.e. the transmission coefficient, as depicted in figure 2.1) at the resonant frequency, f_0.

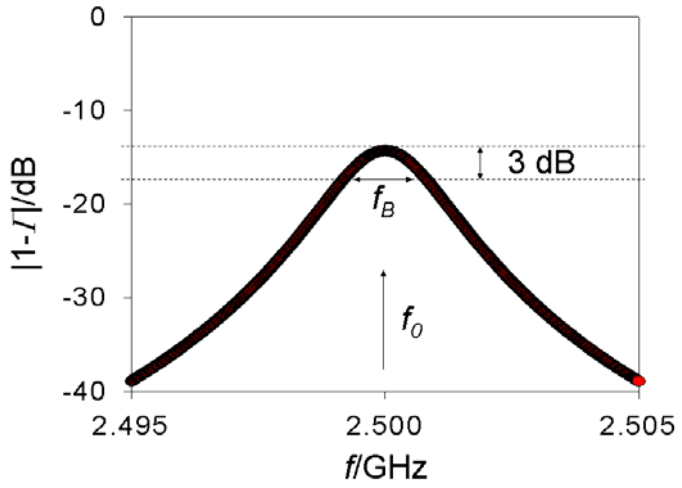

Figure 2.1: A plot of the magnitude of (1- Γ), i.e. the transmission coefficient, as a function of frequency, f, around the resonant frequency of a resonant cavity. The resonant frequency, f_0, and the bandwidth, f_B, are shown.

The cavity quality factor, Q, is determined from the ratio of f_0 to the bandwidth at 3 dB from the minimum, f_B:

$$Q = \frac{f_0}{f_B}. \qquad \textbf{2.4}$$

The introduction of a dielectric sample of volume V_s to a cylindrical resonant cavity of volume V_0 will result in the resonance shifting to a new frequency, f_0', and the quality factor changing to Q'. The dielectric properties of the sample can then be determined from

$$\frac{f_0 - f_0'}{f_0'} = A(\varepsilon' - 1)\frac{V_s}{V_0} \qquad \textbf{2.5}$$

and

$$\frac{1}{Q'} - \frac{1}{Q} = B\,\varepsilon''\frac{V_s}{V_0}, \qquad \textbf{2.6}$$

where A and B are constants relating to the geometry of the cavity and the sample. These can be determined empirically using samples of known dielectric properties. Similar equations exist for other shapes of cavity.

The above calculations are valid only where the sample, and therefore the perturbation, is relatively small. This method is particularly useful for low loss dielectrics but has the disadvantage that it is limited to the resonant frequencies of the cavity.

2.2.3 Open coaxial probe techniques[25]

The coaxial probe is essentially an open-terminated coaxial line. Probes are generally machined from either coaxial cable or connectors, with the outer conductor commonly terminated in a flange. The probe acts as an interface with the test material, and the two must be placed in intimate contact for measurement. Microwave signals are sent along the coaxial line to the probe from where they 'fringe' into the test material before being returned along the line. The dielectric properties of the material can then be determined from measurements of Γ. Various methods are used to model the capacitance and radiation of the probe, and to remove systematic errors due to reflections and loss in the line. The experimental and mathematical methods used for the work reported in this chapter will be discussed in the next section.

Co-axial probing is generally less accurate than resonance methods but is convenient for the measurement of liquids, soft solids, and, because it is non-destructive, for *in vivo* measurements in living systems. The technique also has the advantage that it is a broadband spectroscopy technique. Measurement of hard solids is challenging because the interface between probe and sample must be without air-gaps for accurate measurement. Therefore both sample and probe must be machined as flat as possible.

Coaxial probes have been designed for measurement of solids at elevated temperatures.[27-29] Coaxial measurements are sensitive to temperature as thermal expansion of the probe materials distorts the geometry at the interface,[30] in most cases because the dielectric has a greater thermal expansion coefficient. In order to negate this problem a probe has been made entirely from the same ceramic material but with the conductive parts metallized.[27,28] Another design has solved the problem by including a spring-loaded inner conductor.[29]

2.3 Description of the novel dielectric measurement technique

2.3.1 Introduction

Whilst there have been numerous models and methods for coaxial probe deielectric measurement few are as simple as the one described in this section. The novelty of the method is in the measurement of the scattering parameter for the probe terminated in air, as well as for the probe in contact with the sample. Using a ratio of the two removes the errors due to the electrical length of the probe.

The different aspects of the method will be described in this section starting with a description of the probe used. The general measurement procedure will then be explained including an account of the use of a vector network analyser (calibration and interfacing). Finally the mathematical theory behind the method will be discussed.

2.3.2 The probe

A bespoke probe was manufactured from an SMA (characterised by having a PTFE dielectric, a Z_0 of 50 Ω, and a 3.5 mm inner diameter of the outer conductor) coaxial connector (figures 2.2 (a) and (b)). At one end of the probe is an SMA jack. At the other the connector has been machined back and the outer conductor fitted with a brass flange forming a coplanar open termination of the conductors and the PTFE dielectric. Because the probe is manufactured from brass and PTFE it exhibits good thermal and chemical resistance.

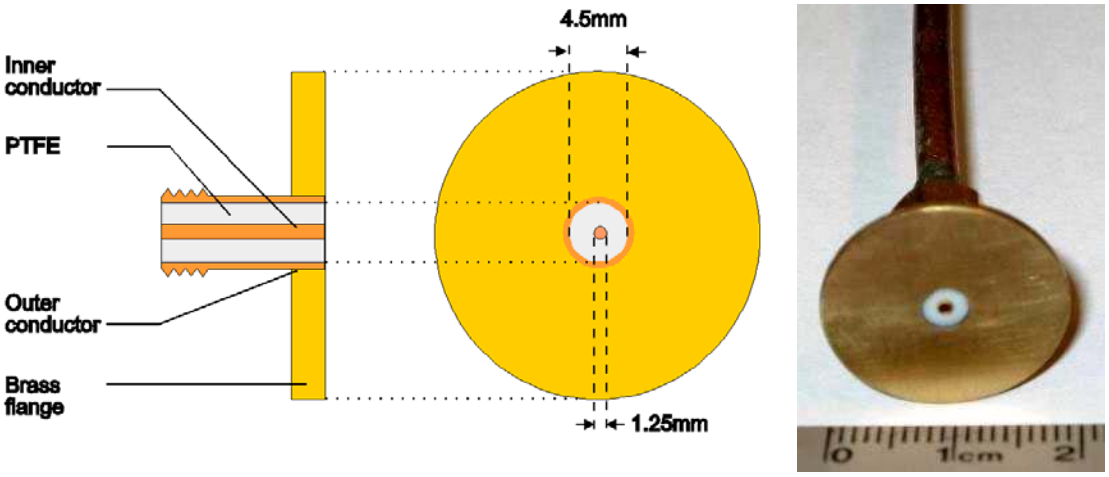

(a) (b)

Figures 2.2 (a) and (b): a) Schematic of of the bespoke probe used for dielectric measurement. The diameters of the inner and outer conductors (shown) are those of the connector from which the probe was derived. b) Photograph of the flat face of the probe connected to semi-rigid coxaial cable (behind), with a rule as an indication of scale.

A probe based on a "k"-connector (Anritsu) was also tested. The dimensions of the coaxial connector are much smaller and therefore the probe radiates less. However, over the frequencies used here (≤ 3 GHz) radiation is not a significant problem. In addition the connectors are more expensive, and the polymer components are less chemically and thermally resistant.

Another SMA-based probe was also fabricated. This was identical to the one shown in figures 2.2 (a) and (b) except the flange was thicker and drilled with holes into which small resistance heaters and a fluoroptic temperature probe could be placed. This allowed the dielectric properties of solid samples to be measured as a function of temperature. The results of these largely unsuccessful trials are recorded elsewhere.[31] However, both SMA-based probes were used interchangeably in the experiments that are reported in this thesis.

2.3.3 The vector network analyser

Measurements of the reflectance coefficient were obtained using a Hewlett Packard 8752A Vector Network Analyser (VNA). VNAs probe devices or materials with AC test signals over a range of frequencies (300 kHz – 3 GHz for the 8752A) and measure the magnitude and phase of

the signal returned. In a typical measurement, an AC current of voltage, V^+, is output from one of the ports on the front of the VNA and conveyed along a coaxial cable to the material to be tested. The voltage, V^-, and relative phase, θ, of the signal returned from the material are then measured at the same port (1-port measurement). The VNA reports the magnitude of the voltage ratio $|V^-/V^+|$ and the phase as the complex number S_{xy}, where x and y are the ports that the signal is measured at and sent from respectively (the letter 'S'' used for this *scattering parameter* should not be confused with the *VSWR* as mentioned in section 2.2.1) A 1-port measurement at port 1 is therefore known as S_{11} and is equivalent to the reflection co-efficient (equation 1.11),

$$\Gamma \equiv S_{11} = \left| \frac{V^+}{V^-} \right| e^{i\theta} . \qquad \textbf{2.7}$$

A 2-port *transmission* measurement of a signal from port 1 measured at port 2 after passing through a device is known as S_{21} and is equivalent to the transmission coefficient, T, and 1- Γ. Thus

$$T = 1 - \Gamma \equiv S_{21} = \left| \frac{V_{trans}}{V_{inc}} \right| e^{i\theta} , \qquad \textbf{2.8}$$

where V_{trans} and V_{inc} are the transmitted and incident voltages and θ is now the phase difference between V_{trans} and V_{inc}.

Scattering parameters are commonly visualised on a polar plot, in which magnitude increases from the centre to the outer circle, and phase increases around the circumference from 0 to 360 (effectively 0) on the right-hand side in a clockwise direction. Figure 2.3 is a polar plot depiction of the responses seen for perfect open, short and matched load devices (see table 1.1) and for a test device or sample giving rise to a reflection magnitude | Γ| and phase difference θ. As the VNA measures S_{11} at a sweep of frequencies the real data returned for a sample or device would be made up of several points on the polar plot. The data for the 3 perfect devices at all frequencies would fall on the same point.

However, if one were to connect a perfect open circuit (we assume for now that such a device is possible) to a VNA by coaxial cable and measure S_{11}, one would not see the data fall on one

point. Rather, the observed response would spiral around the outside of the polar plot. This is as a result of the *electrical length* of the co-axial line.

The phase measured by the VNA is the phase of the test signal after travelling a distance of the order of 10^{-1} m along the cable to the device and then, after reflection, back a further 10^{-1} m. At the lowest frequency measurable by the VNA (f = 300kHz, $\lambda = 10^{3}$ m) reflected test signals will not differ significantly in phase from the test signal sent out, as the wavelength is much greater than the physical length of the coaxial cable. Therefore the point will be plotted at the right-hand side of the polar plot as expected for a perfect open. However, at the highest end of the frequency range of the VNA the wavelength decreases to 10^{-1} m (3 GHz). The wavelength is of the same order of magnitude as the length of the cable and therefore a significant phase change is observed and the point is plotted further round the outside of the polar plot.

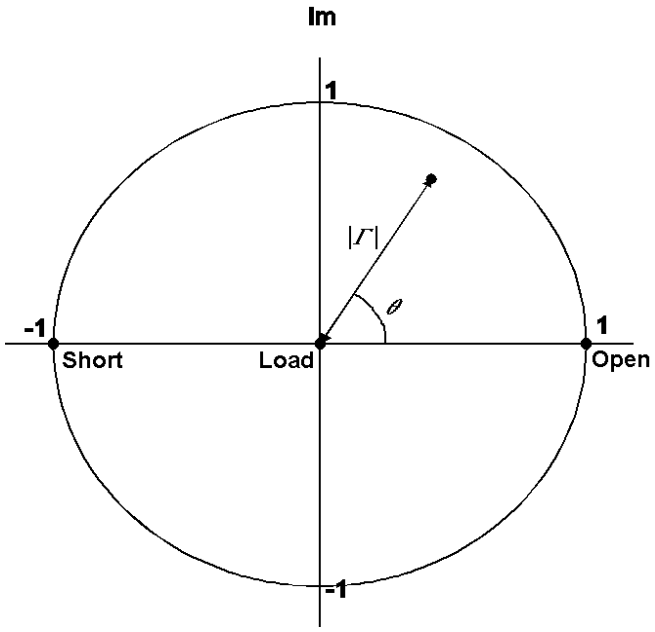

Figure 2.3: A polar plot depicting the S_{11} reponses for perfect open, short and matched load devices and the response for a device or material giving rise to a reflection magnitude $|\Gamma|$ and a phase difference θ.

In addition to the electrical length of the line, real coaxial cable is not perfect and will give rise to losses and reflections that must be removed from the measurement. To cancel out the effects of the electrical length and imperfection of the cable, a calibration procedure is used.

For a 1-port measurement three known responses are required for the mathematical error correction. Three standard physical devices are connected to the end of the co-axial line in turn: a short, an open and a matched load. The VNA measures the responses of each of the three devices and automatically calibrates itself, moving the measurement plane to the end of the co-axial line.

The devices, known collectively as a calibration kit, are supplied with the VNA along with the parameters that reflect their 'imperfections', which must be inputted before the correction. Calibration kits are relatively expensive as they have to be precision engineered and extensively characterised. However, it is worth briefly explaining that, for applications such as this that do not require the highest level of precision, it is possible to create one's own kit. This was necessary for this work to be carried out as the VNA used was inherited without a calibration kit, therefore a kit was therefore created from SMA coaxial connectors.

By machining back the stub end of a jack-to-stub connector until the dielectric and outer and inner conductors were coplanar an open termination was created. Similarly, part of the dielectric was pared back from a jack-to-stub connector to form a recess between the inner and outer conductors. The recess was then filled with solder to form a short. By simply attaching a broadband 50 Ω resistor to a jack-to-jack connector the load was created. All components were purchased from RS. The devices were housed in a single metal box with only the jack connectors showing in order to protect the working ends.

However, these devices are not 'perfect'. The devices were therefore characterised using the VNA after calibration using a borrowed standard Hewlett Packard kit. The electrical length of the each device was then determined from the electrical delay that had to be applied to bring the observed arc to a point. As the impedance of the load is not uniform over all frequencies a compromise impedance was used: 48 Ω was found to give a good calibration. The calibration kit definitions are included in Appendix II, along with the freeware software used to upload the parameters to the VNA.[32]

Once the VNA is calibrated the measurement plane is effectively moved to the end of the coaxial cable. The dielectric probe can then be attached and used to take the required measurements of the sample as described in the following section.

2.3.4 Obtaining data for samples from the vector network analyser

The method requires that for each sample two measurements must be taken: one with the open probe in air and one with the probe in contact with the sample. For each measurement the magnitude of the scattering parameter and the phase are recorded over a range of frequencies. For all measurements reported here the frequency range was 0.06 to 3 Ghz, as 3 GHz is the maximum operating frequency of the VNA and below circa 0.06 GHz the measurement error becomes too large.

The operation of the VNA and the recording of the data would be laborious if carried out manually, therefore a small software application, *Dielectric Donkey* (figure 2.4), was programmed using Microsoft Visual Basic[33] to automate various tasks by sending orders and receiving data via a GPIB interface (Agilent 82357A) between the VNA and a PC. The functions of the program are summarised in table 2.1, but the main function is to download the data from the polar plot seen on the screen of the VNA to a file saved on the PC. The data is saved in the form of a text file with tab-separated columns containing reflectance magnitude, phase and frequency (in that order). A copy of the application along with a text file of the code is included in appendix II.

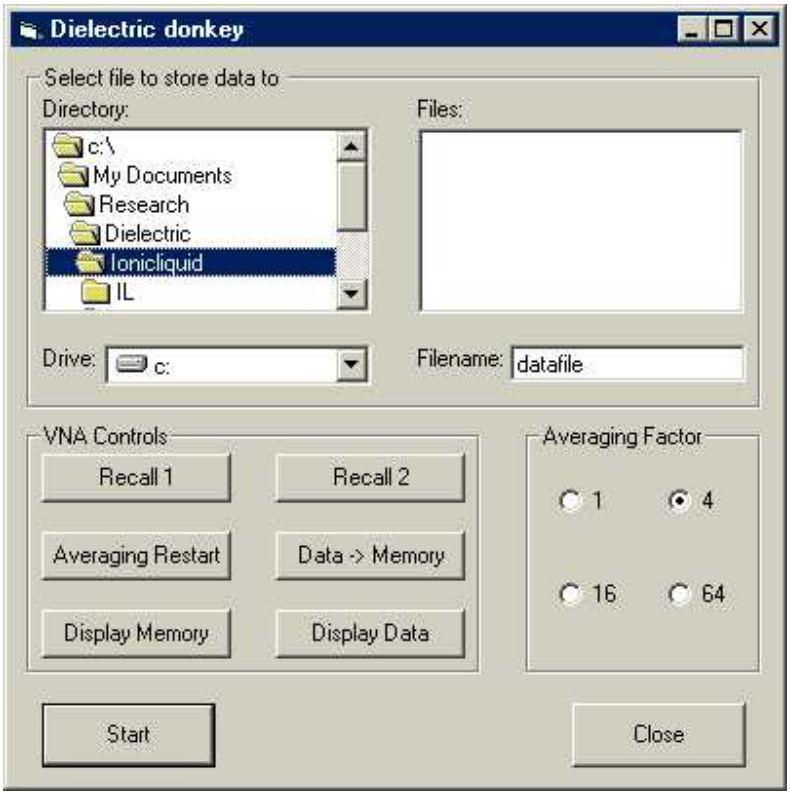

Figure 2.4: Screenshot of Dielectric Donkey, a software application for downloading data from a VNA.

The final step is to transform the two datasets - the probe in air and the probe with sample – into data of the real and imaginary dielectric constants as a function of frequency, that is, dielectric spectra. This mathematical transformation will be described in the following section.

Table 2.1: Summary of the commands for the VNA data download application, Dielectric Donkey.

Command	Function
Directory	Allows the user to choose the directory in which the measurement data file will be stored.
Drive	Allows the user to choose the drive in which the measurement data file will be stored.
Files	Lists files already stored in the selected directory.

Filename	Input of the filename for the measurement data to be stored under.
Recall 1	Recalls the VNA instrument memory state #1.
Recall 2	Recalls the VNA instrument memory state #1.
Averaging restart	Restarts averaging (see Averaging Factor).
Data->Memory	Places the data currently on the VNA screen in the VNA short-term memory.
Display Memory	Places the data currently in VNA short-term memory on screen.
Display Data	Shows current data on VNA screen (default state before Display Memory is selected).
Averaging Factor	Selects the amount of scans over which the data is averaged in the VNA. For averaging factors other than 1 it is crucial that, before starting a data download, averaging is restarted. Otherwise the data on-screen may partly reflect data from a time at which the sample/probe status was different (e.g. before the sample was in contact with the probe).
Start	Starts the downloading of data from the screen.
Close	Closes Dielectric Donkey and sets the VNA screen intensity to 0% (screen intensity set to 100% on start-up).

2.3.5 Mathematical determination of ε_S' *and* ε_S" from the recorded data files

If the calibration had the effect of moving the measurement plane to the interface between the probe and the sample, from equation 1.11, the relationship between the scattering parameter and the impedance of the sample, Z_L, would be

$$S_{11} = \frac{Z_L - Z_0}{Z_L + Z_0}. \qquad \textbf{2.9}$$

If we then model the probe as a capacitor, with capacitance C, the sample impedance can also be described by

$$Z_L = \frac{1}{i\omega C}, \qquad \textbf{2.10}$$

where ω is the angular frequency. The sample admittance, $Y_L = 1/Z_L$, is therefore

$$Y_L = i\omega C . \qquad \textbf{2.11}$$

As $C = A\varepsilon^*$, where A is a constant relating to the probe geometry, we find that

$$Y_L = i\omega A\varepsilon^* , \qquad \textbf{2.12}$$

and substituting in equation 1.1 gives

$$Y_L = i\omega A\left(\varepsilon' - i\varepsilon''\right) = \omega A\varepsilon'' + i\omega A\varepsilon' . \qquad \textbf{2.13}$$

By rewriting equation 2.9 in terms of the sample admittance,

$$S_{11} = \frac{\frac{1}{Y_L} - Z_0}{\frac{1}{Y_L} + Z_0} = \frac{1 - Z_0 Y_L}{1 + Z_0 Y_L} , \qquad \textbf{2.14}$$

we can substitute in equation 2.13 to arrive at an expression,

$$S_{11} = \frac{1 - Z_0\left(\omega A\varepsilon'' + i\omega A\varepsilon'\right)}{1 + Z_0\left(\omega A\varepsilon'' + i\omega A\varepsilon'\right)} , \qquad \textbf{2.15}$$

relating the scattering parameter to the complex dielectric constants. We therefore have a mathematical method for determining ε' and ε'' from S_{11} as all parameters in equation 2.14 are known except A, which can be determined empirically by measurement of a material of known properties.

However, the measurement plane is not at the interface as the probe has an electrical length that is not accounted for in the calibration. It follows from equation 2.7 that the effect of the resulting increase in phase difference, θ, on the scattering parameter can be accounted for by adding a term, $e^{i\theta}$, so that equation 2.14 becomes

$$S_{11} = \frac{1 - Z_0 Y_L}{1 + Z_0 Y_L} e^{i\theta} . \qquad \textbf{2.16}$$

This term is the same in the expression for the scattering parameter measured for the sample,

$$S_{11,S} = \frac{1 - Z_0 Y_{L,S}}{1 + Z_0 Y_{L,S}} e^{i\theta}, \qquad \textbf{2.17}$$

and in the expression for the scattering parameter measured for the open probe in air,

$$S_{11,O} = \frac{1 - Z_0 Y_{L,O}}{1 + Z_0 Y_{L,O}} e^{i\theta}. \qquad \textbf{2.18}$$

Therefore by taking the ratio of $S_{11,S}$ to $S_{11,O}$, the terms for the probe electrical length cancel-out leaving

$$\frac{S_{11,S}}{S_{11,O}} = \frac{1 - Z_0 Y_{L,S}}{1 + Z_0 Y_{L,S}} \cdot \frac{1 + Z_0 Y_{L,O}}{1 - Z_0 Y_{L,O}}. \qquad \textbf{2.19}$$

Substituting expressions for the sample admittance,

$$Y_{L,S} = \omega A \varepsilon_S'' + i\omega A \varepsilon_S', \qquad \textbf{2.20}$$

and the admittance of air ($\varepsilon_{air} = 1$),

$$Y_{L,O} = i\omega A, \qquad \textbf{2.21}$$

into equation 2.19, we ultimately arrive at an equation,

$$\frac{S_{11,S}}{S_{11,O}} = \frac{1 - \left(Z_0 \omega A \varepsilon_S'' + i\omega A \varepsilon_S'\right)}{1 + \left(Z_0 \omega A \varepsilon_S'' + i\omega A \varepsilon_S'\right)} \cdot \frac{1 + Z_0 i\omega A}{1 - Z_0 i\omega A}. \qquad \textbf{2.22}$$

that allows us to determine the dielectric properties of a sample, *ε_S' and ε_s"*. Equation 2.7 shows that the ratio of the scattering parameters, $S_{11,S}/S_{11,O}$, can be determined from the separate measurements of the magnitude and phase of $S_{11,S}$ and $S_{11,O}$ according to

$$\frac{S_{11,S}}{S_{11,O}} = \frac{\left|S_{11,S}\right|}{\left|S_{11,O}\right|} e^{i(\theta_S - \theta_O)}. \qquad \textbf{2.23}$$

The mathematical determination of *ε_S' and ε_S"* from the recorded data files was carried out using the Mathcad mathematical design application.[34] Data over the entire frequency range was read

into a Mathcad worksheet and processed into dielectric property data, which was subsequently saved as another text file (Mathcad format and rich text format copies of the worksheet are included in appendix II). The worksheet also plots a small graph of the dielectric data results (not shown in rich text file). The β factor referred to in the worksheet is equivalent to $A \cdot Z_0$ in equation 2.22 and is effectively used as a calibration constant. $\beta = 1.7 \cdot 10^4$ was found to give good agreement for the probe used.

This method has inherent inaccuracy in that the capacitance model used for the probe (equation 2.12) is only an approximation. A better aperture admittance model is

$$Y_L = iA\omega\varepsilon^* + iB\omega^2\varepsilon^* + iC\omega^4\varepsilon^{*2.5}, \qquad \textbf{2.24}$$

which includes an additional term for the capacitance, $iB\omega^2\varepsilon^*$, and a term for the radiative loss, $iC\omega^4\varepsilon^{*2.5}$ (B and C are additional constants). However, these terms are only appreciable at relatively high frequencies and can be minimised by using smaller coaxial dimensions in the design of the probe.

2.4 Verification of the technique

2.4.1 Introduction

There is very little data of the dielectric properties of materials over a range of frequencies in the literature, although even data at single frequencies is surprisingly rare. However, data for the dielectric properties of three solvents - methanol (MeOH), ethane diol (EtDiol) and dimethyl sulphoxide (DMSO) - were available.[35] Therefore the method was verified against these results. In addition, the parameters of the Debye fit for methanol have been published previously,[36] therefore these were compared against a fit to the measured data.

2.4.2 Experimental

MeOH, EtDiol and DMSO were obtained from Aldrich and dried overnight using molecular sieves. The real and imaginary dielectric constants were determined for each liquid at room temperature (20 °C) over the frequency range 0.06 to 3 GHz by the method described in section 2.3. The measurement for each liquid was carried out in triplicate and the mean and the standard deviation determined for each data point.

2.4.3 Results and discussion

The dielectric spectra recorded for the three liquids are shown in figures 2.5-2.7. Included on the plots are data obtained from a literature source.[35] An indication of the error in the measurement can be derived from the standard deviation determined from the triplicate measurements. It can be seen that the error is inversely proportional to frequency. This is because at lower frequencies (longer wavelength) the measured phase difference is less and the relative error is therefore greater. At the lowest frequencies this error can be comparable in size to the value of ε'' but above around 0.5 GHz it becomes negligible.

On the whole, agreement between the measured and literature spectra is good but there are pronounced differences for ε' for DMSO and ε'' for MeOH and EtDiol. However, even where the difference is greatest, it is not more than 6%. The disparity does not appear to be a systematic error as it is not uniform for all of the liquids. It may just reflect error in the literature data. Fitting the measured dielectric spectra for MeOH to the debye model (equations 1.4 and 1.5) using the graphing and data analysis software Origin[37] (figure 2.8) yielded parameters that are in agreement with those in the literature.

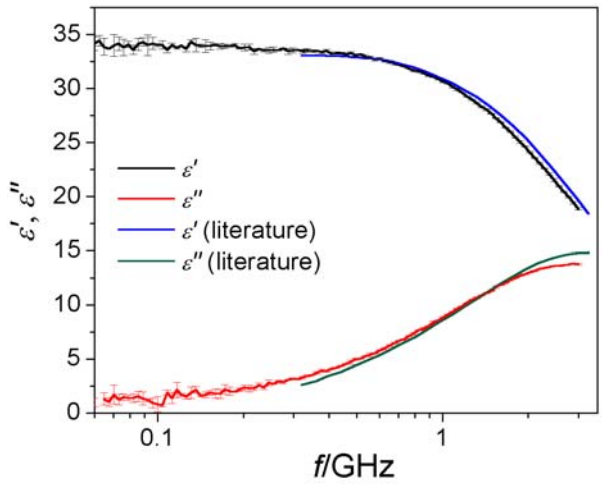

Figure 2.5: Comparison of the measured and literature dielectric spectra of MeOH at 20°C. Error bars for the measured spectra are the standard deviation of 3 measurements.

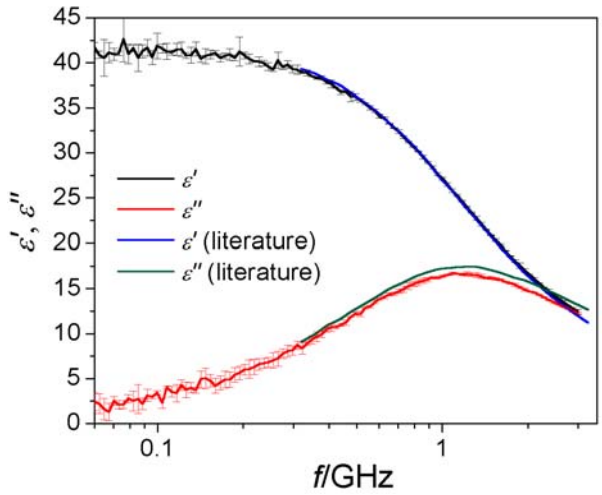

Figure 2.6: Comparison of the measured and literature dielectric spectra of EtDiol at 20°C. Error bars for the measured spectra are the standard deviation of 3 measurements.

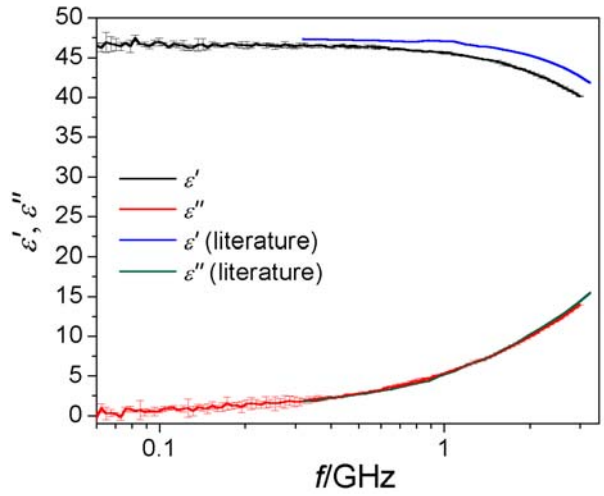

Figure 2.7: Comparison of the measured and literature dielectric spectra of DMSO at 20°C. Error bars for the measured spectra are the standard deviation of 3 measurements.

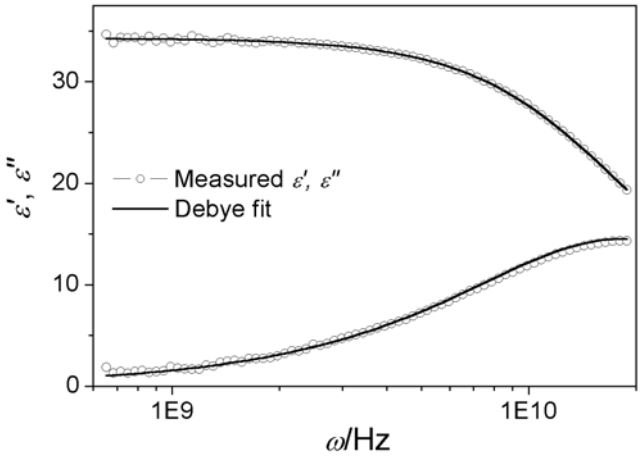

Figure 2.8: Measured dielectric spectrum of MeOH at 20°C and the debye fit to it. The fit parameters were ε_s = 34.3 (literature = 34.8 + 0.5), ε_∞ = 5.2 (4.5 + 0.7), τ = 54 (56 + 2) ps.

2.4.4 Conclusion

Comparison of published dielectric properties and those measured by the method described herein are in agreement to better than 6%. The error in the method is negligible above 0.5 GHz. Therefore the method provides sufficiently accurate dielectric data for probing liquid chemical systems over the range of frequencies relevant to microwave heating.

2.5 The dielectric properties of an ionic liquid as a function of temperature

2.5.1 Introduction

Room temperature ionic liquids are known to heat extremely rapidly in microwaves.[38,39] Along with their other favourable properties (good thermal stability, low vapour pressure), this has made them useful choices for solvent for microwave-assisted chemistry (see review[40]). In some cases, heating is so efficient that it can become uncontrollable. Therefore, ionic liquids can instead be used in small quantities to aid the heating of syntheses that use non-polar solvents such as dichloromethane or hexane.[38,39] The ionic liquid can be chosen to be immiscible in the solvent so that it is easily extracted from the product mixture.

To date the underlying dielectric properties that govern the microwave heating have not been investigated (the dielectric properties of an ionic liquid have been measured[41] but at THz frequencies, far from the principal microwave heating band at 2.45 GHz). In addition, as many ionic liquids are hygroscopic it is important to understand how water content affects their ability to be heated by microwaves. Therefore the dielectric properties of a room temperature ionic liquid, 1-butyl-3-methylimidazolium chloride ([BMIM] Cl), were determined as a function of temperature and as a function of water content.

2.5.2 Experimental

2.5.2.1 Measurement of the dielectric spectrum of [BMIM] Cl as a function of temperature

5 g of the supplied [BMIM] Cl prepared by standard methods[42] was placed in a flask and dried overnight under vacuum at 60°C. Whilst still warm the flask was placed in a hot oil bath and the calibrated dry coaxial probe, a small magnetic stirrer bar and a FISO FOT-H fluoroptic probe linked to a Umi 4 signal conditioner were introduced (figure 2.9). Dry nitrogen was passed through the sealed flask and the liquid was stirred. The dielectric spectrum was measured at intervals using the method described in section 2.3 as the liquid was cooled in a controlled manner from 130°C to room temperature. The scattering parameter spectrum for the probe in air

was measured before introduction to the liquid and, as the arrangement of the coaxial line did not change, was used in the determination of the dielectric spectra at all temperatures.

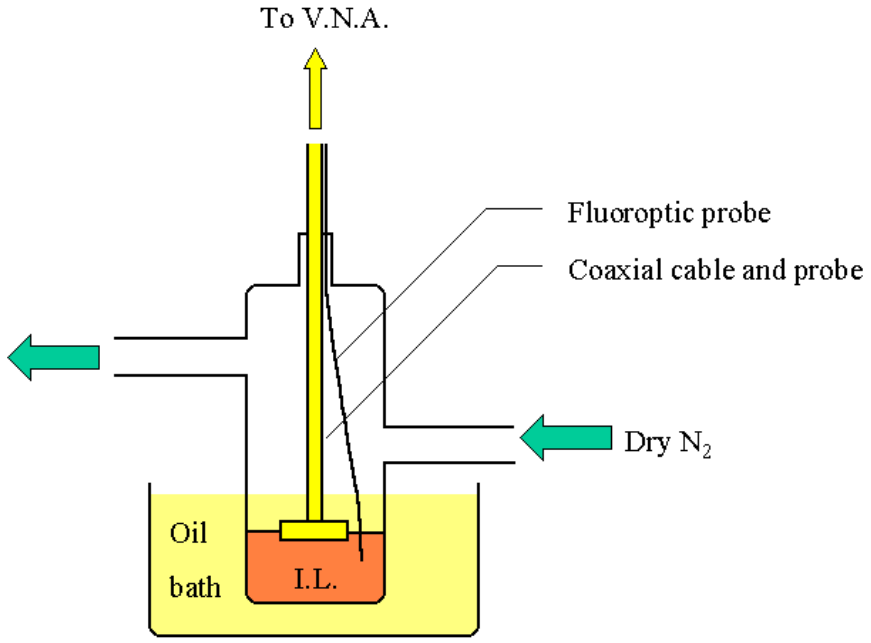

Figure 2.9: Set-up for the measurement of the temperature-dependent dielectric properties of a room temperature ionic liquid (I.L.).

2.5.2.2 Measurement of the dielectric spectrum of [BMIM] Cl as a function of water content

Approximately 2.5 g of [BMIM] Cl were accurately weighed into a small beaker with a magnetic stirrer bar and dried overnight under vacuum at 60°C. The liquid was cooled to room temperature in a dessicator before its dielectric spectrum was measured according to the method described in section 2.3. The dielectric spectrum was subsequently measured as the ionic liquid was progressively diluted with deionised water. A final measurement on pure water was obtained to give the dielectric spectrum at a range of water contents from 0 to 100 %.

2.5.3 Results and discussion

2.5.3.1 The dielectric spectrum of [BMIM] Cl as a function of temperature

The purpose of these measurements was to determine why ionic liquids heat so efficiently. For example, when the ionic liquid probed here was placed in a tube in a CEM Discover microwave reactor and the set temperature and maximum power level set to 90°C and 50 W respectively the temperature was found to overshoot to 180°C after just 25 s of heating. In contrast, for the same settings, water will heat to 90°C with no overshoot over a period of 70 s.

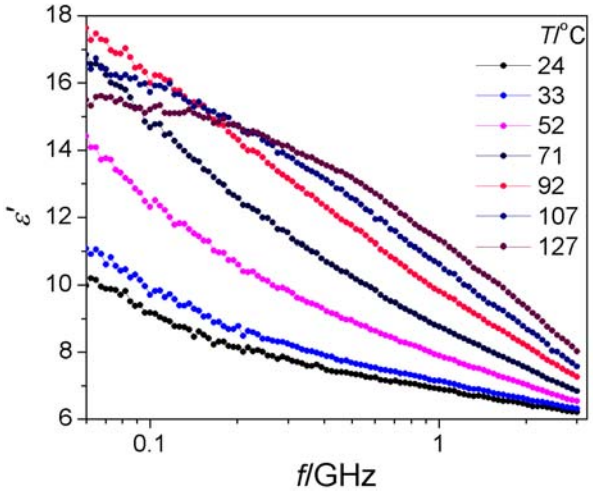

Figure 2.10: The real dielectric constant of [BMIM] Cl as a function of frequency and temperature. For clarity not all measured spectra are shown.

The real part of the dielectric constant of [BMIM] Cl is seen to increase with temperature (figure 2.10) across the frequency spectrum. However, this is not important to the issue. Rather it is the change in the imaginary constant with temperature (figure 2.11) that impacts most on the temperature dependence of the loss tangent and therefore the efficiency of heating.

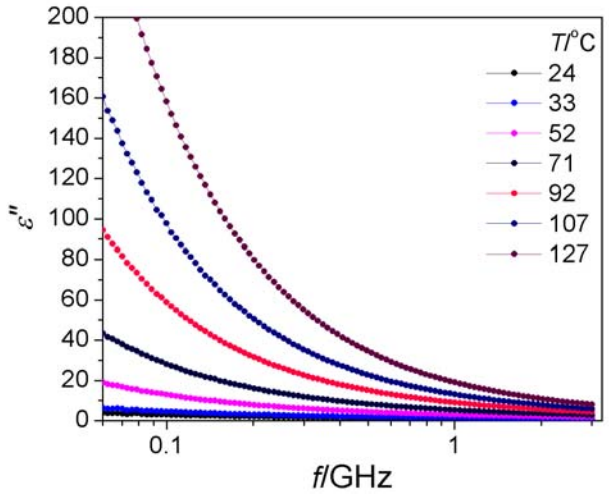

Figure 2.11: The imaginary dielectric constant of [BMIM] Cl as a function of frequency and temperature. For clarity not all measured spectra are shown.

The imaginary dielectric spectrum shows the inverse relation to frequency expected for conductive material. However, it has appreciable magnitude even at higher frequencies and this increases further as the temperature increases. Therefore this material is expected to heat effectively by a conductive mechanism. The loss tangent determined from the real and imaginary parts (equation 1.3) has the same behaviour (figure 2.12). The loss tangent at 2.45 GHz (figure 2.13) exhibits an exponential increase as a function of temperature. For a given power dissipation, $tan\ \delta$ controls the rate of heating. Therefore the change in the dielectric properties with temperature explains the thermal runaway observed when heating the material.

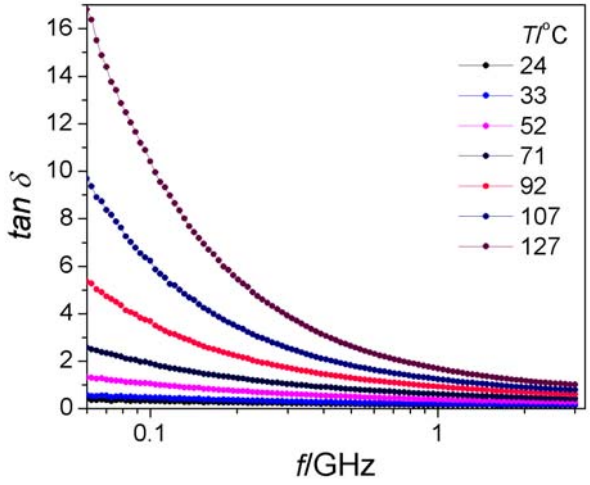

Figure 2.12: The loss tangent of [BMIM] Cl as a function of frequency and temperature. For clarity not all measured spectra are shown.

For dipolar liquids, such as water and alcohols *tan δ* and therefore heating efficiency has a peak at the temperature where the relaxation time, τ, is equal to the reciprocal of the angular frequency of the applied microwaves (see 1.2.1). Heating above this temperature will result in the relaxation time decreasing and *tan δ* and heating efficiency decreasing (for dielectric data as a function of temperature for such liquids see[43]). Therefore thermal runaway is not possible. In any case, heating of the liquid will always reach a limit at the boiling point. However, as the dielectric properties of the ionic liquid are governed by conductive heating, there is no peak temperature and heating efficiency will continue to increase as the liquid is heated leading to thermal runaway. In addition, the boiling point is relatively high and thermal decomposition will occur before this point is reached.

The increase in ε'' as a function of temperature is at least partly due to the decrease in viscosity that results from heating the ionic liquid.[44] Dielectric heating is dependent on the viscosity of the system (equation 1.2). Likewise, a decrease in viscosity will increase the conductivity of the liquid and therefore increase losses due to conduction. As the viscosity of ionic liquids is also known to decreased with addition of a co-solvent, the dielectric properties of [BMIM] Cl as a function of water content discussed in the following section should also exhibit similar behaviour.

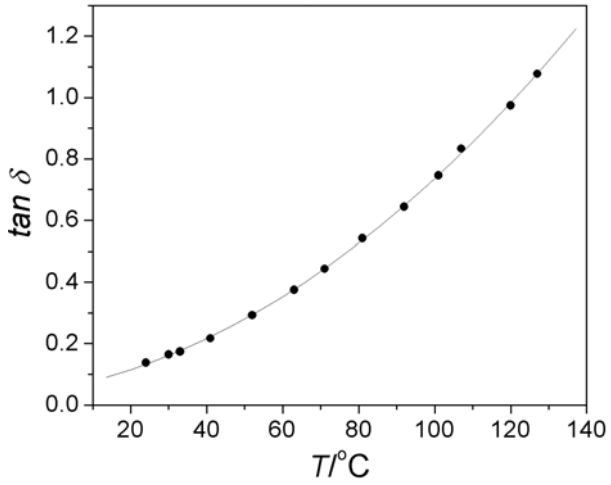

Figure 2.13: The loss tangent of [BMIM] Cl at 2.45 GHz as a function of temperature. The solid line is a fit to an exponential model.

2.5.3.2 The dielectric spectrum of [BMIM] Cl as a function of water content

The change in the real component of the dielectric spectra for ionic liquid/water mixtures from 1:0 (0% water) to 0:1 (100% water) are shown in figure 2.14. They appear to be very similar to that which would be expected from combining the spectra for the two components in the relevant proportions. However, the imaginary component changes in a non-uniform manner with water content (figure 2.15) and is not simply a sum or average of that of the pure components.

At any given frequency, ε'' is at a maximum when the water content is approximately 70% w/w. Consequently, the loss tangent exhibits similar behaviour (figure 2.16). At 2.45 GHz *tan* δ (figure 2.17) increases steeply to a peak at approximately 40% w/w water before falling away again at a lesser gradient. At the peak, the loss tangent is approximately four times greater than it is for the neat ionic liquid. Therefore the incorporation of a co-solvent increases the susceptibility of the ionic liquid significantly and over and above the effect of the combination of the dielectric properties of the two components, presumably because of the effect of lowering the viscosity of the liquid.

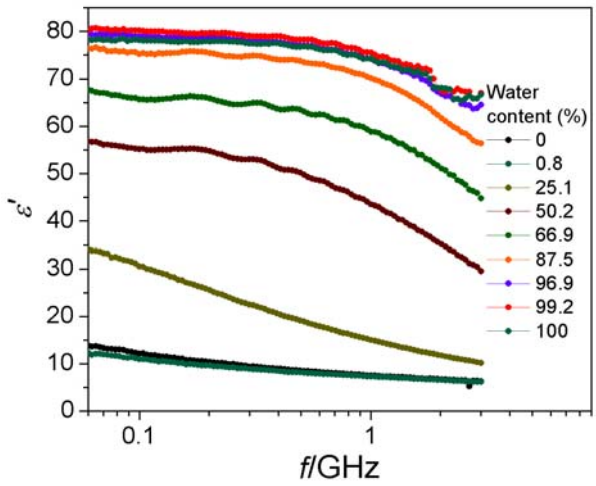

Figure 2.14: The real dielectric constant of [BMIM] Cl as a function of frequency and water content (% w/w) at 20°C. For clarity not all measured spectra are shown.

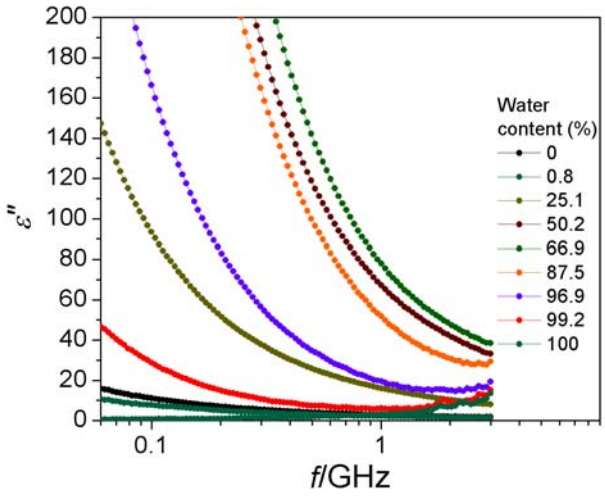

Figure 2.15: The imaginary dielectric constant of [BMIM] Cl as a function of frequency and water content (% w/w) at 20°C. For clarity not all measured spectra are shown.

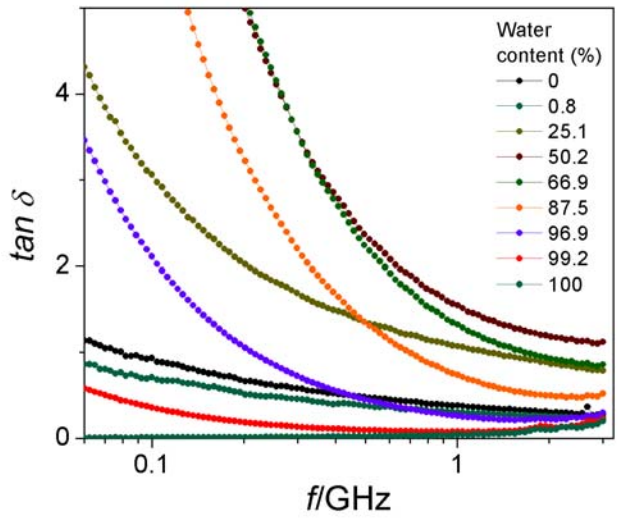

Figure 2.16: The loss tangent of [BMIM] Cl as a function of frequency and water content (% w/w) at 20°C. For clarity not all measured spectra are shown.

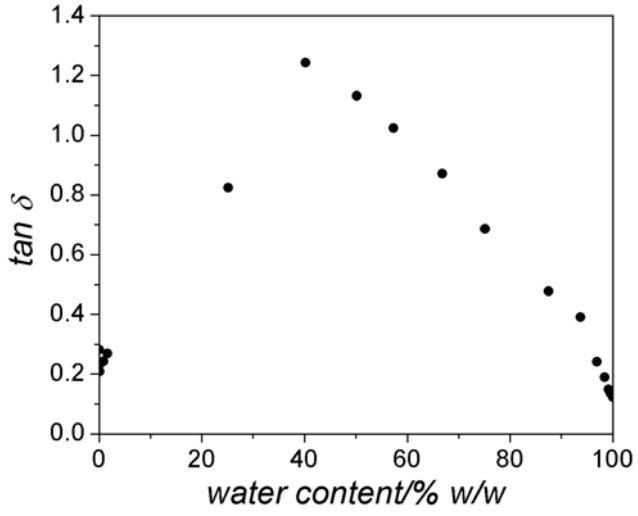

Figure 2.17: The loss tangent of [BMIM] Cl at 2.45b GHz as a function of water content (% w/w) at 20°C.

2.5.4 Conclusions

The first measurements of the dielectric properties of a room temperature ionic liquid as a function of temperature have been obtained. The exponential increase in the loss tangent of the

material as temperature is increased explains the exceptionally efficient microwave heating when compared to dipolar liquids such as water and alcohols for which the loss tangent reaches a peak but subsequently falls away. Thus the thermal runaway observed when heating ionic liquids with microwaves can be explained by the dielectric properties of the substance. The increase in the loss tangent is thought to be due to the decrease in viscosity at higher temperatures.

The effect of adding water to an ionic liquid was determined. Many ionic liquids are hygroscopic and are therefore likely to be wet when used in microwave-assisted syntheses. Additional water was not found to be necessarily detrimental to the microwave heating efficiency of the ionic liquid. In fact up to approximately 40% w/w water it was found to cause significant increase in the loss tangent. This was also thought to be due reduction in the viscosity of the liquid as water is added.

2.6 Determination of the dielectric properties of a microwave-heated industrial process as a function of temperature

2.6.1 Introduction

This section describes the method and findings of a project carried out to probe a microwave-heated industrial process that had been unsuccessfully scaled-up from a laboratory process. The particular stage in the process involves the regeneration of anthroquinone derivatives by passing them in solution over Al_2O_3 in a column. The liquid fraction - the working solution (WS) – also contains aromatic hydrocarbons such as benzene, xylene and 1,2,4-trimethylbenzene, as well as tetrabutylurea and tris(2-ethylhexyl)phosphate. Laboratory tests performed on a relatively small scale using 2.45 GHz microwave irradiation resulted in a much greater rate of regeneration than was possible than for the conventionally heated process. The process was therefore scaled-up to a pilot plant.

At the laboratory scale 2.45 GHz microwaves produced by a 1950 W generator were incident upon a column with a 39 mm ID and a length of 6 cm. The column contained just 74 g of the alumina catalyst. The WS was passed just once through the column at a rate of about 1 L hr^{-1}. The temperature of the WS was found to rise from 25 to 140ºC between the inlet and the outlet

of the column, and reflected power measurements indicated that of the 170 W incident on the sample and column, about 160 W was absorbed.

At the pilot plant scale 915 MHz radiation provided by a more powerful source (maximum 75 kW), was applied to a larger sample: the alumina was held in a column of 20 cm ID and length 1 m, and the WS flow was from 60 to 250 L hr^{-1}. This time just 2-3 kW of power were absorbed and the temperature was typically found to rise from 45 to 140 ºC. The rate of regeneration was found to drop by a factor of about 10 relative to the laboratory test system.

In order to determine why the change from the laboratory set-up to the pilot plant lead to such a change in the efficiency of the process the dielectric spectra of the key components of the reactive system were determined as a function of temperature. This document describes how the measurements were planned and executed and what the findings were before drawing conclusions about possible relations with the change in efficiency of microwave-induced reactivity between the two sets of apparatus.

2.6.2 Experimental

The dielectric properties ε' and ε'' of the working solution and the slurry of the working solution and alumina powder (167g and 50g, respectively mixed by magnetic stirring until all the powder was thoroughly wetted-out, ca. 10 min) were determined at different temperatures. Samples were placed in a round bottom flask under nitrogen with a condenser fitted to avoid loss of any component of the mixture due to evaporation. The flask was heated by an oil-bath and stirred magnetically to minimise physical and thermal inhomogeneity. The calibrated coaxial probe was immersed in the liquid throughout the heating process along with a mercury thermometer to allow temperature measurement (figure 2.18). Dielectric spectra were recorded at temperatures between 20 and 130°C using the method described in section 2.3.

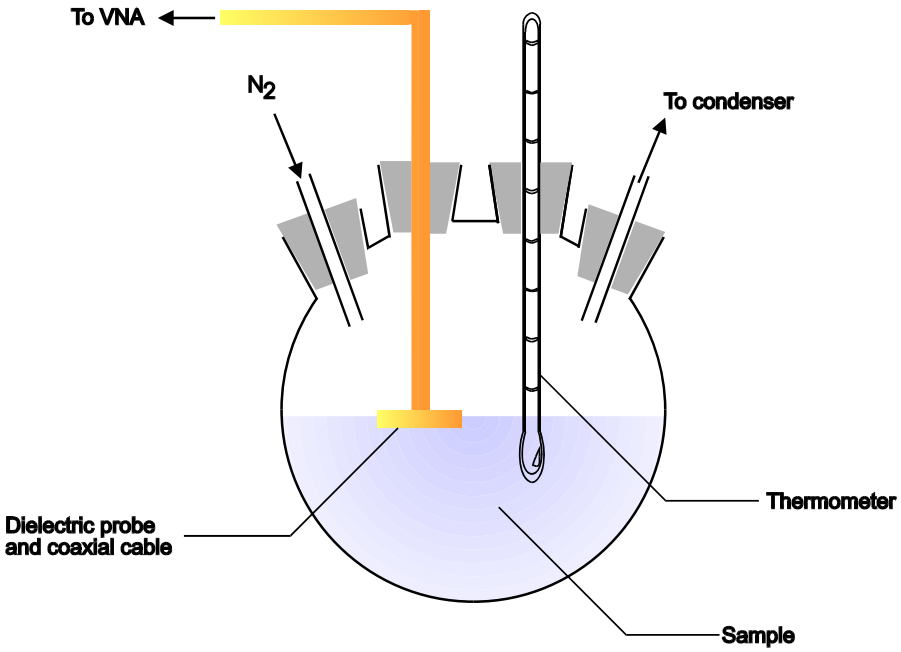

Figure 2.18: Sample vessel and coaxial probe set-up for simulataneous measurement of ε' and ε'' during heating (oil bath) of working solution and slurry samples.

2.6.3 Results and discussion

The values of ε' and ε'' measured as a function of temperature, T, and frequency, f, were used to calculate various secondary properties of the samples including the loss tangent, $tan\ \delta$, and the power dissipation per unit volume, P/V, using the expression,

$$P/V = 2\pi f \varepsilon_0 \varepsilon'' E^2 , \qquad \textbf{2.25}$$

where ε_0 is the dielectric constant of free space (= 8.8 x 10^{-12} F/m) and E is commonly taken to be the root mean squared electric field (the conditions placed on some of these variables are described elsewhere[24]); here we set E arbitrarily as 1 because we were primarily interested in the *change* of P/V with T and f, The penetration depth, D_p, may also be pertinent in defining the effectiveness of microwave radiation in heating the reactive system, and can be expressed as the attenuation of power, P, at a given depth z, which is

$$P \propto e^{-2\alpha z} , \qquad \textbf{2.26}$$

where α is the attenuation factor. D_p is defined as the depth at which the power drops to 1/*e* of its value at the surface (= 1/(2α)). For relatively low-loss materials (($\varepsilon''/\varepsilon'$) << 1) this may be expressed as

$$D_p = \frac{c(\varepsilon')^{1/2}}{2\pi f \varepsilon''}, \qquad \textbf{2.27}$$

where *c* is the velocity of light.

Values of ε', ε'', $tan\delta$ and D_p are given in figures 2.19(a)-(j), together with relative values of *P*/*V*, all as a function of *T* and *f* for WS and the WS-alumina slurry.

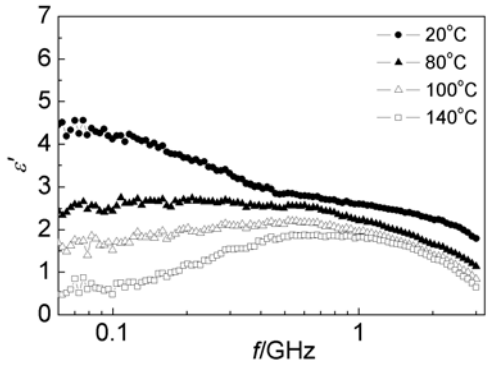
20°C
80°C
100°C
140°C
ε′
f/GHz

(a)

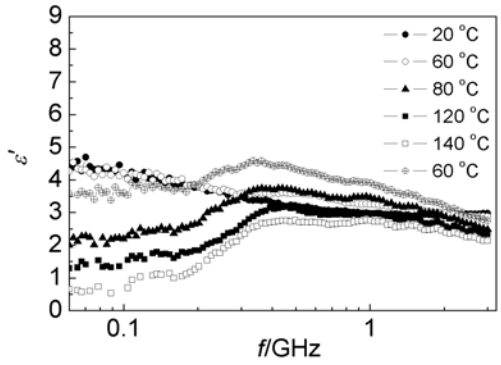
20 °C
60 °C
80 °C
120 °C
140 °C
60 °C
ε′
f/GHz

(f)

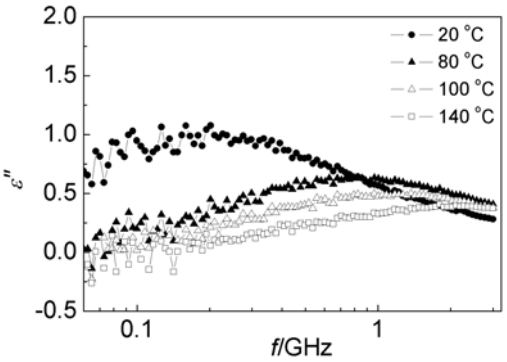
20 °C
80 °C
100 °C
140 °C
ε″
f/GHz

(b)

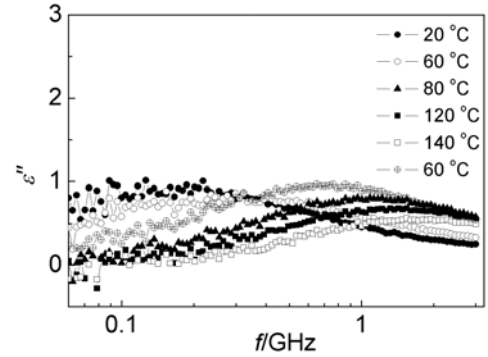
20 °C
60 °C
80 °C
120 °C
140 °C
60 °C
ε″
f/GHz

(g)

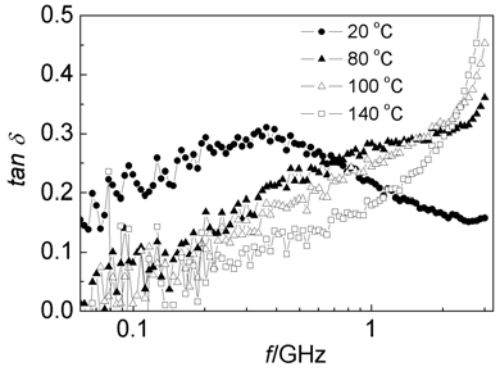
20 °C
80 °C
100 °C
140 °C
tan δ
f/GHz

(c)

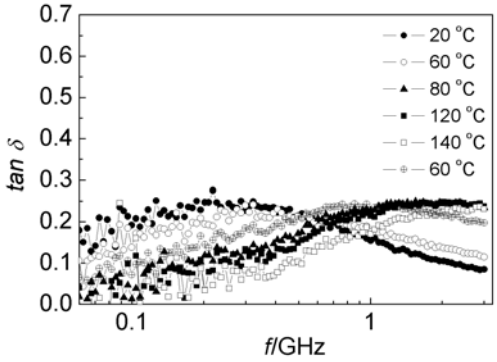
20 °C
60 °C
80 °C
120 °C
140 °C
60 °C
tan δ
f/GHz

(h)

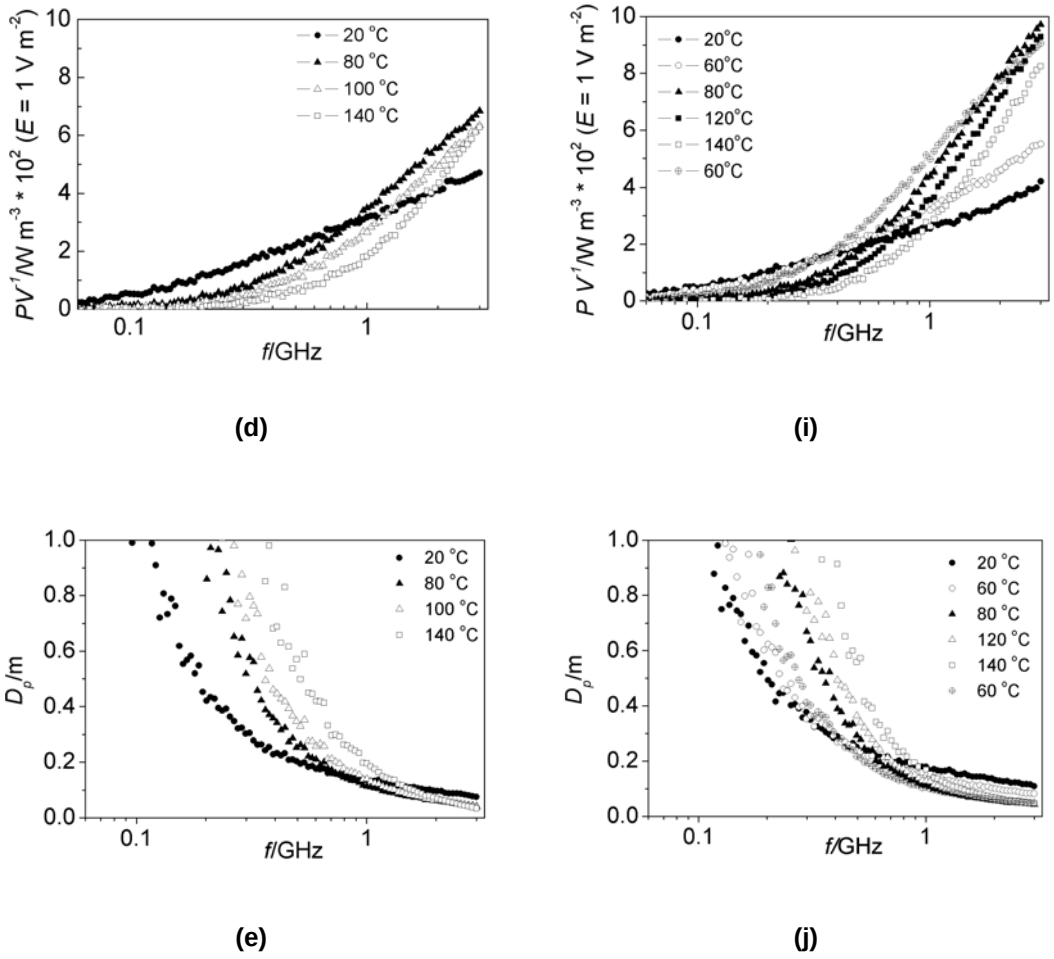

Figures 2.19 (a)-(j): Dependence of ε', ε'', $tan\delta$ and D_p, as well as relative values of P/V with temperatures and frequency for (left, a-e) the working solution (WS) and (right, f-j) a slurry made of WS with alumina.

Table 2.2 gives values for ε', ε'', $tan\delta$ and D_p, and relative values of P/V for frequencies close to 915 and 2450 MHz and at selected temperatures for the WS; table 2.3 provides the same information for the WS-alumina slurry. Precise values given for f arise from the manner in which frequency was swept.

Table 2.2: Dependence of various dielectric parameters for the WS at selected temperatures and frequencies closest to those of the laboratory test system and the pilot plant.

Temperature/ºC, f = 892 MHz	ε'	ε''	tanδ	D_p / m	$P\ V^{-1}$ (E=1)/ W m^{-3}
20	2.66	0.60	0.22	0.15	2.97
80	2.32	0.61	0.26	0.13	3.02
140	1.85	0.30	0.l6	0.24	1.49
f = 2467 MHz					
20	2.09	0.32	0.15	0.087	4.40
80	1.45	0.45	0.31	0.051	6.21
140	1.05	0.39	0.37	0.051	5.31

Table 2.3: Dependence of various dielectric parameters for the WS-slurry system at selected temperatures and frequencies closest to those of the laboratory test system and the pilot plant.

Temperature/ºC, f = 892 MHz	ε'	ε''	tanδ	D_p / m	$P\ V^{-1}$ (E=1)/ W m^{-3}
20	3.09	0.50	0.17	0.19	2.49
80	3.27	0.77	0.22	0.13	3.83
140	2.74	0.45	0.17	0.20	2.25
f = 2467 MHz					
20	2.95	0.27	0.09	0.12	3.72
80	2.67	0.63	0.24	0.05	8.69
140	2.25	0.51	0.23	0.06	7.05

It should be noted that it proved difficult to obtain a consistent response in terms of $\varepsilon'$and ε'' from the slurry. Its properties appeared to depend on the degree of stirring and the period of time

that elapsed between stirring and the measurement period. However, general trends can still be discerned.

Although, due to the complexity of the composition of the system, the dielectric spectra do not follow a simple dipolar relaxation model there does appear to be a maximum in ε'' with respect to frequency. This maximum moved to higher values of f as temperature increased. This is consistent with a decrease in viscosity with increasing temperature that would be expected to shorten the relaxation time, τ. Consequently the maximum in $tan\delta$ moved to higher frequencies as temperature increased. The absorbed power per unit volume rose with frequency for all samples at all temperatures and the change in P/V as the frequency is altered appears to be significantly greater for the slurry compared to the WS (see the last column of the two Tables).

All of the above trends indicate that the laboratory test system, with f = 2450 MHz, was much more likely to be heated than the pilot system, with f = 915 MHz. The underlying physical reason for this probably lies in the characteristic dielectric relaxation period of the system which, at higher temperatures, is somewhat faster than 915 MHz, becoming yet faster as temperature increases.

2.6.4 Conclusions

This study has demonstrated the efficacy of the dielectric measurement method described in section 2.3 and its applicability to the probing of complex chemical systems as a function of temperature. More generally, it has also demonstrated the importance of a thorough understanding of the dielectric properties of a system in the scale-up of microwave-heated processes.

The motivation behind the change of frequency upon scale-up was to increase the wavelength of the radiation and thus increase penetration of the microwaves in line with the increase in vessel dimensions. In this respect the change was successful. However, the impact upon other important aspects of the microwave-heating potential of the system were not considered and consequently the heating of the scaled-up process was less effective.

There are two options for remedying the situation. Firstly, the pilot plant process could be adapted to operate at 2.45 GHz. This would be expensive, not least because good electric field

distribution at larger scale and high microwave frequencies is challenging. However, it has the advantage that the efficiency of heating at this frequency has been proven. The other option would be to alter the dielectric properties of the system such that it heats with the same efficiency at the lower frequency. This option is potentially simpler and cheaper but addition of further components to change the properties would have to be done with care to ensure that it does not effect the chemistry of the process.

2.7 Overall conclusions and outlook

A relatively simple method for the determination of the dielectric properties of materials has been verified and demonstrated for systems relevant to microwave-assisted chemical synthesis. The method was used to obtain the first dielectric data for a room temperature ionic liquid as a function of temperature. The exponential increase in the loss tangent at a given frequency explains the extremely rapid heating and thermal runaway that are observed when such liquids are irradiated with microwaves. It was also found that the addition of water to the ionic liquid increased its microwave-heating potential at room temperature significantly. This is useful knowledge as many ionic liquids are very hygroscopic. It is thought that heating and the addition of water both cause an increase in the microwave susceptibility by lowering the viscosity of the liquid.

The method was also demonstrated in the probing of a microwave-heated process. The decrease in efficiency of the process on scaling-up to a pilot plant could be explained by the decrease in the measured microwave susceptibility of the heated system relative to that at the higher microwave frequency used in the small scale process. The study demonstrates the importance of a complete understanding of the factors that govern the ability of a system to be heated by microwaves, of which the temperature-dependent dielectric properties are a critical part.

There is still relatively little published dielectric data available for solvents commonly used in microwave-assisted chemistry. As the above example shows, without this knowledge the application of microwaves in industrial-scale chemical synthesis is unlikely to be successful. With more literature data and simple and inexpensive methods for obtaining data for individual systems, the scale-up of flow-through processes would become a relatively trivial matter for chemical engineers[45] and microwave heating apparatus could become a more common sight on industrial plants.

3 Measurement of temperature during microwave-assisted solid-phase organic synthesis

3.1 Introduction

Solid-phase techniques are becoming increasingly important in organic synthesis, particularly in the field of drug discovery. Despite the many advantages associated with the methodology, reactions on solid supports are often slow. Using microwaves to heat these reactions goes a long way towards solving this problem. However, little work has been carried out to determine exactly why this is the case. In order that the process of microwave assisted solid-phase organic synthesis (MA-SPOS) might be better understood, a novel *in situ* fluorescence technique for temperature measurement is herein demonstrated. The technique relies on a fluorophore with temperature dependent lifetime covalently attached to the solid support.

This chapter will begin with an introduction to the important principles of solid-phase synthesis and an overview of fluorescence spectroscopy, specifically techniques for the measurement of fluorescence lifetime. This will be followed by a report of component-specific and spatially-resolved measurement of temperature during microwave heating of SPOS resin suspensions. Finally there will be a discussion of further applications of the technique and some of the other problems in MA-SPOS.

3.1.1 Solid-Phase Organic Synthesis[46-48]

Based on the pioneering work of Bruce Merrifield,[49] SPOS became ubiquitous within the field of combinatorial synthesis in the 1980s and '90s. More recently solution-phase chemistry has benefited from the use of solid-supported reagents, catalysts and scavengers.

SPOS was originally developed for the synthesis of peptides and other oligomers. The multi-step synthesis by which peptides are prepared dictates that high yield and selectivity are required at each successive amino acid coupling stage if the final product is to be made in useful quantities. Merrifield realised that by covalently attaching the first amino acid to an insoluble solid support, the work-up after each subsequent amino acid coupling becomes a simple matter of filtering and washing, allowing large excesses of reagents to be employed to drive each reaction to

completion. In the final step the product is cleaved from the support and isolated in high purity (figure 3.1). The technique is applicable to any synthesis in which an initial reagent (with a suitable anchoring functionality, e.g. –OH or -NH_2) is to be transformed over multiple steps. SPOS therefore finds utility in many areas of organic chemistry but is particularly suited to combinatorial synthesis where the ability to automate the procedure is a great advantage.

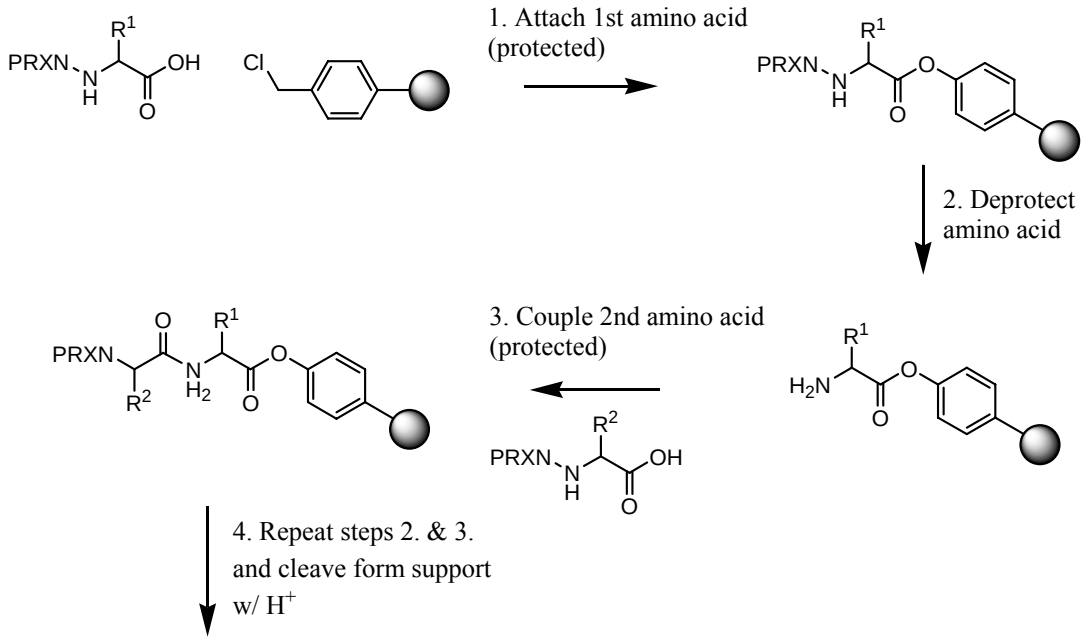

Figure 3.1: The Merrifield methodology of peptide synthesis on a functionalised cross-linked polystyrene solid support (represented here by a sphere).

Combinatorial synthetic strategies[47] were developed to satisfy the pharmaceutical industry's desire to prepare and test large numbers of potential lead compounds rapidly and efficiently. SPOS allows different building blocks to be combined in high yield and thus large libraries of related compounds can be produced by utilising techniques such as 'split and mix' synthesis. The solid support is divided into *n* fractions. Different monomers (e.g. amino acids) are coupled to each aliquot of support in separate reactions. The fractions are then pooled and the process repeated to add a second monomer. By repeating through *x* cycles it is possible to produce n^x different oligomers (e.g. peptides).

In transferring reactions from solution-phase to solid-phase it is often necessary to work through a lengthy process to find optimal conditions for the reaction on the new media. The kinetics can become limited by the rate at which reagents can diffuse through the solid support, which effectively acts as a very viscous solvent. This can mean long reaction times, with increased likelihood of degradation of the polymeric support. The extent to which temperature and pressure can be increased to overcome the slow kinetics is limited by the properties of the support, and the nature of the anchoring bond will normally preclude the use of strong acid or base. In addition to these problems, reaction monitoring is made difficult by the presence of the support. Specialised spectroscopic techniques can be used (e.g. magic angle spinning NMR) but more commonly quantities of the beads are sampled from the reaction and the reacting species cleaved from the support and analysed by conventional methods.

Recent developments in solid-supported chemistry have allowed chemists to side-step many of these problems, combining the best aspects of both solution- and solid-phase. So-called *scavenger resins* can be used in conventional solution-phase reaction to extract excess reagents from the product, simplifying the work-up greatly. Commercially available polymer beads have been designed with functionalities tailored to specifically scavenge virtually any type of organic reagent. Reagents and catalysts are used on solid support in reactions where traditionally they would be difficult to separate from the final product.[48] Expensive or toxic catalysts can be almost completely recovered from the reaction by tethering or 'tagging' them to easily isolable supports, fulfilling the demands of industry to drive towards cleaner and cheaper technology.

3.1.2 The Nature of the Support[50,51]

Up to this point the support has been introduced merely as a quantity of insoluble material that is easily isolable from suspension and to which various chemical species may be anchored. The material may be silicon wafers, glass beads or sheets of paper but by far the most commonly used support is polymer resin in the form of roughly spherical beads. These resins are often depicted in the literature as hard spheres with the reactive species appended to the surface, apparently floating in the surrounding solvent, but this is a misleading image. The reality is that the reactive sites are predominantly *within* the resin sphere, which acts as the medium of the reaction. It has been argued that to neglect the influence of the resin on the reaction is comparable to neglecting the effect of the solvent in liquid-phase chemistry.[52]

The polymeric support used by Merrifield in his original peptide synthesis was polystyrene cross-linked with divinyl benzene (DVB-PS) and chloromethylated to give pendant reactive groups as anchoring points (figures 3.2 & 3.3). Merrifield's resin, as it is known, is still the most commonly used support due to its availability and low cost. The cross-linked polymer beads are normally prepared by suspension polymerisation.[53] Styrene, divinyl benzene (normally 0.5-2%) and a radical initiator are agitated in an immiscible aqueous solution of surfactants to form spherical liquid droplets. The suspension is then heated to activate the polymerisation, yielding solid 'glassy' beads that can be filtered off and washed.

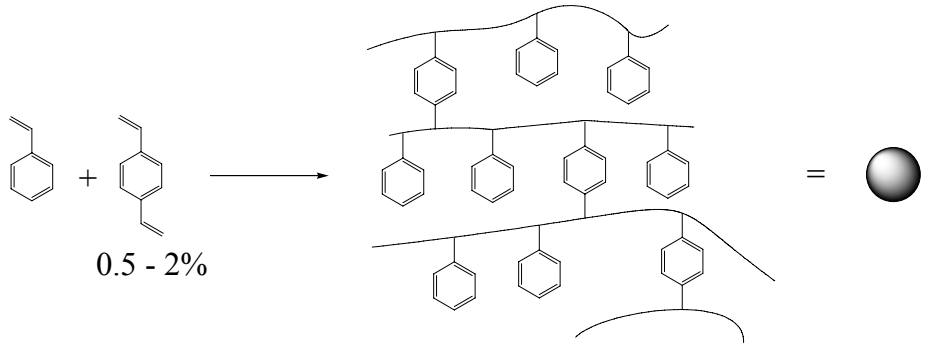

Figure 3.2: Polymerisation of styrene and divinyl benzene to form DVB-PS.

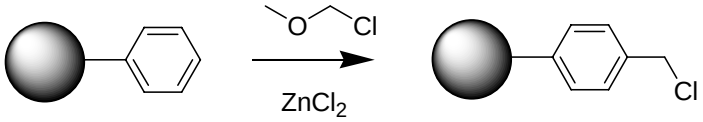

Figure 3.3: Functionalisation of DVB-PS to form Merrifield's resin.

The polymer produced is an amorphous network of interpenetrating polymer chains held together by cross-linking. In the dry state the polymer chains are in contact with one another and the surface area of the resin is low. If, however, molecules of an organic solvent can solvate the chains the polymer can expand or 'swell'. The swelling process is effectively the onset of dissolution of the polymer whereby the chains become fully separated and form a uniform solution. This can never fully occur due to the cross-linking.

The degree to which a particular solvent can induce this effect is governed by the attractive strength between the molecules of the solvent and the polymer. This can be inferred from the

similarity of the solubility parameters, δ (not to be confused with phase lag or skin depth, also given the symbol δ - see chapter 1), of the two substances. A solvent that can expand the network is said to be a 'good' solvent. A very good solvent will expand the network to its elastic limit. The extent to which a resin will swell in a given solvent is reported as the increase in volume per unit mass. A good solvent for a resin will have a swelling value of 4 cm^3 g^{-1} or more; 2 cm^3 g^{-1} or less is considered poor. Swelling of the resin is crucial to solid-phase reactions as it allows reagents to diffuse into the system in order to access reactive sites with enough mobility to react (figure 3.4).

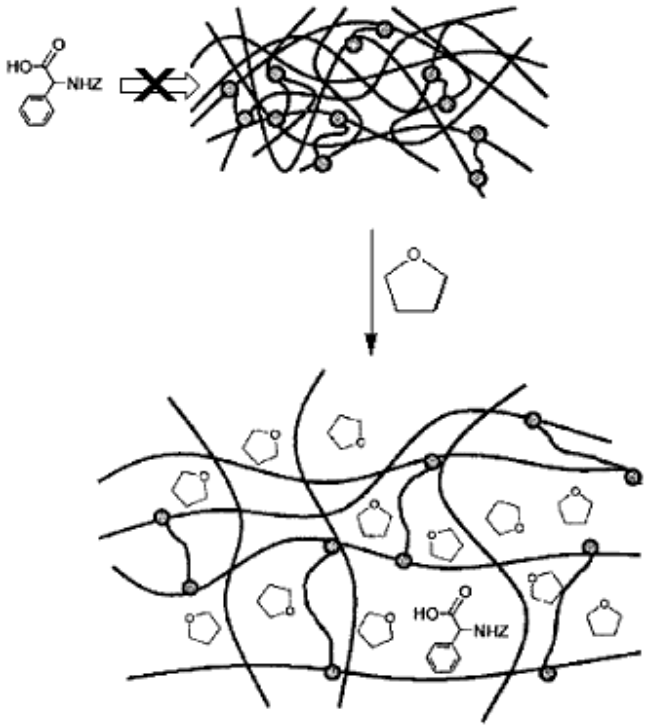

Figure 3.4: Schematic to show the effect on reagent diffusion of swelling a resin with solvent (e.g. tetrahydrofuran).

DVB-PS resins (δ ~ 17-18) have good swelling properties in organic solvents, particularly aromatic hydrocarbons such as toluene (δ = 18.2, Δv ~ 4 cm^3 g^{-1}). DVB-PS is less well suited to more polar solvents such as ethanol (δ = 26.0, Δv ~ 2 cm^3 g^{-1}) and water (δ = 47.9, Δv ~ 1.5 cm^3 g^{-1}). The properties of PS Resins have therefore been modified by using different cross-linkers or by grafting other polymers to the surface of the beads, allowing chemists to carry out SPOS in a

range of solvents.[54,51] The properties of a number of common resins are summarised in table A, appendix III.

3.1.3 Microwave-Assisted Solid-Phase Organic Synthesis (MA-SPOS)[55,56]

Given that one of the principal advantages of microwave assisted chemistry is its speed, it is not surprising that chemists have sought to apply it to SPOS – a procedure whose principal *dis*advantage is sluggish reaction. Where SPOS is used in combinatorial methods for drug discovery programmes the drive to decrease reaction times is especially great, as library production is often a bottleneck in the process.

Prior to discussing the effects of transferring SPOS reactions to microwave-assisted set-ups it should be noted that the choice of solvent is a more complex issue in MA-SPOS. One must consider not only the swelling properties of the solvent, but also the ability of the solvent to be heated by microwaves. In addition to this, an ideal solvent for MA-SPOS should have a high boiling point and be chemically stable at high temperatures. Table 3.1 provides a summary of common MA-SPOS solvents. In general, solvents with loss tangent, *tan* δ, > 0.1 are considered useful for microwave heating. Dimethylformamide (DMF) is one of the most commonly used solvents as it has excellent swelling properties and high loss tangent and boiling point.

Table 3.1: Swelling property, loss tangent and boiling point for common MA-SPOS solvents.[56]

Solvent	DVB-PS swelling / $cm^3\ g^{-1}$	tan δ	bp/°C
Dimethylformamide	5.2	0.161	153
Dimethylsulfoxide	4.2	0.825	189
Tetrahydrofuran	6.0	0.047	65
1,2-Dichloroethane	4.4	0.127	83
Chlorobenzene	-	0.101	132
Nitrobenzene	4.3	0.589	211
Methanol	1.6	0.659	65
Water	1.6	0.123	100

A great deal of literature has been produced, particularly over the last five years, on the subject of MA-SPOS and microwave-assisted combinatorial synthesis.[57,55,56] The majority of the work reports known SPOS reactions that are typically slow to react by conventional heating, producing greater yields and in substantially less time when transferred to the microwave oven. One of the first examples of MA-SPOS was the peptide synthesis by Yu *et al* using an ordinary domestic microwave oven (figure 3.5).[58] It was demonstrated that amino acid coupling could be carried out efficiently in 6 min by microwave heating compared with 30 min at 60 ºC by conventional heating.

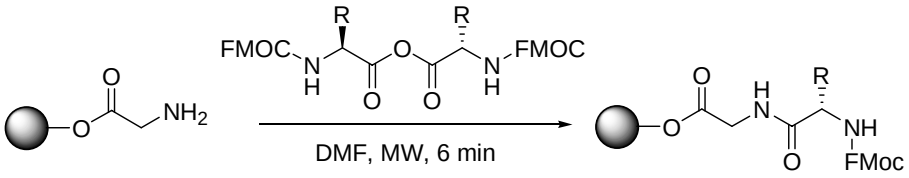

Figure 3.5: Peptide coupling using 9-fluorenylmethyl chloroformate (Fmoc)-protected amino acid anhydride.

There have been many other reports of a wide range of SPOS reactions that have been sped up, made more efficient, or both when heated by microwaves. Yet, in all but a very few of these, there was no monitoring of reaction temperature or pressure during microwave irradiation, making it difficult to infer anything about the possible reasons for the improvement in reaction.

Kappe has used specialised equipment to carry out MA-SPOS with control of power and direct monitoring of temperature from a fluoroptic probe immersed in the solvent, allowing kinetic analysis to be carried out on a variety of reactions (carbodiimide-mediated esterification,[59] acetoacylation and Knoevenagel condensation[60]) on solid support. These analyses have shown that increases in the rate of these reactions, and most probably other reported MA-SPOS reactions, can be attributed to the more rapid (flash) heating and super-heating of solvents that can be achieved using microwaves. It is therefore not necessary to appeal to the notion of a specific microwave effect. Kappe's group has provided further evidence for this in their study of the coupling of a variety of carboxylic acids to chloromethylated resin (figure 3.6). It was found that by stirring to suppress superheating the microwave heated system reacted at the same rate as the conventionally heated system at the same temperature.[61] However, it was found that initially

the microwave heated system proceeded slightly faster (59 versus 37% loading after 15 min). Kappe speculated that this could be due to "additional contributions" from specific coupling to ionic reagents or intramolecular rotation of polar functional groups on the resin.

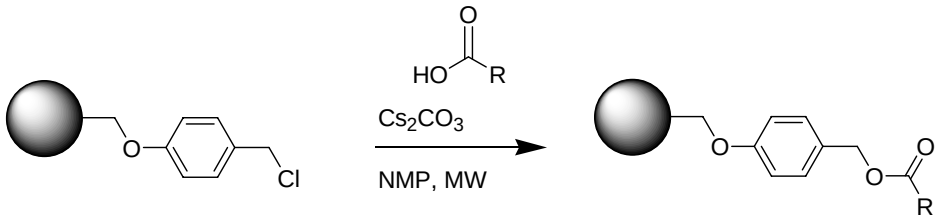

Figure 3.6: Microwave assisted coupling of carboxylic acids to chloromethylated resin.

3.1.4 "In-Resin" Thermometry

In chapter 1 the problems of thermal inhomogeneity and the practical issues of thermometry in microwave heated systems were discussed. It could be expected that in MA-SPOS systems, in addition to the inhomogeneity expected for a liquid, there could be further inhomogeneity in the temperature profile due to the two-phase nature of the reaction mixture. Whether the system is perceived in the traditional sense as 'hard' polymer spheres in solvent or, more correctly, as a viscous solvent-resin mixture, there will almost certainly be differences in the dielectric properties of the components: in the first case because polymers would be expected to be poorer microwave susceptors than many solvents; in the second case because the solvent, as part of the swollen resin, experiences greater viscosity, affecting its dipolar relaxation (equation 1.2, chapter 1). Therefore, the components would be heated to different extents by microwaves and could be at different temperatures. One would expect the system to equilibrate over time; however, since many MA-SPOS reactions are carried out on relatively short time scales the effects could be significant.

Kappe compared the kinetics of a reaction with conventional and microwave heating at the same temperature. However, since the reaction temperature was measured by a fluoroptic probe immersed in the solvent, the measured temperature was actually that of the liquid phase. It is possible that the temperature in the resin could be different in the case of the microwave heated system and this could account for the initial differences in the reaction rates. For a better

comparison it would be necessary to have a thermometer actually in the resin. It is proposed that this could be achieved using fluorescent-labelled resins.

A substantial amount of literature exists on the use of fluorophores for *in situ* thermometry.[62-67] Most of the techniques rely on the temperature dependence of the intensity of peaks in the fluorescent spectrum of the fluorophore but another measurable characteristic of fluorescence that could be used perhaps more accurately as the temperature probe is the fluorescence lifetime.

3.2 Techniques: Fluorescence Spectroscopy

3.2.1 Luminescence, fluorescence and phosphorescence [68]

Fluorescence, like phosphorescence, is a form of luminescence: a process whereby light is emitted as a result of the relaxation of electronically excited states of molecules. The different processes giving rise to luminescent phenomena are most easily explained with reference to a Jablonski diagram (figure 3.7).

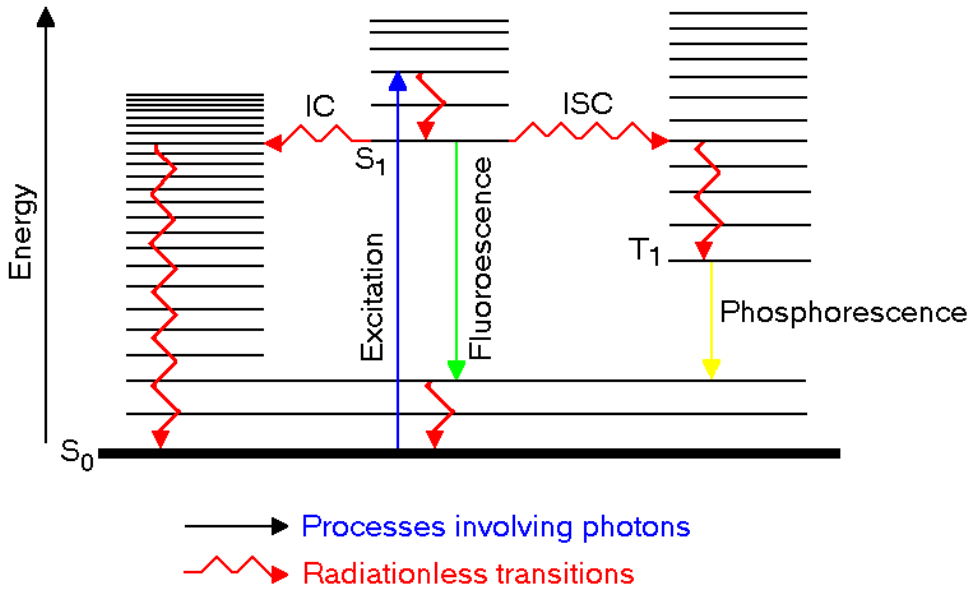

Figure 3.7: A Jablonski diagram illustrating radiative and non-radiative paths of relaxation from an electronically excited state S_1: fluorescence, phosphorescence, internal conversion (IC) and intersystem crossing (ISC).

The first step of any luminescent process is excitation, whereby the luminescent species, a fluorophore or phosphor, absorbs a photon with an energy that corresponds to an electron transition from the ground electronic state, S_0, to the first electronically excited state, S_1. Such electronic transitions are commonly found for delocalised electrons conjugated in double bonds. Therefore the most commonly used fluorophores are aromatic organic molecules. However, ions of certain rare earth elements, such as europium and terbium, also exhibit suitable electronic transitions between shielded *f*-orbital electrons. The fluorophore is excited to a vibrationally excited state as dictated by the Franck-Condon principle but will rapidly relax to the lowest electronically excited state by a process called vibrational relaxation, typically on a timescale of $\sim 10^{-12}$ s.

The molecule can then relax back to the ground state by the slower process of fluorescence (10^{-9} s) with emission of a photon. Because the transition is from the lowest excited state, the energy of the emitted photon is less than that of absorbed photon. Hence the spectrum of the emitted radiation is generally shifted to longer wavelengths relative to the excitation spectrum (Stokes' shift). The effect is further increased by the tendency of the molecule to relax to vibrationally excited states of the electronic ground state. These vibrational states are similar to those of the excited state as the nuclear geometry is not greatly changed during electronic excitation (another consequence of the Franck-Condon principle). As a result, the vibrational detail of the emission spectrum is typically a mirror image of the excitation spectrum.

Another possible radiative relaxation pathway is phosphorescence. Inter-system crossing (ISC) to a triplet state is followed by vibrational relaxation and the emission of a photon. This process is spin-forbidden therefore the timescale is significantly longer than for fluorescence ($\sim 10^{-3}$ s). Relaxation can also proceed by a non-radiative process. Internal conversion (IC) to a vibrationally excited state of the ground electronic state allows vibrational relaxation to the ground state.

3.2.2 Fluorescence lifetime

The observed fluorescence intensity immediately following the excitation pulse, I_0, decays exponentially (equation 3.1) with time according to the fluorescence lifetime, τ as described by the equation,

$$I(\tau) = I_0 e^{-t/\tau}. \quad \textbf{3.1}$$

The lifetime can therefore be defined as the time taken for the excited state concentration to decay to $1/e$ of its original value ($t/\tau = 1$). τ is also defined according to the equation,

$$\tau = \frac{1}{k_{NR} + k_R}, \quad \textbf{3.2}$$

as the inverse of the sum of the rates of the radiative and non-radiative decay, k_R and k_{NR}, respectively.

From equation 3.2 it can be seen that any factor which affects the rate of radiative or non-radiative decay will affect the fluorescence lifetime. The lifetime of several organic fluorophores and inorganic phosphors is observed to decrease with temperature. This temperature dependence can be explained by an increase in the rate of non-radiative decay due to ISC or IC from thermally populated higher vibrational states.[69-71] This dependence will be influenced by solvent polarity, which can change the relative energy, and therefore accessibility, of these states. Following absorption the fluorophore will often have an increased dipole moment. If the solvent molecules also have dipole moments they will orientate around the excited state dipole, effectively lowering the energy of the excited state.

It is also important to consider other factors that can increase non-radiative decay. The term *quenching* refers to a process by which the fraction of molecules that decay radiatively (the fluorescence quantum yield, Φ) is reduced. Quenching occurs when a fluorophore loses its excitation energy to another species either by collision or by electronic coupling.

3.2.3 Steady-state versus time-resolved fluorescence measurement [72,68]

The relatively short lifetime of fluorescence means that measurement of time-resolved fluorescence is in practice difficult, requiring complex and expensive equipment. Therefore, fluorescence is most commonly measured in the steady-state. The sample is illuminated with a continuous beam of light of constant wavelength and the emission intensity recorded as a function of wavelength to give the emission spectrum. Modern instruments also allow the

emission intensity at a given wavelength to be measured as a function of excitation wavelength to yield the excitation spectrum. Due to the nanosecond time-scale of fluorescence the steady-state is reached very quickly after the start of illumination. Therefore the steady-state measurement is simply a time-average of the time-resolved measurement. Integrating the intensity at a given time, *I(t)*, over a long, essentially infinite time-scale gives the steady-state intensity, I_{SS},

$$I_{SS} = \int_0^\infty I_0 e^{-t/\tau} dt = I_0 \tau \,. \qquad \textbf{3.3}$$

It can be seen from equation 3.3 that I_{SS} is proportional to the lifetime, therefore changes in the lifetime can in theory be probed by steady-state measurement. However, as I_0 is dependent upon other factors such as the concentration of the fluorescing species and instrumental parameters, such as fluctuations in the intensity of the excitation beam, it is often very difficult to reproduce measurements between experiments. In addition to this, the time-averaging process results in the loss of potentially useful information. For example, the presence of more than one lifetime in the intensity decay can indicate the presence of different molecular conformations or environments and the relative contribution of the two decay times to the overall decay gives the proportions of molecules in these states.

3.2.4 Time-resolved fluorescence measurement: Time-correlated single photon counting [72,68]

Currently, the most accurate technique for the measurement of decay lifetimes is time-correlated single photon counting (TCSPC). Figure 3.8 depicts the basic components of the set-up and their function. The basis of this method is that for each fluorescence event, an average of less than one emission photon is detected. The time taken between the start of the excitation pulse and the detection of the photon is measured and a count is added to the corresponding time slot (channel). These steps are repeated millions of times and due to the random nature of fluorescence emission the resulting plot of counts versus time will give the decay curve.

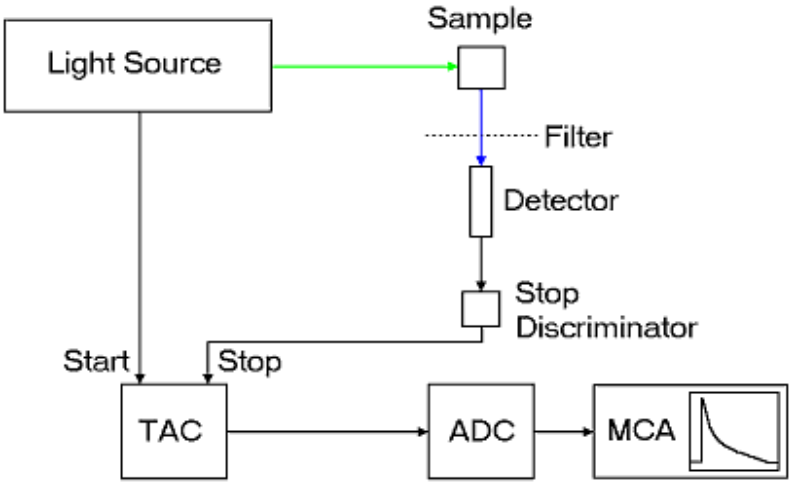

Figure 3.8: Schematic of the basic time-correlated single photon counting (TCSPC) set-up with time to amplitude converter (TAC), analogue to digital converter (ADC) and multichannel pulse height analyser (MCA).

The light source is a tuneable laser that sends bursts of monochromatic light and simultaneously sends trigger signals to the time to amplitude converter (TAC). Light is focused on the sample, commonly a glass cuvette filled with a solution of fluorophore, and the emitted light is detected at 90˚ to the incident beam by the detector - a photomultiplier with an aperture small enough to allow approximately one photon to be detected for each 100 laser pulses. The count level is set this low to prevent biasing the detection of 'early' photons as only the first photon detected is counted. The detected signal is sent to the stop discriminator, which sets a threshold level to remove electrical noise from the signal, and from there to the TAC.

The TAC works as a stopwatch. The start signal from the source starts the charging of a capacitor and the subsequent stop signal from the stop discriminator stops the charging, sending a pulse from the TAC to the analogue to digital converter (ADC). Here the magnitude of this pulse is converted to a numerical value of time. The multichannel analyser (MCA) then records this measurement in a channel on the x-axis (time-axis) according to the numerical value received from the ADC. After many cycles the decay curve is produced as a histogram of the number of counts per channel.

The raw data obtained from a TCSPC measurement must be fitted to a model in order to obtain lifetime information. The decay curve is fitted to an exponential model,

$$R(t) = A + \sum_{i=1}^{i=n} B_i e^{-t/\tau_i} \quad , \qquad \textbf{3.4}$$

with n lifetimes, τ_i, each with a pre-exponential factor, B_i, and an additional background factor, A. Because of the effectiveness of the stop discriminator, the background is usually very low (~1-10 counts in 10000). The number of distinct fluorophore environments or conformations determines the number of lifetimes, n. Systems with a large number of lifetimes can theoretically be fitted to a lifetime distribution although, in practise n is often set to the lowest value that will result in a satisfactory fit and is rarely required to be more than 4. The pre-exponential factor B_i is the relative magnitude of the contribution of τ_i to the overall decay and relates to the relative amount of fluorophore in that environment/conformation.

In practice, as the excitation pulse may have a width comparable to the timescale of the sample decay, the measured curve is a combination of the sample response and the response of the instrument. This complication needs to be addressed in order to obtain a fit that is representative of the sample only. The simplest method is to only fit to data in the 'tail' region of the curve where there is no significant signal due to instrument response. However, *tail fitting* will not recover lifetimes that are short compared to the pulse width. Lifetime information in this region can only be determined using *reconvolution fitting*, where the entire curve is fit to the measured instrument response *reconvoluted* with an exponential model.

3.2.5 Spatially-resolved and time-resolved fluorescence measurement: Fluorescence lifetime imaging microscopy

The technique of fluorescence lifetime imaging microscopy (FLIM) allows spatial resolution of the lifetimes of fluorophores in a sample. A gated CCD camera records a digital image of the fluorescence emitted from the sample over a short time window at a defined delay after an excitation laser pulse. A series of exposures at different delay times is built up into a moving picture showing the decay in fluorescence over time following an initial excitation pulse. As with TCSPC, a portion of the excitation pulse is sent as a trigger signal to determine the start of the delay. The data for each pixel is then fitted to an exponential decay model, as for TCSPC,

resulting in a digital image for which the fluorescence lifetime at each pixel has been determined. The hue or brightness of each pixel denotes the lifetime to show the spatial variation of lifetime throughout the sample.

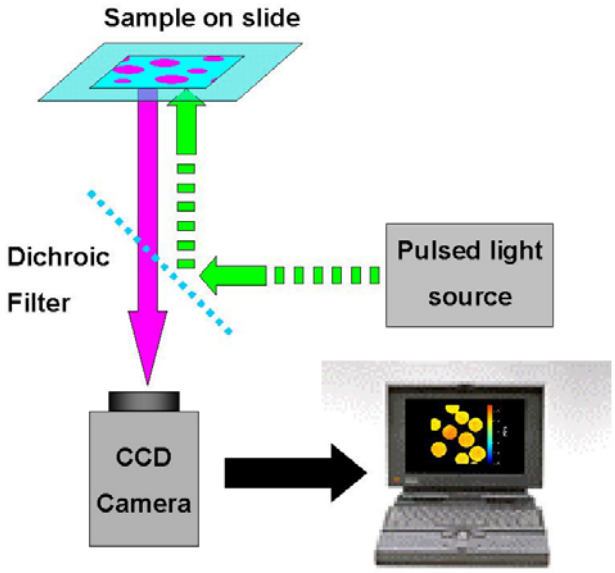

Figure 3.9: Schematic of FLIM measurement set-up.

To obtain data of the same quality as that obtained by TCSPC would require very much longer collection times as the decay curves for each pixel are recorded from the light emitted from only one small area of a sample. Therefore decay curves are generally recorded using fewer channels, each channel here corresponding to a different image. To improve the quality of the data it is common to take the average of a number of exposures for each channel. Pixels of initial intensity below a stated threshold can be removed so that areas of the sample that are 'non-fluorescent' do not complicate the lifetime map.

3.3 In-resin thermometry during microwave heating from TCSPC measurement of the lifetime of a covalently-attached fluorophore

This section describes a method of thermometry that was devised to allow the temperature of the resin beads within a SPOS system to be measured during microwave heating. The fluorescence lifetime of a fluorophore covalently attached to a resin suspended in water is determined over a

range of temperatures using TCSPC, providing a calibration scale that can be used to determine the temperature of the resin during microwave heating. This was motivated by speculation as to whether the resin is heated preferentially over the solvent in which it is suspended.

Remote thermometry of systems based on the fluorescence properties of dyes has been reported before: the thermal profile of a microchannel-microheater chip has been probed by measuring the fluorescence lifetime of a dye solution as a function of distance, flow rate and the voltage passed through the microheater.[73] The novelty of the method reported here is that the thermometry is component-specific. The work described here is a proof of a principle that could potentially be used to remotely determine the temperature of specific parts of systems that are thought to heat inhomogeneously.

Various resin/fluorophore/solvent combinations were tried before a suitable one was found. Some of the unsuccessful combinations are reported to explain the choice of the final combination and to highlight some of the important aspects that must be considered when investigating these systems.

3.3.1 Experimental

All solvents used were HPLC grade and obtained from Aldrich.

3.3.1.1 Preparation of amine functionalised polystyrene (PS-NH_2) labelled to a 1% theoretical loading with dansyl chloride

100 mg of Aminomethylated PS resin (Novabiochem, 1 mmol g^{-1} free amine, 200-400 mesh) was pre-swollen in 0.5 ml of DMF in a 3 ml Whatman filter tube. 5 equivalents of dansyl chloride (Aldrich 99%) and 'non-fluorescent' dansyl analogue (5-chloronapthalene-1-sulfonyl chloride, Toronto Research Chemicals) in the molar ratio 1:99 were dissolved in 0.5 ml DMF along with 65mg (5 equivalents) of diisopropyl ethanolamine (DIPEA, Aldrich) and added to the swollen resin. The tube was sealed and rotated for 16 hr. Resin was then washed using the following protocol: 2 x DMF, 2 x MeOH, 2 x DMF and 4 x DCM. The resin was then tumbled overnight in DMF. DMF was drained off for analysis by steady-state fluorescence before the resin was rinsed with 2 x DCM. An emission spectrum of the DMF washing was measured from 350 to 600 nm using a Spex Fluoromax fluorimeter with excitation at 325 nm, 1 nm bandwidth and a 0.1 s integration period. The DMF/DCM washing protocol was repeated until the

fluorescence of the washings had decreased to a constant level. The resin was finally washed with 4 x DCM and dried under vacuum overnight.

3.3.1.2 Preparation of PS-NH_2 labelled to a 10% theoretical loading with Rhodamine B isothiocyanate (RhdB-ITC)

100 mg of Aminomethylated PS resin (Novabiochem, 0.9 mmol g^{-1} free amine, 200-400 mesh) was pre-swollen in 0.5 ml of DMF in a 3 ml Whatman filter tube. 4.8 mg (0.1 equivalents, 10% theoretical loading) RhdB-ITC (Aldrich) and 65 mg (1 equivalent) of DIPEA in 0.5 ml DMF were added to the resin. The tube was sealed and rotated for 16 hr. Resin was then washed using the following protocol: 3 × DMF, 3 × MeOH, 3 × DCM, 3 × DMF, 3 × DCM, 3 × MeOH, 3 × DMF. The resin was left in the final aliquot of DMF and rotated for 16 hr. DMF was then drained off and analysed by steady-state fluorescence as in 3.3.1.1 except exciting at 555 nm and measuring over 570 to 700 nm. The washing protocol was repeated until the fluorescence of the washings had decreased to a constant level. The resin was finally washed with 4 x DCM and dried under vacuum overnight.

3.3.1.3 Preparation of amine functionalised poly-(ethylene glycol)acrylamide (PEGA-NH_2) labelled to 1% theoretical loading with RhdB-ITC

100 mg (dry weight) of PEGA-NH_2 (0.2 mmol g^{-1} free amine, 300-500 μm, 12.94% w/w in MeOH) was pre-swollen in 4.5 ml of DMF in a 10 ml Whatman filter tube. 0.1 mg (0.01 equivalents, 1% theoretical loading) RhdB-ITC in 0.5 ml DMF was added to the resin. The tube was sealed and rotated for 16 hr. 65 mg (5 equivalents) of DIPEA was added to the tube before a further 24 hr rotation. Resin was then washed using the following protocol: 3 × DMF, 3 × MeOH, 3 × DCM, 3 × DMF, 3 × DCM, 3 × MeOH, 3 × H_2O. The resin was left in the final aliquot of H_2O and rotated for ~ 16 hr. H_2O was then drained off and analysed by steady-state fluorescence as in 3.3.1.1 except exciting at 555 nm and measuring over 570 to 700 nm. The washing protocol was repeated until the fluorescence of the washings had decreased to a constant level. The resin was stored wet (H_2O) and the container wrapped in foil to prevent photo-bleaching.

3.3.1.4 Cuvette holder for simultaneous conventional and microwave heating of samples during TCSPC and FLIM measurement

For initial experiments to determine the temperature dependence of the fluorescence in various systems sample temperature was controlled using a hollow cuvette holder attached to a circulating water bath (Grant LTD 6). However, to heat both conventionally and by microwaves during fluorescence lifetime measurements (figure 3.10) a bespoke cuvette holder was built. The holder is based upon a parallel plate transmission line, with the plates replaced by thicker pieces of metal to allow water to be circulated through the holder and to give it a greater thermal mass.

The advantage of the parallel plate configuration over, say, a waveguide applicator is that complete optical access to three faces of the cuvette is possible at the end of the line. Two of these faces are parallel to one another. Therefore, for TCSPC measurements the excitation light can be introduced through one of the parallel faces and that which is not incident on sample can pass through the other. Emitted light can then be collected from the perpendicular face, where unwanted scattered excitation light is at a minimum.

Microwaves are introduced via a 50 Ω semi-rigid coaxial cable, the inner and outer conductors of which are each connected to one of the two 'plates'. The wave is then propagated along a PTFE-filled parallel plate line to a cavity holding a PMMA 10 × 10 mm cuvette shortened to 12 mm in height. The dimensions of the line and the cuvette cavity, if filled with water, are set to maintain the standard impedance of 50 Ω. For a sample of aqueous solution or suspension this is a good approximation, as the dielectric properties of water will dominate. Two 100 Ω resistors in parallel (equivalent to one 50 Ω resistor) terminate the microwave circuit, providing a matched load.

The two 'plates' have circular bores through them, which are connected to each other at one end. By connecting the other ends to a circulating water bath (Grant LTD 6), the sample temperature, as measured by a fluoroptic probe (Neoptix T1), can be very effectively controlled. A magnetic stirrer mounted on the top of the holder agitates a magnetic 'flea' in the sample to continuously stir the sample.

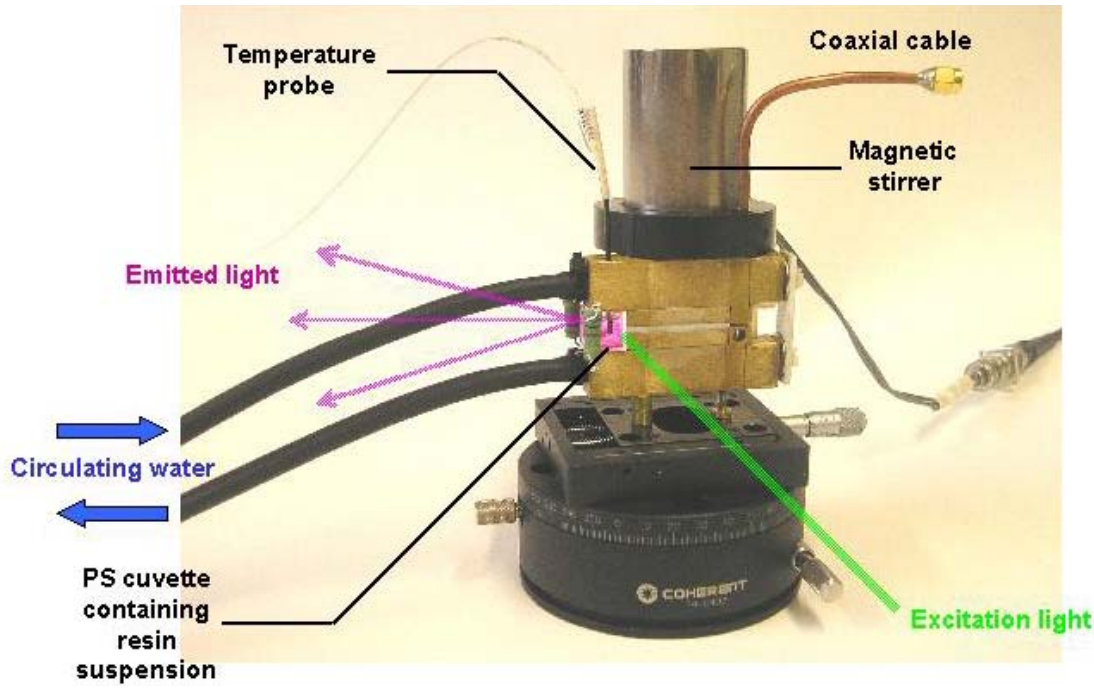

Figure 3.10: Bespoke cuvette holder (pictured mounted on translation table) for conventional and microwave heating of samples and depiction of optical access used for simultaneous probing by TCSPC.

The device can also be used for heating of samples during FLIM measurement. The PTFE filled part of the device can be removed to leave a larger cavity into which a stoppered 10 × 10 mm cuvette can be placed (as the device is orientated in figure 3.10, the longest dimension of the cuvette would be horizontal). The device can then be placed on the microscope table such that one of the long faces is optically accessible to the pulsed light source from below. The temperature probe can be inserted through a hole in the cuvette stopper to give an accurate sample temperature.

3.3.1.5 Temperature dependence of the fluorescence lifetime of dansyl labelled PS resin in DMF

8 mg of dry PS resin (1 % loading of dansyl) suspended in circa 3 ml of DMF in a stoppered clean 10 × 10 mm silica cuvette was placed in the standard cuvette holder/controlled heating

environment along with a small magnetic stirrer bar. The sample was agitated magnetically to continuously resuspend the resin. The cuvette holder was placed within the sample cavity of an Edinburgh Instruments spectrometer attached to a TCC900 TCSPC system. A Ti-Sapphire femtosecond source (Coherent, 10 W Verdi and Mira Ti-Sapphire) was pulse-picked and frequency-tripled to obtain an output of 352 nm. This was focussed on to the sample cuvette and the position and orientation of the holder adjusted to collect the maximum amount of light. The fluorescence was detected by a Hamamatsu microchannel plate photomultiplier (R3809U-50).

The decay of fluorescence emission at 410 nm was recorded over a 50 ns timescale using 2048 channels and to a stop condition of 10000 counts for the peak channel. Decay curves were taken with the water bath/circulator set at temperatures from 20 to 60°C in 10 °C steps after equilibration of the sample temperature. The sample temperature as measured by the fluoroptic probe was recorded. An instrument response was measured to enable reconvolution fitting by collecting at 352 nm. Fitting was carried out using Edinburgh Instruments F900 software.

3.3.1.6 Temperature dependence of the fluorescence lifetime of RhdB labelled PS resin in DMF

6 mg of dry PS resin (10 % loading of RhdB) suspended in circa 3 ml of DMF in a stoppered clean 10 × 10 mm silica cuvette was placed in the same TCSPC set-up as described in 3.3.1.5. The excitation source was adjusted to 371 nm. The decay of fluorescence emission at 575 nm was recorded over a 50 ns timescale using 1024 channels and to a stop condition of 10000 counts for the peak channel. Decay curves were taken with the water bath/circulator set at temperatures from 20 to 60 to 20°C in 5°C steps after equilibration of the sample temperature. The sample temperature as measured by the fluoroptic probe was recorded. An instrument response was measured to enable reconvolution fitting by collecting at 371 nm. Fitting was carried out using Edinburgh Instruments F900 software.

3.3.1.7 Temperature dependence of the fluorescence lifetime of RhdB labelled PEGA resin in water

The modified cuvette was filled with 100 mg of wet PEGA resin (1 % loading of RhdB) suspended in deionised water and placed in the bespoke cuvette holder/microwave applicator along with a small magnetic stirrer bar. The sample was agitated magnetically to continuously

resuspend the resin. The cuvette holder was placed within the TCSPC system described in 3.3.1.5. A pulsed LED source (PicoQuant PDL 800-B) was used to provide excitation light. The output of the source is centred at a wavelength of 500nm but is broad, having significant intensity at the emission maximum of RhdB at 585 nm. Therefore a Schott BG36 filter (transmission at 550 nm = 0.90, at 580 nm = 1×10^{-5}, at 590 nm = 4×10^{-3}) was placed directly in front of the source output to prevent scattered excitation light being counted.

The decay of fluorescence emission at 585 nm was recorded over a 50 ns timescale using 1024 channels and to a stop condition of 10000 counts for the peak channel. Decay curves were taken after equilibration of the sample temperature with the water bath/circulator at set temperatures from 20 to 50 to 20°C in 5°C steps and then from 20 to 30 to 20°C in 2°C steps. The sample temperature as measured by the fluoroptic probe was recorded. An instrument response was measured to enable reconvolution fitting by collecting at 500 nm without the scattering filter in place. Decay curves were fitted to a single exponential model from channels 63 to 1024 with a fixed background of 2 using the FAST global analysis software application.

3.3.1.8 Measurement of the temperature of PEGA resin in water from the fluorescence lifetime of a RhdB label during simultaneous microwave heating

A Hewlett Packard 8752A vector network analyser (VNA) was connected by coaxial cable to the coaxial connector of the cuvette holder via a ZRL-2400LN microwave amplifier. The output frequency of the VNA was then set to 2.45 GHz and the power level set such that the maximum output power of the amplifier (200 mW) would be produced, but the amplifier was not switched on at this stage.

A sample of RhdB labelled resin was prepared and placed in the cuvette holder as in 3.3.1.7 and the water bath/circulator set to 20.0°C. The decay curve was measured as in 3.3.1.7 once the sample temperature was equilibrated with the bath. The amplifier was then switched on and another decay curve measurement was started immediately. After allowing the sample to re-equilibrate with the bath, repeat measurements of the decay curve were taken with and without microwave heating. The decay curves were fitted as in 3.3.1.7.

3.3.2 Results and discussion

3.3.2.1 Temperature dependence of the fluorescence lifetime of dansyl labelled PS resin in DMF

Dansyl chloride (figure 3.11) has previously been used in solid phase support studies as a probe of reactive site distribution and kinetics[74] and to investigate swelling behaviour[75,76]. It is chosen for such studies because until reaction of the sulphonyl chloride group with primary amine (a reaction which it readily undergoes) it is apparently 'non-fluorescent'. Therefore as procedures to produce homogeneously labelled beads are well known it was hoped that its fluorescent properties would also provide a reliable probe of temperature and initial measurements of the lifetime of dansylamide in solution were encouraging.

1 **2**

Figure 3.11: Dansyl chloride (1) and its 'non-fluorescent' analogue, 5-chloronapthalene-1-sulfonyl chloride (2).

PS resin was chosen, as it is the original and still most popular support for SPOS. The properties of DMF that have made it a popular solvent for MA-SPOS - high loss tangent, good swelling properties and a relatively high boiling point – also make it ideal for this study.

It was decided to label the resin to a 1% theoretical loading as high levels of fluorophore prevent excitation light from entering beyond the outer layers of the resin bead. High levels are also likely to lead to self-quenching.[77]. However, as reaction is more rapid than diffusion,[74] a limiting amount of dansyl chloride would be expected to attach only to sites in the outer regions of the resin sphere. A 'non-fluorescent' analogue (figure 3.11) in higher concentration is therefore employed to compete with the dansyl chloride for sites and ensure a homogeneous distribution.

Initial measurements on dansyl labelled PS resin suggested a temperature dependent aspect to its fluorescent decay although it proved impossible to reproduce these effects and the decay was complicated and multi-exponential. It had been assumed that because the unreacted probe is supposedly non-fluorescent, any residual probe in the liquid phase could be neglected. However, from studying the fluorescence intensity of washings of the bead suspension it became clear that there was a significant amount of detectable fluorophore in the liquid phase. The resin had to be subjected to 5 cycles of the washing protocol described in 3.3.1.1 before the fluorescence of the solvent phase decreased to a minimum (figure 3.12).

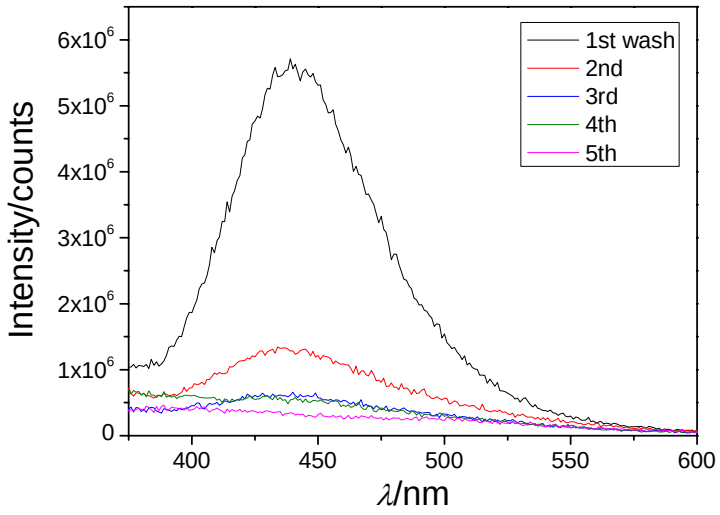

Figure 3.12: Steady state emission spectrum of DMF washings of dansylated PS resin.

It was clear from visual inspection of the decay curves recorded for DMF suspensions of washed beads at different temperatures that there was no significant temperature dependence of the lifetime. Reconvolution fitting revealed that the decay was complicated, exhibiting at least three lifetimes of around 7 (~30%), 2.5 (~50%) and 0.5 ns (21%). The multi-exponential behaviour may be due to the presence of the 'non-fluorescent' analogue, either because it is itself fluorescent, even if only weakly, or because quenching with it provides another non-radiative pathway for decay. In addition, there may still be residual fluorophore leaching into the liquid phase that could be expected to have a different fluorescence lifetime.

The temperature dependence seen in initial measurements was most likely due to the oxygen quenching of fluorophore in the liquid phase and the change in the solubility of oxygen with temperature. In summary, this resin-fluorophore-solvent system was not suitable for this study.

3.3.2.2 Temperature dependence of the fluorescence lifetime of RhdB labelled PS resin in DMF

The temperature dependence of the fluorescence quantum yield of RhdB in aqueous solutions has been used before in remote temperature sensing.[67,64-66] However, as discussed in section 3.2.3, the quantum yield is dependent upon other factors that make reproducible measurement difficult. Reference dyes with temperature independent properties can be used to negate these difficulties.[78,67] However, a method that instead uses the fluorescence lifetime ought to be both simpler and more robust.

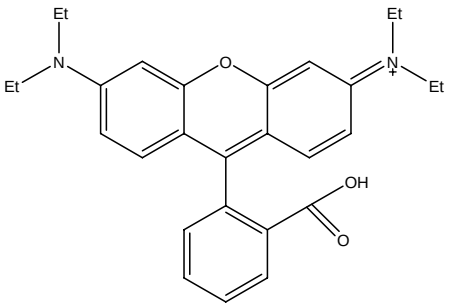

Figure 3.13: Rhodamine B. The isothiocyanate derivative differs in that the benzoic acid ring is substituted with the –N=C=S functionality. This undergoes reaction with primary amine groups on the resin to form a thiourea linkage.

Literature reports state that the fluorescence lifetime RhdB (figure 3.13) also exhibits a strong temperature dependence in water and ethanol.[78,73] However, measurements of RhdB labelled beads in DMF were hindered by low emission count rates. This was partly due to the limitations of the laser source that meant that the principal excitation maximum was not accessible but it was also observed that RhdB fluorescence is strongly quenched in DMF. The quenching quickly becomes apparent if one makes up a solution of RhdB in DMF and leaves it for any length of time. The reasons for this are unclear but it may be that the solvent in some way promotes aggregation of the fluorophore or that the strongly polar nature of the solvent makes internal conversion more favourable.

Despite the low count rates it was still possible to measure the temperature dependence of the fluorescence decay of RhdB on PS resin in DMF. The decay profiles fitted to 4 exponential terms with lifetimes of 0.32, 1.73, 4.06 and 11.95 ns at 20°C. These reduced to 0.23, 1.13, 3.73 and 10.53 ns at 60°C. However, upon cooling back to 20°C the lifetimes were 0.24, 1.43, 4.02 and 11.89 ns. The irreversibility of the system suggests that it is degrading in some way. The most likely reason is that the quenching effect of RhdB increases over a period of time and with exposure to higher temperatures. The higher elevated temperature might also be expected to accelerate solvent degradation of the resin or detachment of RhdB.

The route of all the problems encountered in this system appears to be the strength of the solvent. It was therefore decided to move to an aqueous suspension as RhdB is known to be stable in water and has shown strong temperature dependence in it.

3.3.2.3 Temperature dependence of the fluorescence lifetime of RhdB labelled PEGA resin in water

The change to using water as the solvent necessitated a move to another resin (water is a poor solvent for PS). PEGA (figure A, appendix III) was used as the polyethylene glycol chains imbue the resin with good swelling properties for polar solvents such as water and alcohols. The loading level of RhdB was again kept low (1%) for the reasons stated in 3.3.2.1. However, no 'non-fluorescent' analogue was used to homogenise the loading due to concerns that it would complicate the fluorescence decay behaviour. Instead the resin was left in RhdB solution overnight so that the fluorophore could diffuse evenly throughout the resin before catalyst was added to initiate reaction.

The change of solvent and of excitation source immediately resulted in greater success in measuring decay curves. The curves recorded at different temperatures all fitted to a single exponential model with a χ^2 of less than 1.2. Additional exponential terms would normally be included in the model until a χ^2 of typically less than 1.1 is obtained. However, a rigorous photophysical analysis of the system, determining the number of distinct fluorophore environments and their relative proportion, was not the aim here. Rather, it was to establish that for a given temperature a lifetime representative of the resin system would be reproducibly

obtained, and thus conversely that the temperature of the resin could be confidently determined from measurement of the lifetime.

As figure 3.14 shows, the fluorescence lifetime of RhdB on the resin determined by single exponential fitting exhibits strong temperature dependence, decreasing from approximately 2.1 ns at 20°C to approximately 1.2 ns at 45°C. These values are in good agreement with observations of the lifetime of RhdB in aqueous solution decreasing from 2.1 to 0.6 ns over the range 10 to 60°C[73] and the strong temperature dependence it exhibits in solution in ethanol.[78] The behaviour is reproducible over two heat-up and cool-down cycles and fits well to the quadratic function,

$$\tau = 3.05 - 0.052T + 0.00026T^2 . \qquad \textbf{3.5}$$

Solving the quadratic and simplifying yields an equation,

$$T = \frac{0.052 - \sqrt{0.00104\tau - 0.000432}}{0.00052}, \qquad \textbf{3.6}$$

for determining temperature from a measured lifetime. The standard error (determined using Microsoft Excel[79]) for determining T from τ is 0.52°C.

The temperature within the water-swollen resin can therefore be reliably determined from measurement of the fluorescence lifetime of RhdB covalently attached to it. It should be noted here that the temperature determined can be confidently said to be that of the swollen resin and not the surrounding water, but only because the resin was washed until residual fluorescence in the solution was at a minimum.[†] This was further confirmed by turning off the agitation of the sample when probing in the TCSPC system. With agitation off, no resin beads are incident with the excitation light and no significant fluorescence emission is counted.

[†] Interestingly, the fluorescence quenching reported in the previous section can be quite clearly observed during the washing protocol. As the resin is rinsed in DMF it immediately becomes much less strongly coloured. The effect appears to be completely reversed upon rinsing with the next solvent.

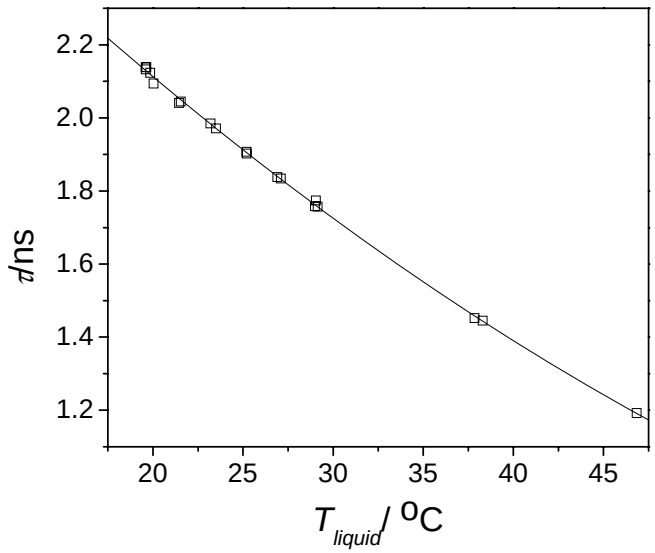

Figure 3.14: Fluorescence lifetime of RhdB-labelled PEGA resin in water as a function of temperature. The data represents two heat-up and cool-down sequences from 20 to 50 to 20°C in 5°C steps and from 20 to 30 to 20°C in 2°C steps. The solid line is a quadratic fit to the data.

3.3.2.4 Measurement of the temperature of PEGA resin in water from the fluorescence lifetime of a RhdB label during simultaneous microwave heating

The hypothesis was that microwaves could preferentially heat the resin with respect to the liquid phase. In order to probe this the fluorescence lifetime of RhdB on the resin, and hence resin temperature, T_{resin}, were measured with the system under conventional thermal control and then subsequently during microwave irradiation of the sample.

The time taken to measure a decay profile is dependent on a number of factors including the resolution of measurement, the emission count rate and the fluorescence lifetime. After optimisation of this system, the shortest possible measurement was not less than one minute and consequently 'real-time' measurement of fluorescence lifetime as microwaves heated the sample was not possible. The experimental approach was therefore to continue water circulation at the same temperature during exposure to relatively low power microwaves so that, over the timescale of the fluorescence measurement, the observed increase in the liquid phase temperature, T_{liquid}, was small. Preferential heating of the resin would be evident from any

increase in T_{resin} above that seen for T_{liquid}. The continued circulation of water would be expected to exacerbate any preferential heating effect as it would cool the liquid phase.

Although this may appear to be an artificial set-up, simultaneous cooling of reaction vessels, either using compressed air or circulating refrigerant, is now commonly exploited in modern applicators for microwave-assisted chemical synthesis. Indeed, in virtually all applications of microwave heating the workload experiences simultaneous cooling from the surrounding ambient conditions.

The results of the experiment are summarised in table 3.2. The first thing to note is that without applied microwaves, and with the sample temperature controlled only by water circulation, T_{liquid} and T_{resin} are in good agreement. This is further verification of the accuracy of the method of in-resin thermometry, as the components of the sample ought to be in thermal equilibrium under these conditions. Furthermore, this is the still the case when the sample has been allowed to return to conventional temperature control and thermal equilibrium after the first period of microwave exposure, demonstrating the reproducibility of the method.

Table 3.2: Comparison of the temperature of the liquid phase, T_{liquid}, (as measured by a fluoroptic probe) and the temperature of the resin, T_{resin}, (as determined from the fluorescence lifetime, τ, of RhdB attached to the resin according to equation 3.6).

Microwave power/mW	T_{liquid}/°C	τ/ns	χ^2	T_{resin}/°C
0	19.8	2.121	1.114	19.83
200	20.0	2.113	1.210	20.02
0	19.8	2.123	1.115	19.78
200	20.0	2.114	1.226	20.00

With applied microwave heating T_{liquid} was observed to increase by 0.2°C. T_{resin}, as determined from measurement of the fluorescence lifetime over the period of microwave exposure, was seen to increase by the same amount. In any case, the increase in T_{resin} is less than the estimate of the error in the measurement (± 0.5°C). The same result was obtained over the two microwave

exposures. Thus, it appears that the resin is not preferentially heated. This may be because the water, of which the swollen bead is predominantly made, is unrestricted and would therefore be expected to have much the same microwave susceptibility as the water in which it is suspended.

Suspending the water-swollen resin in a less microwave susceptible liquid would be expected to increase the chances of preferential heating occurring. To this end, an attempt was made to probe water-swollen PEGA resin suspended in hexane. However, the hydrophilic resin beads agglomerated on introduction to the hydrophobic solvent and could not be suspended. This agglomeration made it impossible to measure the fluorescent lifetime of RhdB on the resin.

3.3.3 Conclusions

As well as the direct outcomes of the work done to test the central hypothesis that motivated this program of research, a number of other interesting findings came to light. Evidence has been found for the reversible fluorescence quenching of RhdB in DMF and reasons for this have been briefly discussed. Probing of resin labelled with dansyl chloride and its analogue (5-chloronapthalene-1-sulfonyl chloride) suggest that the unreacted probe and the analogue can not simply be thought of as 'non-fluorescent'. It seems that the fluorescence decay determined for the dansyl system is complicated by presence of the analogue, either because the analogue is, at least to some extent, fluorescent or because it quenches the fluorescence of the dansyl fluorophore.

Probably the most interesting supplementary finding was that fluorescence measurements suggest that previously recommended protocols[74] for washing SPOS beads are not completely effective. Long, repeated periods of agitation in solvent were required to produce clean resin.

However, the central aim of this work was to develop a means of determining the temperature of a specific component, the resin, in a microwave-heated system and to determine whether it differed from the rest of system due to preferential microwave heating. The results of lifetime measurements of RhdB labelled onto PEGA beads suspended in water demonstrate that an accurate and robust system of thermometry specific to the resin component of the system was developed. Temperature measurement during simultaneous microwave heating was also succesfully demonstrated. It was found that microwave heating does not result in any thermal inhomogeneity between the components of the suspension.

An attempt to use the method to measure the temperature of water-swollen beads in hexane (a system more likely to exhibit selective heating) failed, as a suspension of the two components could not be formed. The next section describes a modification of the technique that allows the fluorescence lifetime of fluorophore, and hence temperature, on single beads of resin to be determined.

3.4 Spatially resolved thermometry during microwave heating from FLIM measurement of the lifetime of a covalently-attached fluorophore

This section describes a method of thermometry that was devised to allow the temperature of individual resin beads within a SPOS system to be measured during microwave heating. As in section 3.3 the fluorescence lifetime of a fluorophore covalently attached to a resin is determined over a range of temperatures to provide a calibration scale that can be used to determine the temperature of the resin during microwave heating. However, in this case Fluorescence Lifetime Imaging Microscopy (FLIM) is used to determine the fluorescence lifetime. Using this method, a map of the lifetime (and therefore temperature) distribution over the sample can be produced.

This was motivated by the desire to probe water-swollen resin immersed in non-polar solvent as it was thought that this system would be more likely to exhibit selective microwave heating. The water-swollen resin will not suspend in non-polar solvent and so cannot be probed by the method described in section 3.3. However, this work also represents a proof of a principle that could potentially be used to remotely determine the temperature distribution in any systems that are thought to heat inhomogeneously.

This is not the first example of *in-situ* spatially-resolved thermometry during microwave heating: a contemporaneous report describes 2-D temperature measurements of aqueous solutions in a microwave cavity.[67] A temperature map of an illuminated slice of the workload is produced from the measured intensity of RhdB in solution. As reproducible measurement of fluorescence intensity is difficult, a reference dye, Rhodamine 101, which is not sensitive to temperature, is also in the solution. The emission intensities of both dyes are simultaneously recorded on separate CCD cameras after splitting the emission with a dichroic mirror. The images are then

mechanically and electronically aligned before producing an image of the relative intensity, which can then be scaled to produce a 2-D temperature map.

The novelty of the work described here is that the temperature measurement is specific to one component of a two-phase system. In addition, as the method uses the more robust fluorescence lifetime as the measured probe of temperature only one fluorescent probe is required and the optical measurement set-up is much simpler.

3.4.1 Experimental

3.4.1.1 Preparation of amine functionalised poly-(ethylene glycol)acrylamide (PEGA-NH_2) labelled to 100% theoretical loading with RhdB-ITC

The procedure for preparation of resin with 1% theoretical loading (3.3.1.3) was followed except 25 mg (2.5 equivalents, 250% theoretical loading) RhdB-ITC was used.

3.4.1.2 Temperature dependence of the fluorescence lifetime map of RhdB labelled water-swollen PEGA resin in water and in hexane

A small quantity of wet resin was allowed to settle on the base of a 3 ml quartz cuvette filled with either deionised water or hexane. The cuvette was placed in a hollow cuvette holder attached to a circulating water bath (Grant LTD 6) and placed on the sample stage of a Nikon TE300 inverted microscope configured for epifluorescence. The cuvette holder was open at the base, allowing optical access to the cuvette. Excitation light was sourced from the pulsed LED described in 3.3.1.7, reflected from a dichroic mirror and focused through an objective (Nikon 10 ×, 0.45 aperture) on to the sample in the base of the cuvette. The emitted fluorescence was collected through the same objective and passed through a Nikon G2A dichroic filter (transmission 510-560 nm, emission 580 nm) and imaged onto a Picostar HR-12QE gated intensified CCD camera system (LaVision GMBH, Berlin).

The instrument response was determined to be 800 ps by reflection of the excitation light from a mirror. 1375 × 1039 pixel images were taken with a 600 ps gate width, in steps of 200 ps over a 12 ns range (60 channels). Each image was the average of 10 exposures of 1300 ms each. The exposure time was chosen to give a peak intensity of 3000-4000 for the brightest image. The measured background signal was subtracted from each image. The decay curve for each pixel

was tail-fitted to a single exponential decay using the Picostar DaVis module in DaVis 6.2 software application. Lifetime maps were produced by assigning a colour from a 16-bit pseudocolour scale to each pixel according to its lifetime. Pixels with a count below a threshold of 700 in the brightest image were coloured black. The software was also used to determine an average lifetime for each bead by fitting over the largest square that could be fit in to the image of each bead.

Lifetime maps were produced for a collection of beads in water with the water bath/circulator set at temperatures between 20 and 50°C during heat-up and cool-down in 2°C steps between 20 and 30°C and subsequently in 5°C steps. A FISO FOT-H fibre optic temperature sensor linked to an Umi 4 signal conditioner was used for temperature measurements of the liquid phase. The sensor was introduced into the cuvette through a hole in the PTFE stopper. Maps of a collection of beads in hexane were taken in the same way.

3.4.1.3 Spatially-resolved thermometry during microwave heating of water-swollen PEGA resin in hexane from fluorescence lifetime mapping of RhdB covalently attached to the resin

The microwave generator and applicator set-up originally designed for simultaneous heating during neutron scattering measurements and described in 4.2.2.2 was used to heat samples. The waveguide applicator was placed horizontally on the sample stage such that one of the ports designed for neutron beam access was used for insertion of a 3 ml quartz cuvette, and the other for optical access to the base of the same cuvette. A small quantity of water swollen RhdB labelled PEGA resin was allowed to settle on to the base of the cuvette and the cuvette was filled with hexane. The waveguide was tuned so that the cuvette was at a maximum of the electric component of the microwave field in the direction of the transverse wave motion. The electric field at the inside surface of the waveguide is theoretically zero. Therefore the base of the cuvette was raised slightly from the bottom of the waveguide by two microscope slides, although the field strength will be non-zero here anyway as microwaves will breach the port to some extent.

Lifetime maps were produced during two different heating regimes. In the first, the sample was heated with a microwave power level of either 50 or 100 W until the system reaches quasi-

equilibrium, where the heat loss from the sample is equal to the heating due to absorbed microwave energy. Only at this point were lifetime maps recorded. In the second regime, lifetime maps were recorded immediately after microwave power (at either 100 or 200 W) had been switched on and therefore whilst the temperature was increasing. In both cases, before microwave heating, lifetime maps were produced with the sample at room temperature. A fresh sample was made up for each experiment. The temperature of the liquid phase was measured with a FISO FOT-H fibre optic temperature introduced into the cuvette through a hole in the PTFE stopper.

The method and apparatus described in 3.4.1.3 were used to record fluorescence lifetime maps and determine average lifetimes for individual beads. However, the physical attributes of the sample environment necessitated an objective with a longer focal range (Nikon 10×, 0.30 aperture). Because of the smaller aperture of the objective longer exposure times were required. Images for the quasi-equilibrium measurements were an average of 5 exposures of 3000 ms and taken in 200 ps intervals, giving a total acquisition time of approximately 15 min. Images for the measurements during heating had to be produced more quickly and were therefore an average of 5 exposures of 1000 ms and taken in 500 ps intervals – a total of approximately 2 min.

3.4.2 Results and discussion

3.4.2.1 Temperature dependence of the fluorescence lifetime map of RhdB labelled water-swollen PEGA resin in water and in hexane

Fluorescence lifetimes of RhdB on a sample of water swollen resin (table 3.3) exhibit strong temperature dependence in both water and hexane, as would be expected from the TCSPC measurements on suspensions of RhdB labelled resin described in section 3.4.1. The dependence and the even distribution of the lifetime across the bead, illustrated by the evenness of colour, are sufficient to allow temperature differences as small as 2°C to be visually discerned. However, also clear from table 3.3 is the difference in lifetimes seen on different beads at the same set temperature.

The probable reason for this is that different beads have different distributions of fluorophore. For this experiment, the resin was reacted with an excess of RhdB to give 100 % loading because the exposure times required for lower loadings were prohibitively long. Some reports

have suggested that this can lead to uneven distribution of fluorophore because there is a greater concentration of reactive sites at the surface.[80] However, it appears that this result was arrived at because high levels of fluorophore prevent light from passing beyond the outer layers and increase the probability of fluorescence from within the bead being reabsorbed before it escapes to be detected.[77,81] The distribution can therefore be expected to be even throughout each bead and differences between beads can not be explained by differences in the degree of loading of reactive sites as all should be labelled.

Therefore the difference in distribution is either because the manufacture of the resin produces beads with different amounts of reactive sites per unit mass, or because, due to differences in the extent to which they are able to swell, they ultimately have different amounts of reactive sites per unit volume. Both would have the effect of changing the effective concentration of RhdB within the resin. Higher concentration would result in closer packing of fluorophore molecules and therefore greater likelihood of self-quenching or reabsorption of fluorescence, thus reducing the average fluorescence lifetime.

Whilst this is a satisfactory explanation, the inhomogeneity in lifetime across a sample of beads is clearly an obstacle to using lifetime mapping as a basis for thermometry during microwave heating. The differences observed between beads are further highlighted in figure 3.15, a plot of the change in average lifetime of 7 of the beads pictured in table 3.3 as a function of temperature. The temperature dependence for each bead appears to be uniform, following a similar curve to that observed in the TCSPC experiment, although the lifetimes obtained are shorter. This is most probably as a result of the higher loading of RhdB here, which will increase self-quenching and shorten the lifetime.

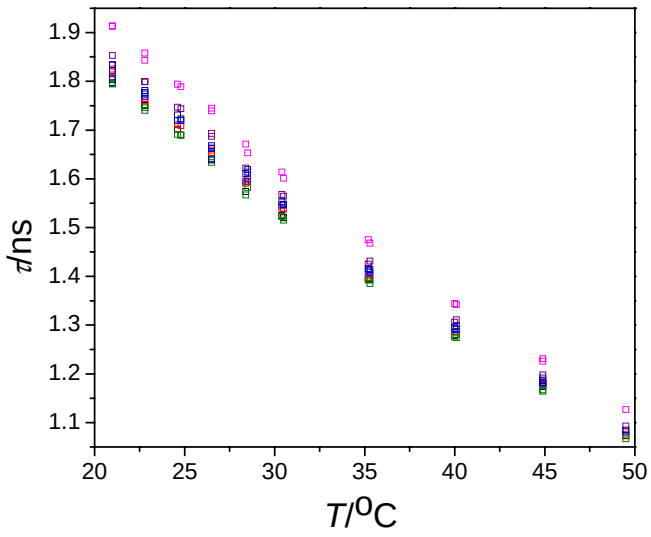

Figure 3.15: Average fluorescence lifetime of 7 RhdB-labelled PEGA resin beads (each represented by a different colour here) in water as a function of temperature. The data represents heat-up and cool-down between 20 and 50°C.

It was found that if, instead of plotting τ, the percentage change in τ from 21°C is plotted against temperature (figure 3.16), the curves for the beads are seen to overlap. That is, the percentage change for all beads as temperature increases to 50°C and decreases back to 21°C is, within a certain error, the same. The quadratic function,

$$\%\Delta\tau = 42.1 - 2.23T + 0.0113T^2, \qquad \textbf{3.7}$$

is a good fit of the behaviour. Solving the quadratic and simplifying yields an equation,

$$T = \frac{2.23 - \sqrt{3.08 + 0.0453(\%\Delta\tau)}}{0.0227}, \qquad \textbf{3.8}$$

for determining temperature from $\%\Delta\tau$.

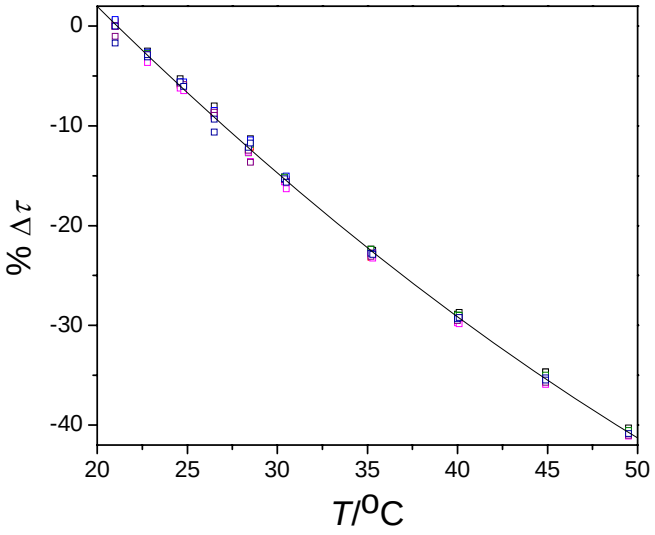

Figure 3.16: Percentage change in average fluorescence lifetime, % $\Delta\tau$, of 7 RhdB-labelled PEGA resin beads in water as a function of temperature. The data represents heat-up and cool-down between 20 and 50°C. The solid line is a quadratic fit to all the data points.

Therefore if τ is determined for a bead at 21°C, the temperature of that bead can subsequently be determined from a measurement of τ. In fact, from one measurement of τ for a bead at a known temperature, τ_T, and equation 3.7, the expected percentage change in τ for that temperature, $\%\Delta\tau_T$, can be determined. τ at 21°C, $\tau_{21\,°C}$, can then be predicted according to

$$\tau_{21°C} = \frac{\tau}{1 + \frac{\%\Delta\tau_T}{100}}. \qquad \textbf{3.9}$$

With this value, $\%\Delta\tau$ and consequently the bead temperature, T_{bead}, can be determined at any time thereafter from a single measurement of τ.

In fact, because τ recorded at 21°C after the heat-cool cycle was not exactly equal to that measured at the start of the heating cycle, $\%\Delta\tau$ at 21°C as determined from the quadratic fit is not exactly 0 ($\%\Delta\tau_{21\,°C} = 0.188$). Consequently the expression,

$$\tau_{21°C} = \frac{\tau}{1 + \frac{\%\Delta\tau_T - \%\Delta\tau_{21°C}}{100}}, \qquad \textbf{3.10}$$

should, for completeness, be used in place of equation 3.9. This level of exactitude is probably unnecessary: a difference of 0.188 appears negligible when the error in the measurement is considered. Nevertheless equation 3.10 will be used in determinations of temperature in the next section. The standard error (determined using Microsoft Excel[79]) for determining T_{bead} over the range 20-50°C from $\%\Delta\tau$ is 0.59°C.

The percentage change in fluorescence lifetimes of RhdB on water-swollen beads in hexane exhibit the same behaviour as they are heated to 50°C (figure 3.17). The data fits well to equation 3.7, but with a larger estimated error (± 0.65°C). However, points representing lifetimes measured during cool-down (not shown) deviated significantly from the curve as the lifetimes were shorter than those measured during heat-up. For example, the τ measured at 21°C for one particular bead was 1.715 ns after cool-down versus 1.801 ns before heating.

Clearly, heating and subsequently cooling the sample changes the average fluorophore environment, presumably by allowing hexane to ingress into the beads. Hexane would be expected to decrease the swelling of the bead (non-polar hydrocarbons are poor solvents for PEGA) and thus increase the effective fluorophore concentration. Moreover, increased hexane concentration would also decrease the polarity of the average fluorophore environment. Both of these effects are consistent with the observed reduction in fluorescence lifetime.

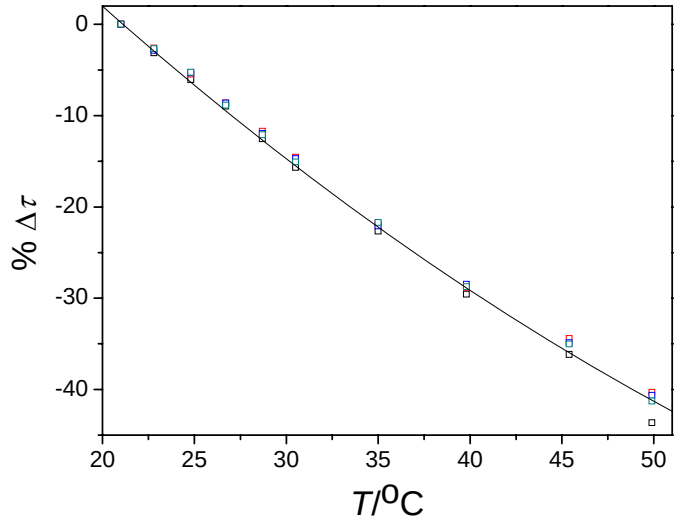

Figure 3.17: Percentage change in average fluorescence lifetime, % $\Delta\tau$, of 4 RhdB-labelled water-swollen PEGA resin beads in hexane as a function of temperature. The data represents a heat-up between 20 and 50°C. The solid line is a quadratic fit to all the data points.

Nonetheless, the results demonstrate that, provided the sample is not subjected to more than one cycle of heating, the temperature of water-swollen PEGA beads in hexane can be determined from the fluorescence lifetime of RhdB labels. The following section is a discussion of the results of utilising this temperature dependence to determine the difference, if any, between the temperature of the beads and that of the surrounding hexane during microwave heating.

Table 3.3: Lifetime maps of water-swollen RhdB labelled resin beads in water and in hexane at temperatures between 20 and 50°C. For each temperature an image of a collection of beads is shown alongside a close-up of a single bead. Pixel colour denotes fluorescence lifetime according to the pseudocolour scale included.

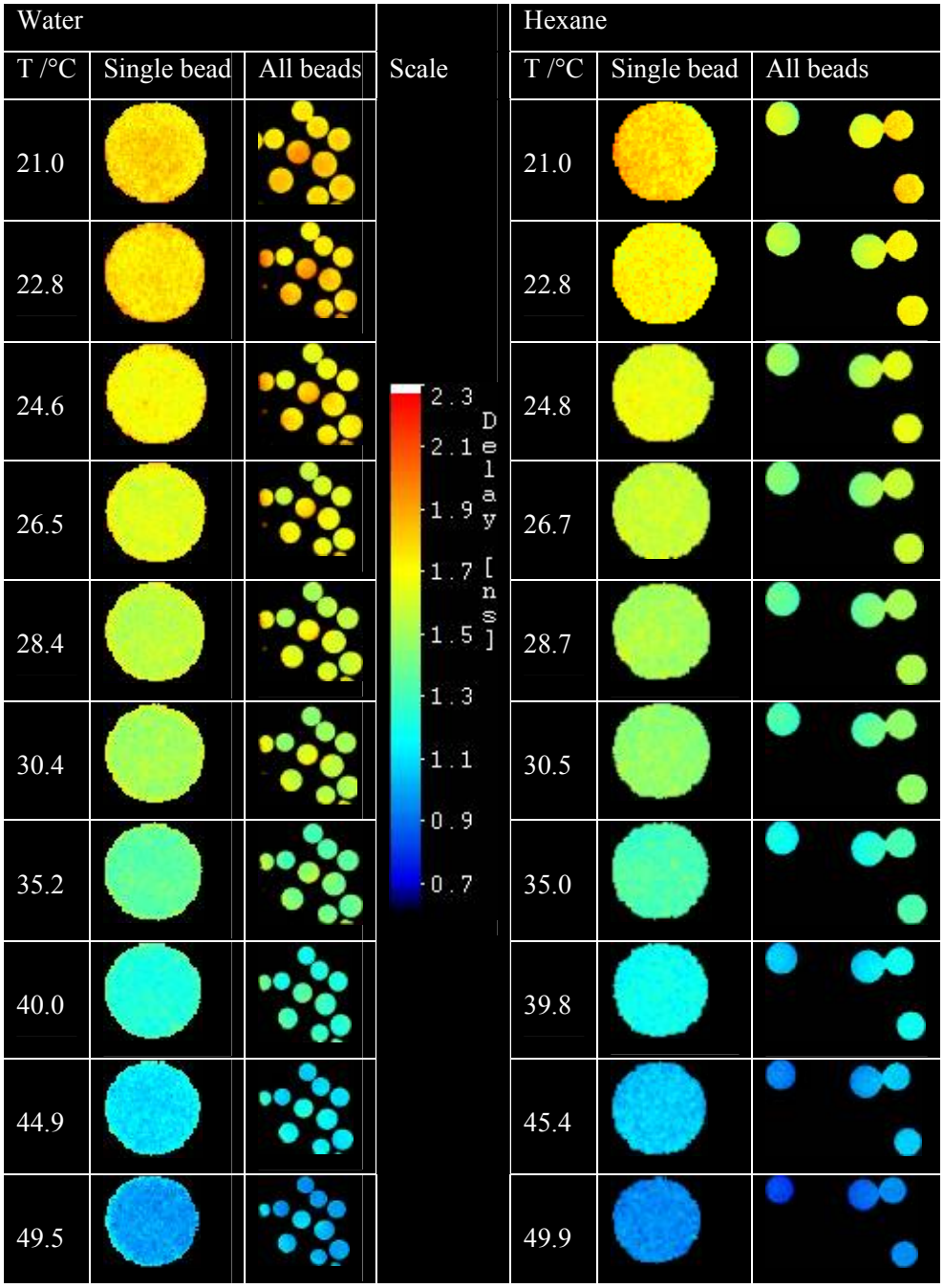

3.4.2.2 Measurement of the temperature of water-swollen PEGA resin in hexane from the fluorescence lifetime of a RhdB label during simultaneous microwave heating

A system was designed so as to offer the best chance of microwave heating resulting in thermal inhomogeneity. Therefore the temperature of water-swollen resin beads in hexane was determined during microwave heating. It is an artificial system in the sense that it would not be used in MA-SPOS. However, if no selective heating could be found for this system, as was the case for water-swollen resin in water (3.4.1), then it is most unlikely that any 'real' MA-SPOS system would exhibit inhomogeneous heating.

The results of probing temperatures after the sample had been heated to a quasi-thermal equilibrium state by microwaves are summarised in table 3.4. With the sample at thermal equilibrium with ambient conditions, T_{liquid} as measured by the fluoroptic probe, and T_{bead} are in agreement. This is dictated by the method as the initial calculation of $\%\Delta\tau_T$ (using equation 3.7) assumes, justifiably, that this is the case in order to determine temperatures at points in the future.

It was thought that after microwave heating, the beads - swollen as they are with strongly microwave-absorbing water - might be at a higher temperature than the surrounding hexane, which has a much lower *tan* δ (0.020 versus 0.123 at 20°C and 2.45 GHz). However, the results in table 3.4 indicate that this is not the case: T_{liquid} and T_{bead} are, within the estimated error, the same for both beads after quasi-equilibrium has been achieved with a microwave power levels of both 50 and 100 W. If the beads do heat selectively, which is almost certainly the case, they equilibrate with the surrounding hexane over a timescale shorter than the measurement of the fluorescence lifetime.

Table 3.4: Comparison of the temperature of the liquid phase, T_{liquid}, (as measured by a fluoroptic probe) and the temperature of two water-swollen beads, T_{bead}, (as determined from the fluorescence lifetime, τ_{bead}, of RhdB attached to the resin according to equations 3.8 and 3.10) after thermal equilibrium had been achieved with different microwave irradiation conditions.

Microwave power/W	T_{liquid}/°C	τ_{bead1}/ns	T_{bead1}/°C	τ_{bead2}/ns	T_{bead2}/°C
0	22.2	1.65	22.2 ± 0.5	1.59	22.2 ± 0.5
50	26.2	1.53	26.4 ± 0.5	1.47	26.3 ± 0.5
100	30.0	1.45	29.4 ± 0.5	1.40	29.3 ± 0.5

It was thought that quickly measuring lifetime maps *during* heating would give the best chance of observing thermal inhomogeneity in the sample as the system would have less time to equilibrate. Care was taken in preparing the sample to ensure that a larger number of beads could be mapped for this experiment, giving a better indication of the error of the results (table 3.5). The timescale of fluorescence lifetime mapping was such that, over the course of the measurement, T_{liquid} increased significantly with applied microwaves. Therefore a temperature range is quoted.

Table 3.5: Comparison of the temperature of the liquid phase, T_{liquid}, (as measured by a fluoroptic probe) and the temperature of five water-swollen beads, T_{bead}, (as determined from the fluorescence lifetime, τ_{bead}, of RhdB attached to the resin according to equations 3.8 and 3.10) during heating with different microwave irradiation conditions. For clarity, τ_{bead} is not shown in this table.

Microwave power/W	T_{liquid}/°C	T_{bead1}/°C	T_{bead2}/°C	T_{bead3}/°C	T_{bead4}/°C	T_{bead5}/°C
0	21.8	21.8	21.8	21.8	21.8	21.8
100	21.8-22.4	21.7	21.9	21.4	22.1	21.9
200	22.4-23.8	23.3	23.2	22.7	23.9	23.0

No evidence of selective heating of the beads is observed: during microwave heating at both power levels T_{bead} is, within the estimate of error, the same as T_{liquid} during the lifetime measurement. T_{bead} varies significantly across the sample (22.7 to 23.9°C at 200 W) but the variation is within the standard error in the measurement. The system, as probed by this method, is continually seen to be in thermal equilibrium because the rate of heat transfer is too great compared to the timescale of the measurement.

A time constant for the conductive dissipation of thermal energy from a sphere of water of radius a can be estimated from

$$\tau_\kappa \approx \left(\frac{1}{4\pi}\right)\frac{C\rho}{\kappa}a^2 \text{ .}^{14} \qquad \textbf{3.11}$$

For a sphere in water (at 298 K heat capacity per unit volume, $C\rho$, = $4.2\cdot10^6$ J m^{-3} and thermal conductivity, κ, = 0.6 W m^{-1} K^{-1} s^{-1}), the time constant will be of the order of $5\cdot10^5\cdot a^2$. Therefore if we approximate the water-swollen resin bead to a sphere of water of radius $5\cdot10^{-4}$ m (500 μm) we arrive at an estimate for the time constant of the thermal re-equilibration of $2.5\cdot10^{-2}$ s. The relaxation will be longer in hexane (at 298 K $C\rho = 2.3\cdot10^6$ J m^{-3} and $\kappa = 0.12$ W m^{-1} K^{-1} s^{-1}) but still orders of magnitude shorter than the timescale of the measurement, which was of the order of $1\cdot10^2$ s.

As a general rule, a system can be treated as if it were in thermal equilibrium if the rate of the change of absolute temperature, $dT/dt \ll T/\tau_\kappa$.[14] The shortness of the time constant for this system means that a very large heating rate ($T/\tau_\kappa \approx 300/2.5\cdot10^{-2} \approx 12000$ K s^{-1}) would be required for the system to be away from thermal equilibrium. As it is, dT/dt was approximately 0.03 K s^{-1}.

Thermal inhomogeneity was observed in the previously mentioned report of *in-situ* measurement of temperature during microwave heating of aqueous solutions,[67] but there the volume of the region of solution being heated ($a \approx 1\cdot10^{-2}$ m) and heating rate ($dT/dt \approx 2$ K s^{-1}) were much greater and the measurement time ($5\cdot10^{-1}$ s) much shorter. dT/dt and T/τ_κ (≈ 6 K s^{-1}) were comparable, and the system was therefore not in thermal equilibrium.

3.4.3 Conclusions

A novel technique for spatially-resolved measurement of temperature by fluorescence lifetime imaging microscopy has been demonstrated. Lifetime maps of fluorophore covalently attached to beads of SPOS resin were used to determine the bead temperature during conventional and microwave heating. Visual inspection of the lifetime maps of a sample of resin beads over a range of temperatures shows that a difference of 2°C can be discerned. By plotting the percentage change of the average lifetimes of individual beads as a function of temperature, the temperature of beads can subsequently be determined with an estimated error of better than ±1°C.

Selective microwave heating of the MA-SPOS system was not observed. This was despite the fact that the liquid and solid phase components of the system were chosen to have a much greater difference in microwave susceptibilities than would be found in a 'real' SPOS system. In addition, the bead and liquid temperatures were probed *during* heating so that the more susceptible component of the system is being continually pumped with energy and therefore less able to thermally equilibrate with the other component. We conjecture the thermal conductivity of the liquid media is sufficiently good to result in the system re-equilibrating before any selective heating can be observed. Estimates of the time constant for re-equilibration suggest that, for the heat-up rates used here, the system is effectively in equilibrium.

3.5 Overall conclusions and outlook

3.5.1 Thermal inhomogeneity in MA-SPOS

Two related novel techniques for *in-situ* determination of the temperature of suspended solid-phase organic synthesis resin beads during microwave heating have been demonstrated. Both rely on the temperature sensitive response of the fluorescence lifetime of a dye, Rhodamine B, covalently attached to the resin. The first technique uses time-correlated single photon counting to determine the lifetime, and therefore temperature, within the resin component of the sample as a whole. The second method, using fluorescence lifetime imaging microscopy, yields a 2-D map of lifetime that can be scaled to indicate the distribution of the temperature of specific beads.

The bulk, component-specific measurement of resin temperature was used to determine the temperature difference between water-swollen resin and the water in which it was suspended during microwave heating. The second, spatially-resolved technique was used to probe the temperature of water-swollen beads in hexane. The two components of this system were chosen for the large difference between their microwave susceptibilities in order to maximise the possibility of selective heating by microwaves. This system does not suspend well and would not be observable by the first method.

Both techniques were found to be reliable, accurate and precise to within an error of better than ± 1°C. However, in neither case was any selective heating of the resin by microwaves observed. From estimates of the thermal relaxation time constant for a heated resin bead it is calculated that the system is effectively in thermal equilibrium for the heating rates used. Therefore, even if the resin is selectively heated, the small size of the beads and the good thermal conductivity of the system determine that thermal inhomogeneity would only occur in MA-SPOS when heating rates approach hundreds or thousands of degrees per second. Even microwave flash heating is not this rapid. Therefore both calculation and experiment agree that thermal inhomogeneity due to selective heating of the resin in MA-SPOS is not a problem.

3.5.2 Other applications for the technique

Whilst the relative temperature of the components of MA-SPOS is now not in doubt, the determination of the temperature of the system as a whole is still often problematic. The difficulties in thermometry in microwave-heated systems were discussed in chapter 1. Current commercial laboratory microwave applicators predominantly use infrared temperature measurement, as fluoroptic probes tend to be less robust and are difficult to incorporate in closed-vessel systems. However, infrared thermometry is essentially a surface temperature measurement and requires calibration to obtain representative values for the bulk.

It has been shown that the temperature determined for dye-labelled resin beads are representative of the bulk; therefore they could be used simply as thermometers. The beads described here are limited to use in solvents in which the resin will swell and in which the dye has a significant temperature response, narrowing their applicability to aqueous and alcohol systems. However, beads fabricated from more inert materials, such as glass or silica, and impregnated with inorganic fluorophores could be used in all but the most aggressive environments. The

temperature dependence of the lifetimes of inorganic "thermographic phosphors" such as Y_2O_3:Eu have been utilised extensively in thermometry applications[8], forming the basis of most fluoroptic probe techniques. Remote probing of phosphor-containing beads could offer robust and highly sensitive (± 0.05°C) thermometry for microwave-heated systems.

Broadening the perspective further, the same principle could be used for determining the temperature in specific components or regions of solid-state microwave-assisted synthesis or in any applications where thermal inhomogeneity might be expected.

3.5.3 Microwave susceptible beads

It was noted in section 3.1.3 that the choice of solvent for MA-SPOS is crucial as it must be compatible with the resin and have reasonable microwave susceptibility. This limits the chemistry that can be carried-out as solution phase components must also be compatible with the solvent. Therefore SPOS resin beads that are themselves microwave susceptible would remove one of the criteria for solvent choice and make different chemistries more accessible.

It has been shown in this report that, for beads of the size typically used in SPOS, even if microwave heating is selective for the bead it will not lead to thermal inhomogeneity. Therefore microwave-susceptible beads could facilitate the homogenous microwave heating of SPOS suspensions in microwave-transparent solvents (assuming that the suspension is adequately agitated to remove bulk thermal gradients). This was effectively demonstrated by the heating of a suspension of water-swollen beads in hexane.

Incorporating conductive species into the resin would yield more robust microwave-susceptible beads. This could be done by entrapment of particles of metal or graphite during formation of the beads, or by grafting or copolymerisation with conductive polymers. The preparation of composite resin beads containing conducting polymers has been demonstrated, although for different reasons.[82] Producing composite beads for MA-SPOS would almost certainly be challenging – preparation of SPOS resin beads is a notoriously *black* art[46] – but would allow the benefits of microwave heating to be utilised over an even broader spectrum of polymer-supported chemical technologies.

4 *In situ* probing of the effects of microwave irradiation upon structural changes in model biological systems

In chapter 1 the question of whether or not low power microwave radiation, such as that emitted by mobile telephones, could perturb living systems to an extent sufficient to cause damage was discussed. This highlighted the lack of research carried out to investigate the possibility of specific microwave excitation of relatively large biological molecules and systems such as proteins and lipid membranes. In this chapter, two novel *in situ* techniques for directly probing the structural changes of model biological systems during microwave irradiation are described.

The first technique utilises small angle neutron scattering to probe the transitions between various polymorphic phases of a phospholipid system as it is heated, both conventionally and with microwaves. The second technique allows the thermally induced folding/unfolding of a protein to be followed by means of circular dichroism spectroscopy during simultaneous microwave irradiation. The techniques were used to discern whether or not irradiation results in any measurable differences in the transitions probed compared to samples heated conventionally. The results of these experiments are discussed with reference to the extent to which they provide evidence for or against non-thermal microwave interactions.

4.1 In situ probing of thermally induced phase transitions of a model membrane lipid, DOPE-Me, in the presence of microwaves

4.1.1 Introduction

4.1.1.1 Interactions between microwaves and lipids

It has been previously proposed that specific excitation of polar lipid molecules found in biological membranes could provide a mechanism of interaction between microwaves and living systems. It was suggested that an electric field oscillating at microwave frequencies could resonate with correlated motions of lipids in a collective response of the membrane system to the field.[83] Alternatively, an applied field could be expected to induce a dipole in individual lipid

molecules.[84] These moments would be parallel in adjacent lipids, and therefore repulsive. The effect of both hypothetical interactions would be to decrease the structural order of the system. This has been experimentally probed by testing the effect of microwaves upon the permeability of membranes. Testing *in vivo* is often difficult due to problems with reproducibility, therefore planar lipid bilayer membranes are frequently used as models of biomembranes. The effect of microwave exposure upon their permeability has been probed using a variety of techniques.

The degree of leakage of fluorescent dye from liposomes exposed to microwaves has been measured and was found to be the same as for liposomes conventionally heated to the same extent.[85,86] Liposome permeability as probed by light scattering was found to be greater for samples exposed to microwaves for 5 hr than for samples thermostated at the same temperature over the same period.[87] IR and NMR spectroscopy indicate that this is due to structural changes in acyl chain packing with no appreciable changes to the headgroup. Conductivity measurements have been used to probe ion transport across bilayer membranes during microwave exposure.[88] Changes in current and capacitance do not suggest a resonance effect and are commensurate with a small increase in temperature.

In most studies changes to the structure of membranes have been tested after exposure to microwaves or have been indirectly probed by measurement of related properties of the system. The study reported herein is the first to directly measure changes in the structure of a lipid system *in situ* during microwave heating. A model lipid, DOPE-Me, was probed by small angle neutron scattering during both microwave and conventional heating.

4.1.1.2 DOPE-Me

1,2-dioleoyl-sn-glycero-3-phosphoethanolamine-N-methyl (DOPE-Me, also known as N-Monomethylated dioleoylphosphatidylethanolamine) has been widely used as a model lipid in studies to improve understanding of membrane fusion and the effect of additives upon it (e.g.[89]), largely because it readily forms non-lamellar phases. At room temperature, vesicles of the lipid in water dispersions form in a lamellar (L_α) phase. However, as the molecule (figure 4.1) is cone-shaped, having a greater cross-section at the fatty acid end than at the polar headgroup, it experiences monolayer curvature strain. At higher temperatures (> 50 °C) this strain overcomes the energy cost of bilayer disruption allowing the layers to separate and form into other phases (figure 4.2): the inverse cubic phase (the so-called plumber's nightmare, Q_{II}) and the inverse

hexagonal phase (H_{II}). The behaviour of the system around these transitions is complex and governed at least partly by kinetics.[90,91] Lamellar and non-lamellar phases can exist simultaneously over a range of temperatures and, at a given temperature, competition between Q_{II} and H_{II} is determined not only by the relative thermodynamic stability of the phases, but also by their rates of formation.

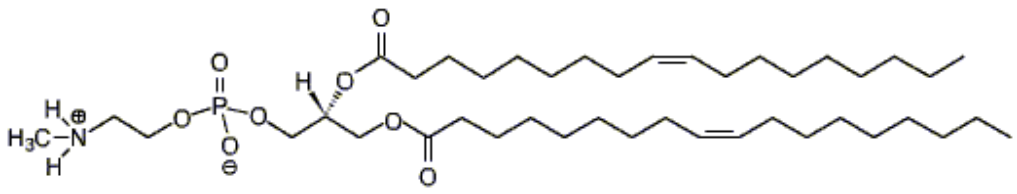

Figure 4.1: DOPE-Me.

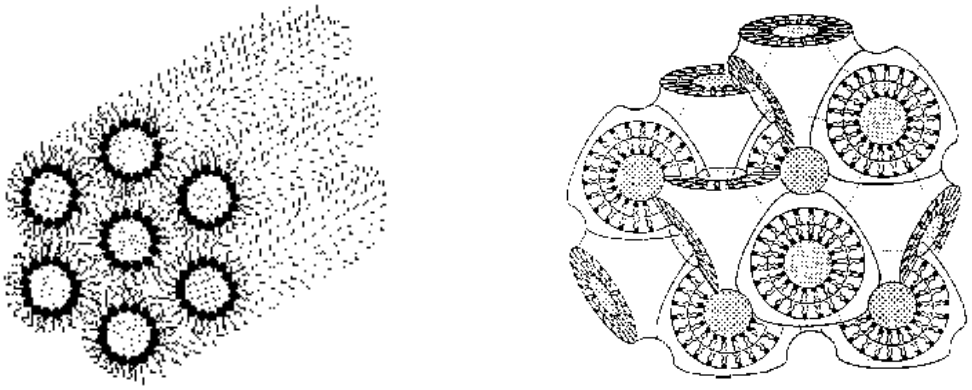

(a) **(b)**

Figures 4.2 (a) and (b): Schematics of the structure of the a) inverted hexagonal and b) inverted cubic phases.

4.1.1.3 Small angle neutron scattering (SANS) as a probe of lipid polymorphic structure [92]

A typical chemical bond is 0.1 nm (1 Å) long. A lipid having one or more C_{18} alkyl chains and a headgroup of 10 bonds length, as DOPE-Me does, can therefore be expected to have a length of around 3 nm and form a lamellar structure with a repeat distance of around 6 nm. Thermally moderated neutrons produced at research facilities typically have associated wavelengths of

between 0.1 and 1 nm (*c.f.* 400-700 nm for visible light) and is therefore ideal for probing the structure of these systems by means of elastic scattering. X-rays with comparable wavelengths can be generated and are also used for diffraction studies of lipid polymorphism. However, there is a fundamental difference between scattering of neutron and electromagnetic radiation. Whereas light and X-rays are scattered by the electrons surrounding atomic nuclei, neutrons are scattered by the nuclei themselves.

The main consequence of this is that the neutron scattering cross-section of an atom is not proportional to the number of electrons, and hence atomic number, *Z*, as with X-rays, but rather varies irregularly with *Z*. Thus neutrons can easily differentiate between different elements and isotopes, which makes them particularly useful in solving crystallographic structures of large molecules. In addition, because the interaction between neutrons and matter is weak, neutron radiation is much more penetrating than X-rays. Therefore samples with relatively long pathlengths or samples in unusual sample environments (furnaces, cryostats *etc.*) can be probed.

The diffraction pattern produced from a small angle neutron scattering (SANS) experiment can yield information about size, shape and orientation of species such as lipids. The dependent variable measured in a SANS experiment is the differential cross-section, given by the expression,

$$\frac{\delta\sigma}{\delta\Omega}(Q) = N_p V_p^2 (\Delta\delta)^2 \, P(Q) S(Q) + B_{inc}, \qquad \textbf{4.1}$$

where N_p is the number concentration of scattering bodies (subscript 'p' for 'particle'), V_p is the volume of one scattering body, $(\Delta\delta)^2$ is the square of the difference in neutron scattering length density (known commonly as the contrast), $P(Q)$ is the shape factor, $S(Q)$ is the interparticle structure factor, Q is the modulus of the scattering vector and B_{inc} is the incoherent background signal. It is beyond the scope of this review to explain all the terms in this equation, but this information is well covered elsewhere.[92,93]

The differential cross section is determined from the recorded flux of scattered radiation, $I(\lambda,\theta)$, and a knowledge of certain instrument and sample-dependent parameters. For a detector element

of dimensions $dx \times dy$ positioned at a distance, L, and angle, θ, the flux scattered into a solid angle element $\Delta\Omega$ ($= dx\, dy / L^2$) is related to the differential cross-section according to

$$I(\lambda,\theta) = I_0(\lambda)\Delta\Omega\eta(\lambda)TV\frac{\delta\sigma}{\delta\Omega}(Q), \qquad \textbf{4.2}$$

where I_0 is the incident flux, η is the detector efficiency, T is the sample transmission and V is the volume of sample illuminated by the beam.

In a SANS experiment the differential cross-section is measured as a function of the scattering vector, Q, to give a diffraction pattern. Q is the magnitude of the difference between the incident, k_i, and scattered, k_s, wavevectors (figure 4.3) and is given by

$$Q = |Q| = |k_s - k_i| = \frac{4\pi}{\lambda}sin\frac{\theta}{2}. \qquad \textbf{4.3}$$

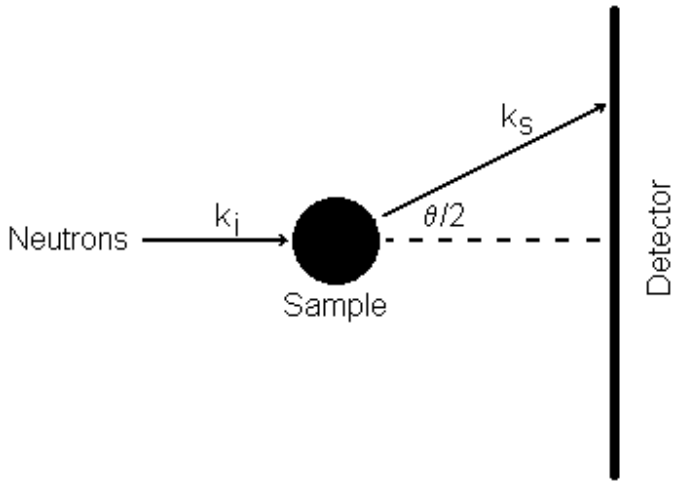

Figure 4.3: Incident, k_i, and scattered, k_s, wavevectors resulting from the elastic interaction of a neutron beam with a scattering sample and the angle subtended between the two, $\theta/2$.

By substituting into Bragg's law of diffraction,

$$\lambda = 2d\,.sin\frac{\theta}{2}, \qquad \textbf{4.4}$$

it is possible to convert a peak in Q into a distance,

$$d = \frac{2\pi}{Q}. \qquad \textbf{4.5}$$

A distance could relate to a lamellar repeat length or a cell parameter of a cubic or hexagonal structure. Q therefore has units of inverse length (typically $Å^{-1}$).

4.1.2 Experimental

4.1.2.1 Sample preparation

DOPE-Me was added to D_2O, agitated using a vortex mixer and freeze/thawed 6 times using liquid nitrogen to yield a 1 mM white suspension. DOPE-Me was purchased from Avanti Polar Lipids. D_2O was obtained from Aldrich. The sample was placed in 2 mm quartz cuvettes.

4.1.2.2 Conventional and microwave heating during diffraction

A heater/sample changer manufactured at ISIS was used for conventional heating. The samples are supported in a metal block heated by a circulating water bath and the assembly is insulated and enclosed. The bath is controlled remotely and the temperature of the sample environment is logged automatically.

Microwave heating was carried out using a bespoke waveguide applicator (figure 4.4) attached to an Aztex AX2110 1 kW generator. A PTFE holder attached to a removable plate holds the cuvette in the centre of the waveguide, in line with the neutron beam passing through ports in the long sides of the guide. A step motor allows movement of the terminal end of the guide to change the position of the microwave field maximum relative to the sample. A fluoroptic probe (Neoptix T1) immersed in the sample such that the tip is at the same height as the centre of the beam allows direct monitoring of sample temperature. A signal is fed from the fluoroptic conditioner to a PC that maintains the desired temperature by varying the power output of the microwave generator.

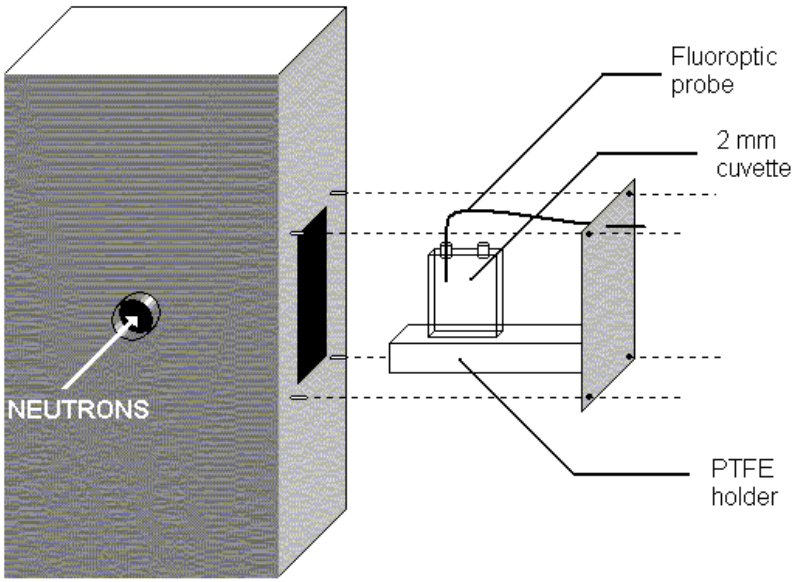

Figure 4.4: Bespoke waveguide applicator for heating of samples during *in situ* neutron diffraction.

4.1.2.3 In situ neutron diffraction

Neutron scattering experiments were carried out at the ISIS facility (Oxford, UK) using the LOQ instrument. ISIS is a spallation neutron source using a 200 μA, 800 MeV synchroton operating at 50 Hz to accelerate and direct protons at a tantalum target, producing circa 12 neutrons per proton impact. LOQ, the SANS instrument at ISIS, has a Q-range of 0.06-10 nm^{-1}.

Diffraction patterns were taken as temperature was stepped between 35 and 68°C. Step size was initially 5°C but was decreased above 50°C to capture more information around the phase transitions.

4.1.3 Results and Discussion

Figures 4.5 (a) and (b) show the patterns taken during conventional and microwave heating and the evolution of the pattern as temperature was increased. Figures 4.6 and 4.7 show the same data but mapped onto a real temperature scale and plotted as 2D (4.6) and 3D (4.7) contour plots.

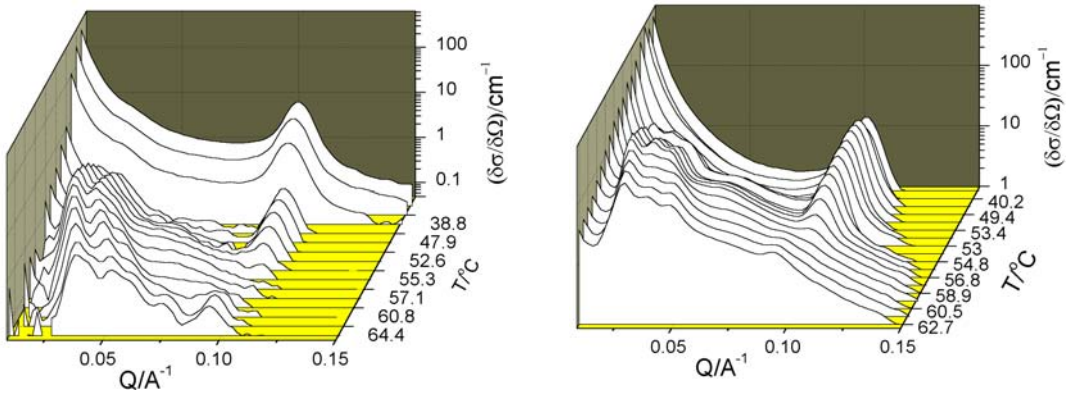

(a) **(b)**

Figures 4.5 (a) and (b): Evolution of SANS patterns for Me-DOPE during a) conventional and b) microwave heating.

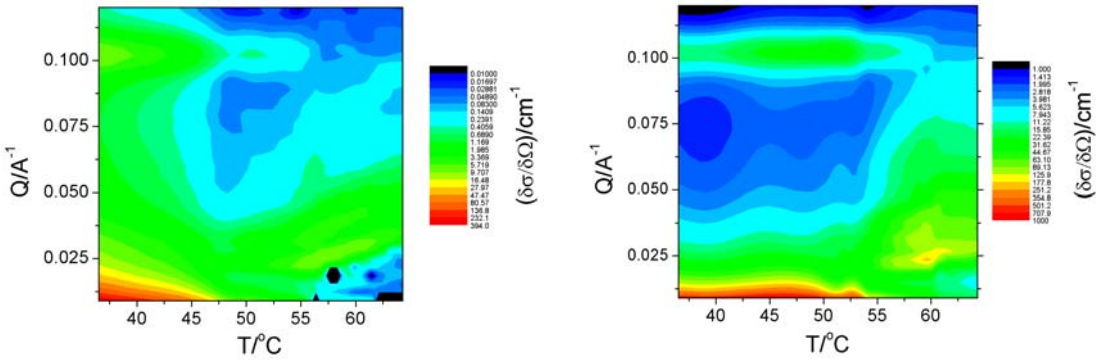

(a) **(b)**

Figures 4.6 (a) and (b): 2D contour plots of the change in the SANS pattern of Me-DOPE as a function of temperature for a) the conventionally heated sample and b) the microwave heated sample.

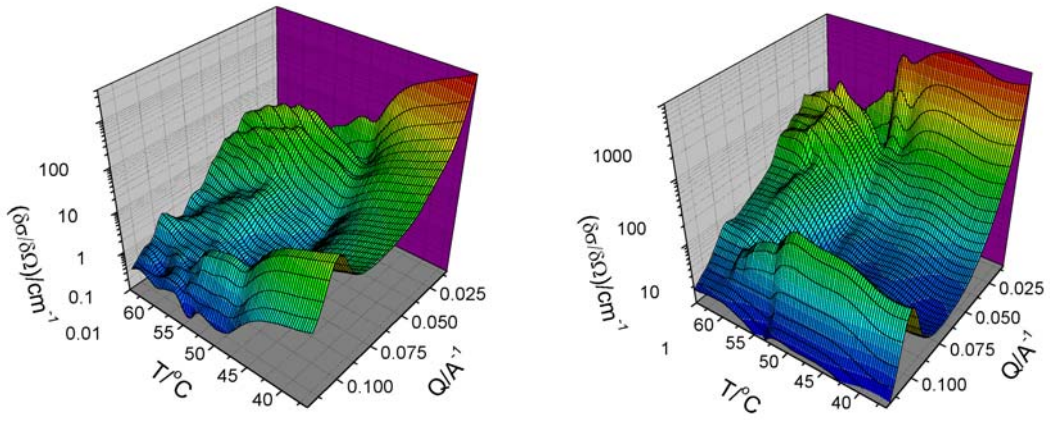

(a) **(b)**

Figures 4.7 (a) and (b): 3D contour plots of the change in the SANS pattern for Me-DOPE as a function of temperature for a) the conventionally heated sample and b) the microwave heated sample

The most noticeable difference between the conventionally and microwave heated cases is that the value of differential cross-section at any given Q is initially lower for the conventionally heated system and decreases further with temperature (particularly above 45 °C) whereas it remains relatively constant for the microwave heated system. There are two possible explanations for this.

The first is that the preparation of the lipid suspensions was not sufficiently standardised. Samples were agitated using a vortex mixer until the suspension appeared uniformly turbid. Therefore some samples could have been agitated for different amounts of time and could potentially have different amounts of suspended lipid or different sized vesicles. This could explain the differences in initial intensity. Secondly, as the sample is heated some of the lipid becomes less well suspended and floats to the top of the vessel. Depending on the relative position of the neutron beam the amount of lipid 'seen' by the neutrons could therefore decrease as the temperature increases and lipid floats above the neutron-probed volume of the cell. This would result in a fall-off of the observed intensity with temperature.

Both of these factors, and others, could feasibly be contributing to the problems in the reproducibility between heating methods. Because of this it is not useful to directly compare the

intensity of peaks for the microwave and conventionally heated systems at a given temperature. However, by plotting the position (figure 4.8) and height (figure 4.9) of the principal peaks as a function of temperature, it is possible to observe the evolution of the different phases and compare the temperatures at which they appear and disappear for the two heating methods. The position and height of the peaks plotted were determined at each temperature either by fitting to a Gaussian model, in the case of the best-resolved peaks, or by using the peak finding tool in the Origin graphing and data analysis software.[37]

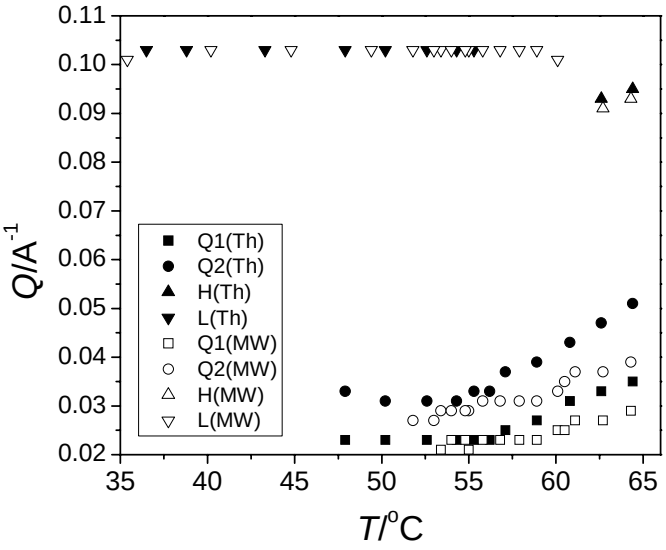

Figure 4.8: Change in the position of peaks corresponding to the lamellar phase (L), the cubic phase (Q1 and Q2) and the hexagonal phase (H1) as a function of temperature for conventionally (Th) and microwave (MW) heated samples.

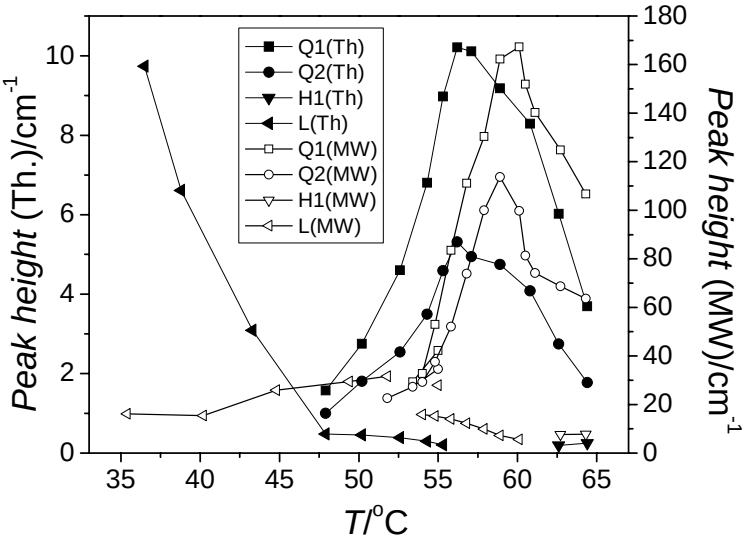

Figure 4.9: Change in the height of peaks corresponding to the lamellar phase (L), the cubic phase (Q1 and Q2) and the hexagonal phase (H1) as a function of temperature for conventionally (Th) and microwave (MW) heated samples.

At low temperatures a sharp diffraction feature at Q = 0.10 Å^{-1} is observed. This corresponds to a lamellar repeat distance of 61 Å, which is consistent with previous reports.[90,89,91] Above around 50ºC peaks are observed at Q ~ 0.02 and 0.03 Å^{-1} (d ~ 270 and 200 Å). Above 58ºC a third peak can also be resolved in the microwave-heated sample at Q ~ 0.04 Å^{-1}. Fitting the patterns recorded at 64ºC to a multiple gaussian model allowed 5 peaks to be resolved for both heating systems. The peaks are in a spatial ratio of √2: √3: √4: √6: √8 and therefore most likely correspond to the (110), (111), (200), (211) and (220) reflections of the Q_{II} phase described by Gruner *et al*.[91] At 62ºC and above a final peak is observed for both heating systems at Q ~ 0.095 Å^{-1} (d ~ 65 Å). This can be ascribed to the principal reflection of the H_{II} phase that is known to form after the Q_{II} phase.

Comparing the plots for the different heating methods reveals differences in the temperatures of formation of the different phases. Apart from the sharp fall-off of the height of the lamellar peak observed in the conventionally heated sample over the range 36 to 48°C, possible reasons for which are stated above, the plots for the different heating methods have very similar profiles although they appear to be shifted relative to one another in temperature. In both cases the position of the lamellar peak is almost completely constant until it disappears at 56 and 60°C for

the conventionally and microwave heated cases respectively. There are similar offsets in the temperature of the first appearance (at 48 and 52°C), the maximum height (at 56 and 60°C) and the change in position of the Q_{II} peaks. However, the first observed appearance of the H_{II} phase is at the same temperature (62°C) for both heating methods.

All of the above observations indicate that the transition from lamellar to cubic phase occurred at a higher temperature when the lipid sample was heated by microwaves. Before speculating upon the nature of a microwave-specific effect on lipid phase transitions other possible reasons for the observed differences should be considered.

One problem when probing the phase behaviour of lipids is in definitively stating the temperature of transitions. It is difficult to discern where one phase ends and another begins, as phases often co-exist and the temperature at which reflections characteristic of a certain phase appear and disappear is dependent upon the resolution of the patterns obtained. Determining the points of phase appearance or disappearance by extrapolating to a point of zero peak height would require an understanding of the evolution of the peak height with temperature that cannot be justifiably inferred from the data. For this reason no transition temperatures are reported here. However, a temperature difference is clearly observed in the phase formation of lipid heated by different methods. It is apparent, not only in the temperature at which the Q_{II} phase is seen to appear and disappear but in the entire evolution of the phase, whether followed by the change in peak position or height.

There are certain factors that are known to affect reproducibility in DOPE-Me systems. Gagne *et al*[94] state that it is imperative to start from a common state; therefore they incubated samples at 0-2°C over a period of 24 hr. Gruner *et al* state that several freeze/thaw cycles, as were carried out here, should be sufficient to reset the system.[91]

Cherezov *et al*[90] observed that the behaviour of the system is also very sensitive to the rate of heating as phase formation is governed at least partly by the rates of formation of competing phases. Doubling the ramp rate from 1 to 2 °C.hr^{-1} resulted in their observed L_{α}/Q_{II} transition temperature, $T_{L/Q}$, increasing from 58 to 62 °C. Therefore it is clear that ramp rate could cause variation in the transition temperature to the extent observed here.

The average ramp rate below 56°C (figure 4.10) was greater for the microwave-heated case due to the greater efficiency of this heating method. A higher $T_{L/Q}$ would therefore be expected for this sample. However, it is difficult to state how much higher as ramp rate varied significantly during the course of the heat-up. This is mainly because patterns were recorded at smaller temperature steps around the phase transitions but also because the importance of heating rate was not fully appreciated at the time of carrying out the experiment and repeating the experiment was not possible because of limited access to the facility.

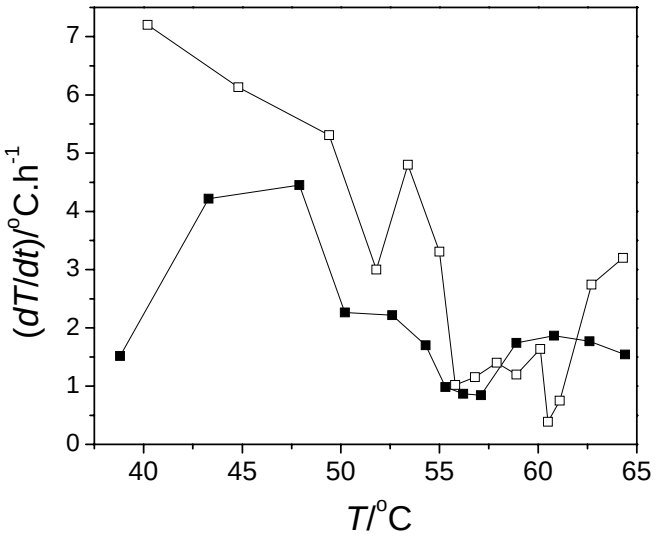

Figure 4.10: Rate of conventional (solid squares) and microwave (open squares) heating during as a function of temperature.

The difference in the observed $T_{L/Q}$ could also be due to the temperature recorded for samples, T_{rec}, not being representative of the temperature of the lipid sample 'seen' by the neutrons, T_{lipid}. Either T_{rec} for the microwave-heated sample was higher than T_{lipid}, or T_{rec} for the conventionally-heated sample was lower than T_{lipid}.

The conventionally-heated sample was left for more than 15 min at each temperature so that the sample temperature could equilibrate with the temperature of the environment before recording the scattering pattern. Any thermal gradient would therefore be small and would be expected in the other direction; i.e. the sample temperature could lag behind that of the environment and

therefore be cooler at a given time. It is therefore highly unlikely that T_{rec} should be 4°C lower than T_{lipid}.

Temperature gradients could feasibly exist in the sample heated by microwaves. As discussed in chapter 1, masses heated by microwaves are often hotter at the centre than they are towards the outside surface. However, for the phase behaviour difference to be explained by thermal inhomogeneity, the opposite would have to be true; the temperature recorded by the fluoroptic probe towards the side of the cell, T_{rec}, would have to be greater than the temperature of the neutron-probed sample volume, T_{lipid}, at the centre of the cell.

The way in which microwaves were applied in this experiment might be expected to produce a thermal gradient in the direction of wave propagation. As the magnitude of the microwave field strength varies along the length of the waveguide it is conceivable that there would be variation in temperature in the sample cell in the same direction. However, the fluoroptic probe was positioned such that the tip was level with the centre of the neutron beam in this direction in order to negate this effect.

Bulk thermal inhomogeneities can therefore not explain the different phase behaviour observed in the microwave and conventionally heated samples. However, the higher temperature of Q_{II} formation when heated by microwaves could be explained by a smaller scale thermal gradient. Each of the different polymorphic lipid phases consist of regions made up of water and regions made up of the alkyl chain portion of the lipid molecules. The water rich regions would be expected to absorb a great deal more microwave energy than the alkyl chain regions. This could result in a thermal gradient whereby the lipid molecules making up the alkyl chain region would experience a lower temperature than the bulk. Non-lamellar phases would therefore appear to form at higher measured temperatures.

However, for this thermal gradient to be set-up the transfer of thermal energy between the water molecules and the lipid molecules would have to very poor. The system is relatively fluid and the head portions of the lipid molecules are in intimate contact with the water region. Efficient transfer of energy would therefore be expected. The timescales for the thermal relaxation for much larger entities were estimated in chapter 3 and found to be much too short to allow thermal inhomogeneity to be sustained.

It appears that an additional effect would have to be at play in order for a thermal gradient to be responsible for the observed increase in the Q_{II} transition temperature. The possibility of explaining the observations by means of athermal microwave effects should therefore be discussed.

The coherent resonance of lipid systems, as proposed by Frölich (but discounted by Adair[13]), would, to some extent, disrupt the lamellar phase. As the transition to non-lamellar phases requires bilayer disruption it might be expected that irradiated samples would undergo the transition at a lower temperature. However the opposite was observed in this experiment. From a thermodynamic perspective the results suggest that, at a given temperature, either the lamellar phase is more stable, or the cubic phase is less stable when heated by microwaves. This could be explained by the different responses to microwave irradiation that would be expected for these phases.

The polar head regions of lipid molecules possess dipoles that would be expected to attempt to align with the electric field component of an applied microwave field and therefore with each other. In the lamellar phase, although bilayers are slightly curved, forming 'onion skin' vesicles over large scales, neighbouring lipid molecules and therefore their dipoles are similarly aligned. Alignment of the dipoles to the applied field would not cause major disruption to the overall structure. However, in the cubic phase lipid orientation varies over a much smaller scale. This phase would therefore be relatively destabilised by the impetus for lipid alignment. The hexagonal phase and transition structures that are believed to form during phase transitions, such as the stalks and trans-monolayer contacts proposed by Cherezov,[90] would also be destabilised by this effect. However, as the hexagonal polymorphic structure only varies in 2 dimensions, as opposed to 3 in the cubic phase, it would be destabilised to a lesser extent than the cubic phase.

The extent of destabilisation for each of the phases would therefore be in the order $Q_{II} > H_{II} > L_{\alpha}$. Therefore this effect would explain the differences in the phase behaviour observed when lipid sample is heated by microwaves: the larger temperature range over which L_{α} exists before Q_{II} begins to preferentially form and the lesser range over which Q_{II} exists before the transition

to H_{II}, although this second observation is only evidenced by the two data points corresponding to the hexagonal phase.

4.1.4 Conclusions

Bespoke microwave heating equipment was used to carry out the first *in situ* probing of the polymorphic structure of a lipid, DOPE-Me, during microwave heating. A significant difference was observed in the evolution of the system when compared to a conventionally heated sample; the transition from the initial lamellar phase to the cubic Q_{II} phase occurred at a temperature approximately 4°C greater.

This anomaly in the microwave-heated case cannot be explained by any expected bulk thermal gradients. A nano-scale thermal gradient as a result of the selective heating of water by microwaves could result in the observed difference. However, this explanation requires supplementary explanation as to how the energy transfer between water and lipid molecules could be poor enough to allow a thermal gradient of several °C to exist over the scale of tens of Ångstroms.

The observation could be interpreted as a destabilisation of the Q_{II} phase by the applied microwave field. A possible explanation for this is that the impetus for the lipid dipoles to align with the electric field component of the microwaves, and therefore with one another, makes it less favourable for the system to adopt a structure where lipid dipoles are not aligned.

A simpler explanation is provided by previous observations that transition temperatures in these systems can be elevated to the extent reported here if ramp rate is sufficiently increased. In this experiment the ramp rate was indeed greater when the sample was heated by microwaves. However, the variation of ramp rate during heat-up makes it extremely difficult to determine whether a transition temperature increase of this magnitude could be expected due to this effect alone. Ideally, the experiment would be repeated with a constant heating rate during both conventional and microwave heating.

4.2 In- and Ex situ probing of β-lactoglobulin thermal denaturation in the presence of microwaves

4.2.1 Introduction

4.2.1.1 Interactions between microwaves and proteins

The low frequency vibrational modes predicted for coherent lipid systems would also be expected for proteins, providing a potential mechanism of non-thermal microwave coupling by resonance absorption.[11] In addition, it has been shown that microwave frequency collective twist excitations or 'wring' motions of chain molecules could also be sustained by proteins due to the topological constraint exerted upon them by their environment.[15] Resonance with these modes could impair the function of proteins by altering their conformations or even causing the chains to break.

However, there is a paucity of experimental reports to provide evidence for or against the existence of these mechanisms of interaction. De Pomerai *et al* report that aliquots of bovine serum albumin exposed to microwaves (1.0 GHz, *SAR* = 15-20 mW kg^{-1}) had a greater degree of aggregation as determined by light scattering than samples shielded from radiation.[95] The temperature of irradiated samples was measured by thermocouple at the end of exposure, and found to be insufficiently elevated to account for the increased aggregation. However, the authors of this report have since raised doubts about the accuracy of these results. It has been found that the applicator used is responsible for significant power losses and is itself heated during microwave exposure. The results were not reproduced when the exposure was repeated in an improved, lower loss, applicator.[19]

However, tuna myoglobin exposed to microwaves (1.95 GHz, *SAR* = 5 mW g^{-1}, 2.5 hr) exhibited no differences when compared to non-exposed protein in terms of structure as probed *ex situ* by absorption spectroscopy, circular dichroism and fluorescence lifetime measurement.[96]

It has been reported that thermophilic enzymes are inactivated by exposure to microwaves at elevated temperatures.[97] Enzyme solutions were exposed to microwaves (10.4 GHz) in a waveguide surrounded by a water jacket at a constant temperature of 30°C. Microwave power

levels were set such that the sample would reach desired temperatures (70, 80 and 90°C) at the point at which the cooling effect of the water jacket and microwave heating are in balance. *SAR*, as determined from reflected power measurement, was between 1.5 and 3.1 W g^{-1}. Samples were taken over the course of exposure and analysed *ex situ* by enzyme activity assay, steady state fluorescence measurement and circular dichroism.

The time and temperature dependent inactivation was ascribed to microwave-induced structural change revealed by the fluorescence and circular dichroism measurements. As non-exposed samples were stable at the same temperatures, it was concluded that microwaves affect the enzymes by a non-thermal mechanism. However, this relies on reliable sample temperature measurement. An assumption was made that placing the thermocouples in the sample perpendicular to the electric field would ensure that they were unaffected by microwave exposure.

Another study[98,16] following the reversible "cold" denaturation process of a protein at low temperature in the presence of urea by optical rotation reported that a short microwave pulse (estimated *SAR* = 250 W kg^{-1}) increased the rate of structural change by two orders of magnitude. It was speculated that this was due to resonance excitation of coherent modes in the protein proposed in an earlier paper.[15] The effect is apparently not seen after a sham exposure procedure without microwaves and the step changes observed are not reproduced by temperature jumps of the magnitude that the irradiation was measured to produce.

However, the exposure environment is far from ideal as the sample cell must be removed from the polarimeter for irradiation and then replaced. In addition, the heating effect of microwave exposure was only measured after the sample had been withdrawn from the cavity and therefore had time to cool. Therefore the temperature jumps induced by conventional means may not have been an accurate reproduction of those due to microwave exposure. Furthermore, microwave induced temperature increases will occur over a much shorter timescale than could be achieved by conventional heating. The implication of a non-thermal effect is therefore questionable and it would be greatly preferable to probe the system during irradiation and with accurate temperature measurement.

Only one literature example of *in situ* measurement of proteins during microwave exposure is known.[99] In this report, the structure of crystallised hen egg-white lysozyme were probed by X-ray diffraction during exposure to microwaves. The crystals were irradiated (8 GHz, $P \leq 3$ W) using a well-characterised (in terms of electric field distribution) slab-line waveguide geometrically optimised for access to the sample for X-ray diffraction.

High power levels were found to result in lattice distortions due to loss of water. At lower power levels displacement factors were found to be consistent with the heating effect expected due to microwaves. The large scale, power-independent displacements predicted by resonance coupling theories were not evidenced. These results are not transferable to in-vivo proteins though, as a critically important component on the system - the aqueous environment – is missing.

In the study reported herein, changes in the near UV CD response during the thermal unfolding of β-lactoglobulin are used to probe the effects of microwave irradiation on the process. For the first time, protein solution is irradiated *in situ* whilst its structure is simultaneously probed by CD measurements. The effects of microwave heating on the extent of irreversible denaturation are also probed by *post mortem* CD and fluorescence spectroscopy of the intrinsic tryptophan fluorophore and 1-anilino-8-naphthalene sulfonate (ANS), an extrinsic probe of hydrophobicity.

4.2.1.2 β-lactoglobulin

β-lactoglobulin (BLG) is a water soluble globular protein found in bovine and other mammalian milks. Its function is still debated but from the presence of a ligand-binding site with a high affinity for hydrophobic molecules and its similarity in this respect to other members of the lipocalin family it has been inferred that it probably has a role in the transport of retinol or other hydrophobic molecules.[100] It is a relatively small protein with a molecular mass of 18300 and having 162 amino-acid residues.

The native protein adopts a dimeric β-barrel structure at neutral pH but undergoes a well-studied[101-104] thermally induced structural change at different temperatures depending upon the pH of solution and the presence of denaturants such as urea. Circular dichroism (CD) and steady-state fluorescence techniques have shown that on heating beyond around 70°C the change is partially irreversible.[103] The effects of heat treatment were initially studied to better

understand the processes that lead to the problem of 'fouling' during milk processing but the relative ease of isolation and good stability of the protein mean that BLG is often used as a model in folding/unfolding studies. Two of the most common methods of studying this folding and unfolding are circular dichroism and fluorescence spectroscopy, both of which will explained in the following sections.

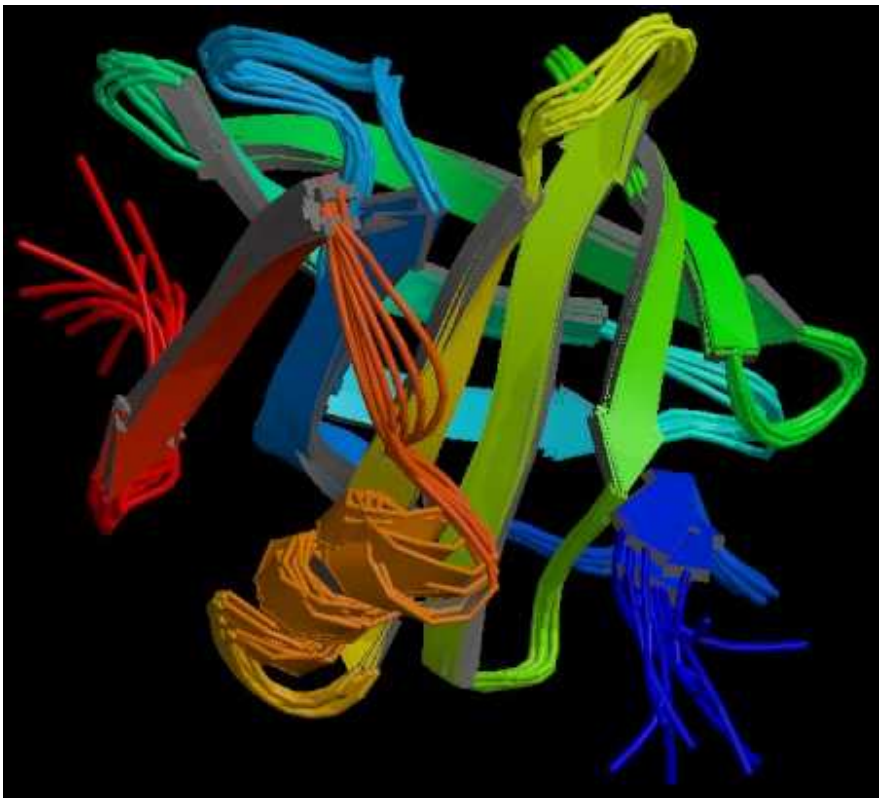

Figure 4.11: Schematic of the strucutre of β-Lactoglobulin as determined by X-ray diffraction, showing its characteristic β-barrel and the α-helix (orange).[105]

4.2.1.3 Circular dichroism as a probe of protein structure[106]

Circular dichroism is the differential absorption of left and right circularly polarised components of plane-polarised radiation. For this to occur, a chromophore must be chiral either due to its intrinsic structure, by covalent linking to a chiral centre or by being placed in an asymmetric environment. Left and right polarised light passed through an achiral sample will be absorbed to the same extent, therefore recombining the two components will result in plane polarised light.

However, if one of the components is absorbed to a greater extent by a chiral chromophore the result of recombination will be elliptically polarised light.

In practice the two components are generated by passing plane-polarised light through an isotropic material such as quartz that is modulated by a piezoelectric crystal subjected to an AC field (50 kHz). The quartz emits circularly polarised light at the extremes of the field modulation. The absorption of the two components, A_L and A_R, are measured separately after passage through the sample and the result is either reported as the difference in absorption, ΔA (= A_L - A_R), or the ellipticity, θ (= tan^{-1} b/a , where a and b are the major and minor axes of the resultant ellipse), in degrees. ΔA and θ are related by the simple relationship: θ = 32.98 ΔA. Dichroism is measured as a function of wavelength in order to build up a spectrum. ΔA is typically of the order of only 10^{-4} absorption units, corresponding to an ellipticity of around 10 m°, therefore care is required to obtain good results.

The aromatic amino acid side chains of phenylalanine, tyrosine, and tryptophan absorb in the near UV between 250 to 290 nm. Their CD spectra often reflect their placement in chiral environments due to tertiary folding of the polypeptide chain. Near UV CD therefore provides a sensitive probe for following structural change during unfolding of proteins.

The near-UV CD spectrum of native and thermally denatured BLG is shown in figure 4.12. The ellipticity bands at 292.5 and 285 nm are thought to be due to one of the two tryptophan residues in the protein (Trp^{19}). This residue is located within the central hydrophobic β-barrel of the protein and is surrounded by a number of side chains of other residues. It is thus in a more chiral environment than the other more externally located tryptophan residue (Trp^{61}) and therefore is thought to make a greater contribution to the near-UV CD spectrum. The magnitude of the bands decrease with increasing temperature as the protein unfolds and the side chain packing around the Trp^{19} becomes less.

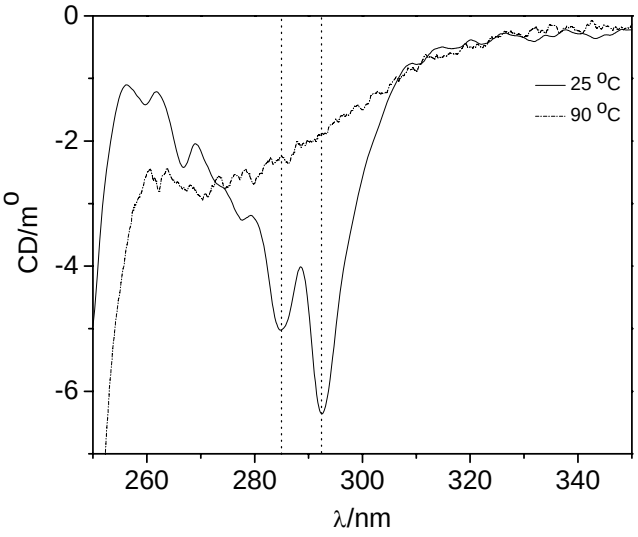

Figure 4.12: The change in CD spectrum of BLG on heating a solution of the protein from 25 to 90°C (solution prepared as 4.3.2.6, spectra recorded as 4.3.2.4 but over the range 350-250 nm). The absorption bands at 292.5 and 285 nm due to tryptophan are higlighted.

4.2.1.4 Steady-state fluorescence as a probe of protein structure[68,107,101]

All aromatic amino acid residues can theoretically provide intrinsic fluorescent probes of protein structure. However, the absorption spectra of tryptophan and tyrosine overlap. Consequently in proteins containing both residues the fluorescence excitation of the latter can pass to the former by means of energy transfer. In addition, it is only possible to selectively excite tryptophan. These complications and the relatively low quantum efficiency of phenylalanine in water (0.02 compared to 0.14 and 0.13 for tryptophan and tyrosine respectively), mean that in practice tryptophan is the most commonly studied intrinsic probe.

The fluorescence properties of tryptophan provide highly sensitive probes of local environment. Increases in the polarity of the residue environment result in the peak emission, λ_{max}, shifting to higher wavelength and the intensity of emission decreasing. During unfolding tryptophan residues located within the hydrophobic core of proteins become more exposed to aqueous buffer, thus the degree of denaturation can be determined from the steady state fluorescence spectra of the residue.

Extrinsic fluorescent probes allow one to look at other aspects of protein structure such as the surface of the protein. For example, ANS is a conformation sensitive hydrophobic probe that binds to a number of proteins. A decrease in the polarity of ANS environment, such as when it binds to surface hydrophobic pockets, leads to changes in spectral properties. In free water ANS has a λ_{max} of 515nm whereas the protein-bound probe typically has a λ_{max} of between 470 and 490 nm and significantly enhanced emission intensity. ANS fluorescence can therefore be used as a sensitive probe of changes in the hydrophobic sites during unfolding and hence as an indicator of the degree of protein denaturation.

4.2.2 Experimental

4.2.2.1 Materials and equipment

BLG (A & B, Sigma, approximately 90% PAGE), ANS (NH_4^+ salt, Fluka, >97.0%), NaCl (Fisher, analytical grade) and $NaH_2PO_4.H_2O$ (AnalaR) were used as bought. A Grant LTD 6 water bath/circulator was used for heat treatment of BLG samples and temperature control during fluorescence measurements. A Julabo 5 water bath/circulator and a Jasco PTC-423S Peltier cuvette holder controlled temperature during CD measurements. Fluorescence measurements were carried out using a Spex Fluoromax fluorimeter. CD measurements were carried out using a Jasco J-810 spectropolarimeter. A Hewlett-Packard 8752A Vector Network Analyser was used as a source of microwaves for *in situ* experiments. The signal was amplified with a Minicircuits ZRL 2400-LN microwave amplifier and power levels were determined using a Hewlett Packard 435B Power Meter. A CEM Discover controlled microwave heater was used for the *ex situ* experiments. A FISO FOT-H fibre optic temperature sensor linked to an Umi 4 signal conditioner was used for temperature measurements. The probe can be used to monitor temperature during microwave irradiation and is accurate to within 0.05 °C.

4.2.2.2 Buffer preparation

For probing of the high temperature irreversible unfolding βLG was buffered in 10 mM sodium phosphate, 60 mM sodium chloride at pH 6.8. This was prepared by dissolving 0.685 g of $NaH_2PO_4.H_2O$ and 1.753 g of NaCl in 475 ml deionised H_2O. The pH was adjusted to 6.8 using concentrated NaOH solution and the solution was made up to 500 ml with deionised H_2O.

For probing of the low temperature reversible folding/unfolding BLG was buffered in 50 mM sodium phosphate, 60 mM sodium chloride, 3 M urea at pH 6.8. This was prepared by dissolving 0.390 g $NaH_2PO_4.2H_2O$, 0.350 g NaCl and 18.018 g urea in 90 ml deionised water. The solution was then made up to pH 6.72. The pH was adjusted to 6.8 using concentrated NaOH solution and the solution was made up to 100 ml with deionised H_2O.

4.2.2.3 Conventional and microwave heat treatment for ex situ analysis of the irreversible denaturation of BLG

BLG was dissolved in sodium phosphate/sodium chloride buffer to a concentration of 0.2 mg mL^{-1}. ANS was added to give a concentration of 50 μM. 4 mL samples of this solution were heated in sealed glass tubes to temperatures between 50 and 94 °C for 15 minutes. For each temperature one sample was heated conventionally in a water bath and another was heated using the CEM Discover instrument. The temperature during microwave heating was monitored using the infrared temperature sensor in the instrument. The temperature reported by the instrument during the heating of a dummy sample was checked against the reading reported from a fluoroptic probe immersed in the sample and found to be out by as much as 5 °C at the higher end of the temperature range. Temperatures reported by the instrument were subsequently calibrated using these results. The actual temperature during conventional heating, as opposed to the set temperature of the water bath, was determined in the same way. Samples were cooled in ice water immediately after heating. All samples were stored at 4 °C and heated and analysed within 4 days of the original solution being made up.

4.2.2.4 Ex situ analysis of the irreversible denaturation of BLG

Fluorescence spectra of intrinsic tryptophan fluorescence and ANS were recorded in a fluorimeter. Samples were placed in clean disposable PMMA 10 mm fluorimeter cuvettes in a water circulation temperature-controlled cuvette holder at 20 ^oC and left for 10 min to equilibrate. The emission spectrum of the intrinsic protein fluorescence due to tryptophan was measured between 315 and 400 nm with excitation at 295 nm. The emission spectrum of ANS was measured between 450 and 550 nm with excitation at 475 nm. All spectra were measured with a bandwidth of 1 nm, an integration time of 1 s and excitation and emission slits set at 5 nm. λ_{max} for each spectrum was determined using the fluorimeter software and the intensity at this position was recorded.

CD values at 292.5 nm were determined by scanning between 295 and 290 nm. Sample solution was placed in a 10 mm fluorimeter cell rinsed with buffer and a small portion of sample. The cuvette was placed in a peltier-controlled cell holder at 20.0 ^{o}C and left to equilibrate for 15 min before scanning at a rate of 50 nm min^{-1} with a 2 s time constant, 1 nm band width and an averaging factor of 10. Spectra were corrected for buffer and cuvette aberrations by subtracting a scan of pure buffer.

4.2.2.5 Microwave applicator for in situ CD measurements

An applicator based on a square coaxial transmission line was designed to enable simultaneous irradiation of a sample solution during CD measurement. The applicator fits over the top of a 10 × 10 mm cuvette so that the cuvette can be placed in a Peltier cuvette holder for automated control of sample temperature. A coaxial SMA to stub connector was fitted with a length of platinum wire to act as the inner conductor of the coaxial line (figures 4.13 (a) and 4.14 (a)). The cuvette top component of the device (figure 4.13 (b)) was machined from brass with a PTFE insert that provides a lid for the cuvette. The brass walls act as the outer conductor of the line. The modified connector is attached to the cuvette top with screws in three of the four corners. At the fourth corner is a hole that extends fully through the cuvette top for a fluoroptic probe.

With all the components together and fitted over the cuvette (figure 4.14 (b)) a circular-to-square coaxial line transition is formed. Dimensions of the inner and outer conductors were chosen to preserve the standard impedance as best as possible along the length of the line (see chapter 1, section 1.2.2). The impedance of square coaxial line can be determined from

$$Z_0 = \frac{138.06}{\sqrt{\varepsilon^*}} log_{10} \frac{D}{d}, \quad \textbf{4.6}$$

[108]

where D and d are the dimensions of the outer and inner conductors respectively. Calculations based on the dielectric response of water at 2.45 GHz result in an ideal D/d ratio of 1848 and therefore an impossibly thin inner conductor. The thinnest practical platinum wire (0.4 mm diameter) was used for its biological inertness.

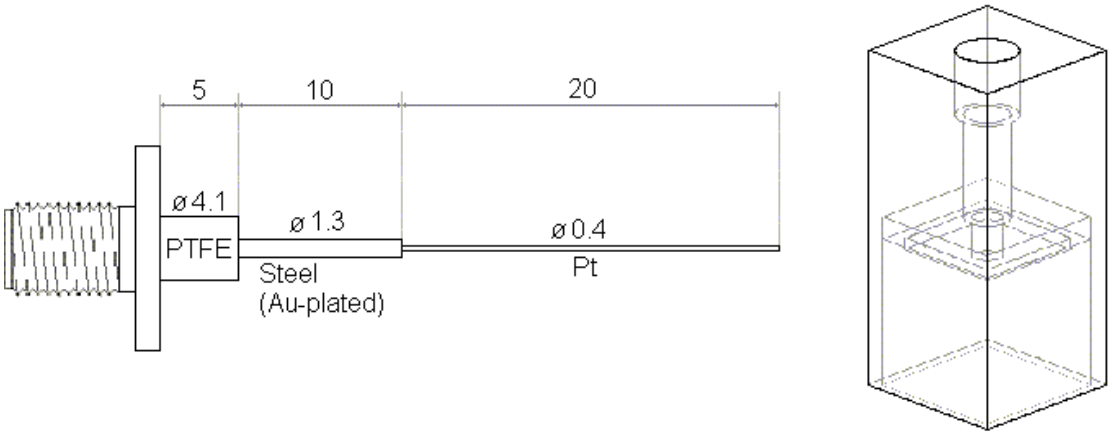

(a) **(b)**

Figures 4.13 (a) and (b): Schematics of the modified coaxial connector ((a), dimensions in mm) and cuvette top ((b), screw fixings not shown) components of the applicator.

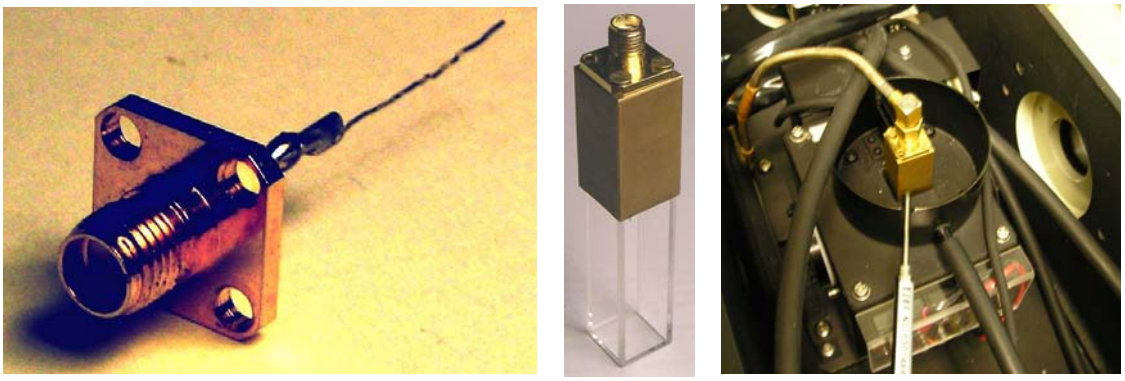

(a) **(b)** **(c)**

Figures 4.14 (a)-(c): Photographs of the modified coaxial connector (a), the complete applicator fitted over a cuvette (b), and the applicator and cuvette fixed in the peltier controlled holder inside the sample chamber of the CD spectrometer (c).

The assembly was designed to fit into the peltier holder in such a way that the wall of the holder and the walls of the cuvette top form an almost seamless outer conductor for the coaxial line. The metal base of the holder completes what is, ignoring the windows for optical access,

essentially a closed cavity. The reflectance of this cavity was determined over a range of frequencies using a network analyser. Reflectance spectra recorded with the cuvette filled with 3.5 g aliquots of each of the two buffers used (figure 4.15) are similar. The absorbance is strongest around 700-900 MHz (~ 80-90%) but is appreciable at 1.8 and 2.45 GHz (~ 10%).

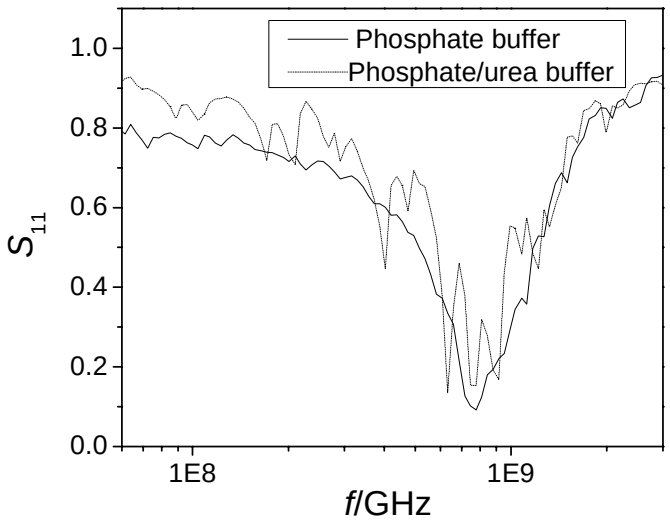

Figure 4.15: Reflectance of the microwave applicator/peltier cuvette holder cavity for a cuvette filled with 3.5 g of each buffer.

4.2.2.6 In situ probing of the high temperature irreversible unfolding of βLG

1 mg/ml BLG solution in sodium phosphate/sodium chloride buffer was prepared and stored at 4°C for a period of no more than four days. A 10 mm quartz fluorimeter cuvette, rinsed with buffer and a small portion of sample solution, was filled with 3.5 g of the sample and a small magnetic strirrer bar was added. The bespoke microwave applicator was fitted over the cuvette before it was placed within the peltier cuvette holder in the CD instrument sample chamber. The microwave applicator was then connected to the microwave source using coaxial cable and the fluoroptic probe was inserted so that the sensitive tip was immersed in the sample.

The sample was allowed to equilibrate at 20°C for 30 min after which the CD response at 292.5 nm was measured using a variable temperature program from 20-90°C, a scan rate of 30°C hr^{-1} and a data pitch of 0.2°C. This procedure was repeated with continuous microwave irradiation of 10 mW power at frequencies of 0.9, 1.8 and 2.45 GHz for the duration of each run. The

microwave frequencies used for irradiation were chosen for specific reasons: 0.9 and 1.8 GHz are frequencies used for mobile telephones and 2.45 GHz is the frequency used in domestic microwave ovens and has therefore been used in the majority of studies of the effects of microwaves on biological systems.

The sample temperature was not found to vary significantly from the temperature of the peltier holder. The fluoroptic probe was therefore not used for subsequent experiments.

The procedure was repeated but with power levels set so that 0.5 mW of power would theoretically be absorbed at frequencies of 0.9, 1.8, and 2.45 GHz. The amplifier was not required for these power levels.

4.2.2.7 In situ probing of the low temperature reversible unfolding of βLG with urea

1 mg/ml BLG solution in sodium phosphate/sodium chloride/urea buffer was prepared and stored at 4°C for a period of no more than four days. The sample and applicator were prepared as in 4.3.2.6. Sample was allowed to equilibrate at 0°C for 30 min after which the CD response at 292.5 nm was measured using a variable temperature program from 0-20°C, a scan rate of 30°C hr^{-1} and a data pitch of 0.1°C. The peltier cuvette holder was immediately set to 0° and the sample was left until the CD response indicated re-equilibration before the procedure was repeated with different irradiation conditions.

Experiments were run in two sets using one sample for each: In the first set a profile was recorded with no irradiation and then with irradiation at 0.2 mW absorbed power level and frequencies of 0.9, 1.8 and 2.45 GHz; in the second a profile was recorded with no irradiation and then with irradiation of 0.9 GHz frequency and absorbed power levels of 0.1, 1.0 and 10 before a final repeat run without microwave irradiation was recorded.

4.2.3 Results and Discussion

4.2.3.1 Ex situ analysis of the irreversible denaturation of BLG by conventional and microwave heat treatment

The change in each probe parameter (ellipticity, fluorescence intensity etc.) is plotted against treatment temperature to produce a denaturation profile, which indicates the degree of irreversible structural change on heating to a given temperature either conventionally or by microwaves.

Normalised percentage change in ellipticity at 292.5 nm with denaturation temperature was plotted for both the conventionally and microwave heated (figure 4.16). Normalising so that for each profile the lowest value is 0 and the highest is 100 allows the shape of profiles to be compared.

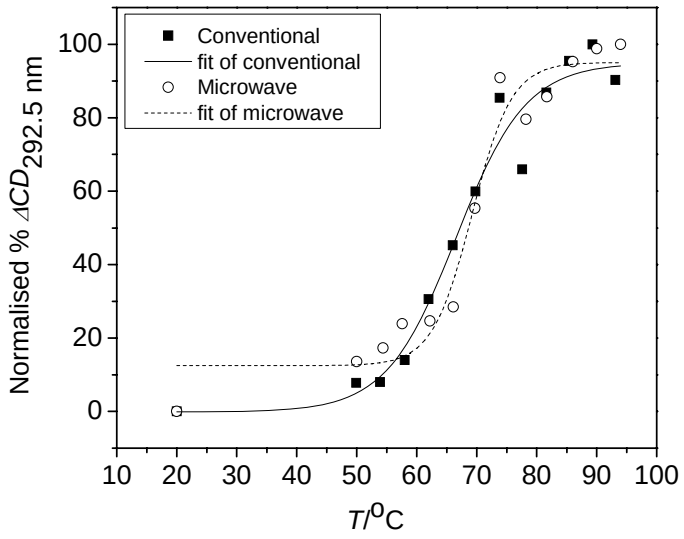

Figure 4.16: Profiles of conventional and microwave irreversible denaturation probed by ellipticity at 292.5 nm. Best-fit lines for a sigmoidal model are shown.

From visual inspection the profiles for conventional and microwave heating are similar. The *mid-point* or *melt* temperature, T_m, was determined from a sigmoidal fit using the graphing and data analysis programme Origin.[37] The value was the same, within the margins or error reported by Origin, for the conventional and microwave-heated cases (table 4.1). The microwave-heated profile differs from the conventionally heated profile in having greater gradient, dy/dx, at T_m

indicating a narrower transition. However, no estimate of the error for this value is available from the fit and the quality of the data is insufficient to fit a peak to the derivative, the width of which would yield information about the width of the transition.

Profiles were also plotted from the change in ANS emission intensity as a function of temperature (figure 4.17). ANS fluorescence intensity increases as its environment becomes more hydrophobic. Heat-treatment of BLG irreversibly alters hydrophobic pockets on the protein to which ANS can bind, apparently increasing the hydrophobicity of these sites. Hence intensity increases as a function of treatment temperature.

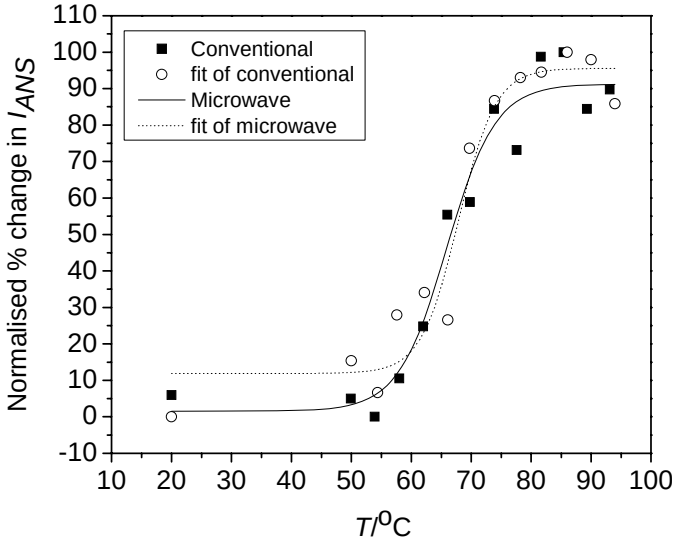

Figure 4.17: Profiles of conventional and microwave irreversible denaturation probed by ANS fluorescence intensity. Best-fit lines for a sigmoidal model are shown.

T_m values (table 4.1) showed no difference between heating methods and were in line with values determined from ellipticity. As with the ellipticity profile, microwave heating results in greater dy/dx when compared to conventional heating but no estimate of the error in this value is available.

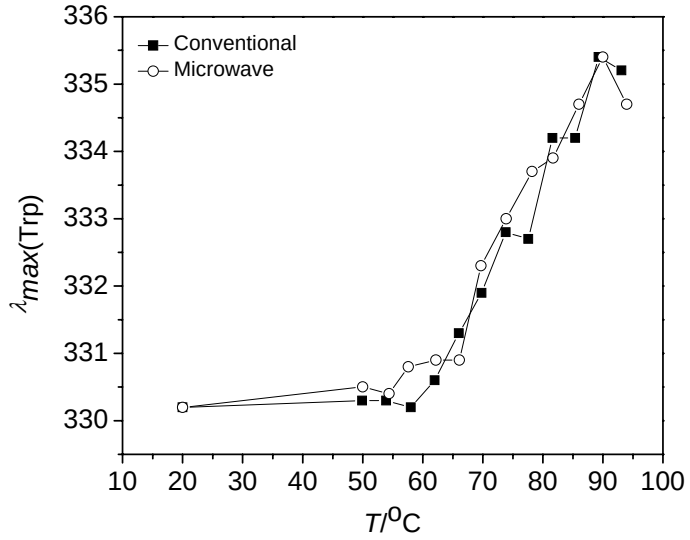

Figure 4.18: Profile of conventional and microwave denaturation probed by tryptophan emission maximum wavelength.

Profiles of the tryptophan emission maximum (figure 4.18) were also fitted to a sigmoidal model (not shown). As expected, λ_{max} increases above 50 °C indicating that the residue environment irreversibly changes to become more polar as a result of incomplete refolding. The values of T_m are higher than those gained from ellipticity and ANS fluorescence probes, indicating that the changes that higher temperatures are required to irreversibly to change the Trp in this manner. However, there is again no significant difference between the conventional and microwave-heated samples. *dy*/*dx* was the same as for both heating methods.

Table 4.1: T_m of BLG determined from sigmoidal fits of conventional and microwave irreversible denaturation profiles from different probes.

Probe	T_m/ °C, Conventional (Error)		T_m/ °C, Microwave (Error)	
%ΔCD	66.6	(1.5)	69.2	(1.2)
$\%\Delta I_{ANS}$	65.9	(1.3)	67.9	(1.3)
$\lambda_{max(Trp)}$	76.3	(2.0)	73.2	(1.3)

Table 4.2: *dy/dx* ($T=T_m$) determined from sigmoidal fits of conventional and microwave irreversible denaturation profiles for BLG probed by different methods.

Probe	*dy/dx* ($T=T_m$)/$^oC^{-1}$, Conventional	*dy/dx* ($T=T_m$)/$^oC^{-1}$, Microwave
%ΔCD	4.1	6.2
$\%\Delta I_{ANS}$	5.5	6.7
$\lambda_{max(Trp)}$	0.20	0.21

Intrinsic tryptophan emission intensity, I_{Trp}, and ANS emission maximum wavelength, $\lambda_{max(ANS)}$, decrease and increase respectively with increasing heat treatment temperature as expected but the profiles (figures 4.19 and 4.20) were of insufficient quality for any comparison between the heating methods. The large relative errors are a result of the relatively small changes in the values after heat treatment.

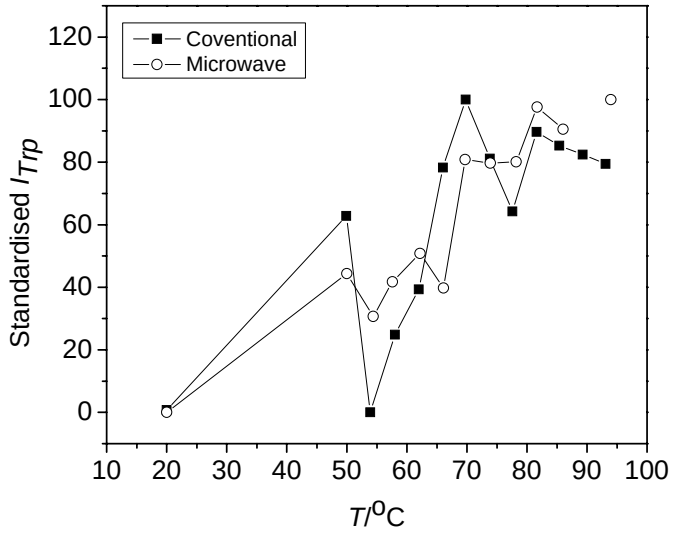

Figure 4.19: Profiles of conventional and microwave irreversible denaturation probed by tryptophan fluorescence intensity.

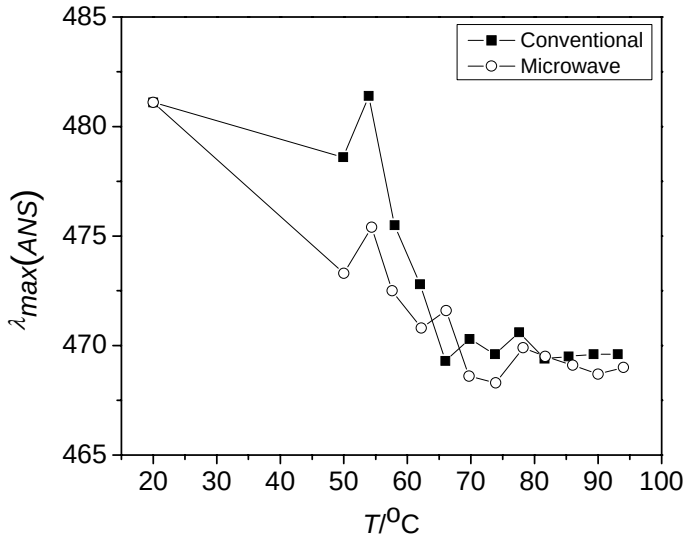

Figure 4.20: Profiles of conventional and microwave irreversible denaturation probed by ANS emission maximum wavelength.

Overall, no significant difference was been observed between conventional and microwave heating for the irreversible denaturation of BLG. However, this may have been due to the large error in the determined parameters. This is a reflection of the small number of data points for each profile, which was limited by the number of samples that can be prepared, treated and analysed before the solution deteriorates. The *in situ* measurements described in the following sections provide more accurate determination of parameters as numerous data points can be recorded during the thermal denaturation process.

4.2.3.2 In situ analysis of the irreversible denaturation of BLG by conventional and microwave heat treatment

Figure 4.21 is a typical thermal denaturation profile recorded by *in situ* measurement. The profile could be fit to a sigmoidal model to yield T_m, as long as a sloping baseline is also included. However, *thermal melting curves* in biological systems are more accurately and informatively fitted to the van't Hoff relationship,[109,110]

$$\frac{d(lnK)}{d(1/T)} = \frac{-\Delta H_{vH}}{R}. \qquad \textbf{4.7}$$

This model relates the shape of the denaturation curve to two fundamental parameters: T_m and the transition or van't Hoff enthalpy, ΔH_{vH}. K is the equilibrium constant for the transition from the native, N, to the denatured state, D, and given by

$$K = \frac{[D]}{[N]} = \frac{1-f}{f}, \qquad \textbf{4.8}$$

where f is the fraction of molecules in the native state. f can be determined from the fractional change in the observed signal.

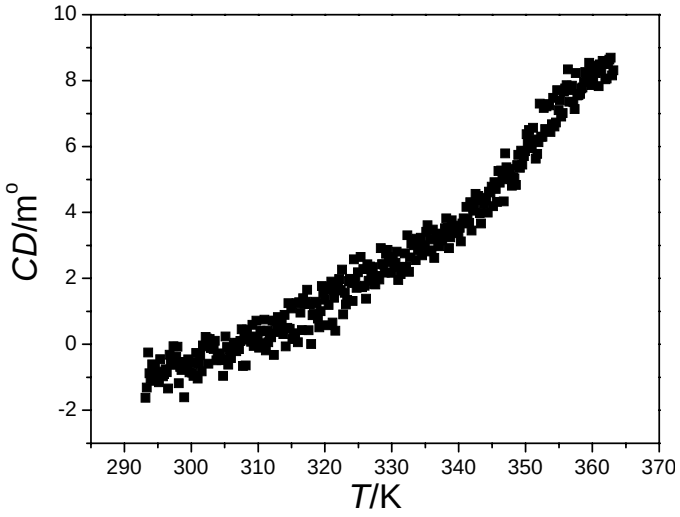

Figure 4.21: A typical denaturation profile or *melting curve* for BLG based on *in situ* measurement of the ellipticity at 292.5 nm.

The observed signal for each of the states will have a temperature dependence, hence it is necessary to subtract lower and upper sloping baselines to determine the fractional change. Uncertainty in determining these baselines will inevitably lead to uncertainty in the fundamental parameters obtained from the fit. This is often a problem where the transition is relatively low or high in the temperature range of aqueous solutions and therefore little data is available for the 'flat' regions below or above the transition.

An alternative is to fit to the *differential* melting curve. The differential plot of any denaturation signal (ellipticity, fluorescence intensity etc.) will supposedly fit to

$$\frac{d(signal)}{dT} = Af(1-f)T^2, \quad \textbf{4.9}$$

where A is a scaling factor. However it was found that this is only suitable where the transition is very clear, that is, 'peak' $d(signal)/dT$ >> 'flat' $d(signal)/dT$. Therefore an additional scaling factor is required to account for the flat regions and the expression becomes

$$\frac{d(signal)}{dT} = A_1 f(1-f)T^2 + A_2 . \quad \textbf{4.10}$$

Substituting equation 4.8 into the integrated form of the van't Hoff equation (4.7),

$$K = exp\left[\frac{-\Delta H_{vH}}{R}\left(\frac{1}{T_m} - \frac{1}{T}\right)\right] \quad \textbf{4.11}$$

and solving for f yields an expression,

$$f = \frac{1}{1 + exp\dfrac{\Delta H_{vH}(T_m - T)}{T_m RT}}, \quad \textbf{4.12}$$

that, together with equation 4.10, relates the differential change in the observed signal to the two thermodynamic parameters that govern the transition.

Therefore all denaturation profiles were differentiated, smoothed by adjacent point averaging and fitted simultaneously to equations 4.10 and 4.12 using Origin. Figure 4.22 shows a van't Hoff fit to the differential plot of the data in 4.21. While the fit to the flat region is relatively poor, the fit to the peak is much better and it is in this region that the thermodynamic parameters are determined. The results of the fits to high temperature denaturation profiles recorded with different irradiation conditions are summarised in table 4.3.

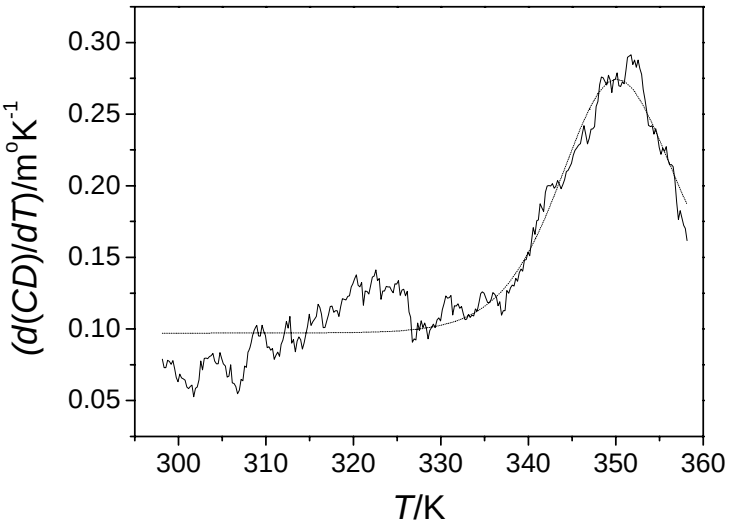

Figure 4.22: Smoothed differential plot (solid line) of the denaturation curve in figure 4.21. The broken line is a fit to the differential van't Hoff model: $f = 1/(1+(\exp((\Delta H*(T_m-x))/(T_m*8.314*x))))$; $y = (A_1*f*(1-f)*(x\text{^}2))+A_2$.

Table 4.3: Results of van't Hoff fits to high temperature denaturation profiles for BLG with different irradiation conditions.

Frequency/GHz	Absorbed Power/mW	T_m/K	ΔH_{vH}/kJ mol^{-1}
N/A	0	345.8 ± 0.15	-261 ± 8
N/A	0	346.7 ± 0.15	-211 ± 6
0.9	0.5	345.2 ± 0.14	-236 ± 7
1.8	0.5	347.0 ± 0.17	-256 ± 9
2.45	0.5	346.1 ± 0.08	-294 ± 6
0.9	8.0	350.4 ± 0.17	-189 ± 5
1.8	2.0	349.9 ± 0.16	-229 ± 7
2.45	1.5	348.2 ± 0.14	-243 ± 7

The T_m and ΔH_{vH} determined for solutions of BLG not subjected to irradiation during heating are in reasonable agreement with values determined previously (T_m = 343.2 ± 0.2 K, ΔH_{vH} = 195 ± 10 kJ mol^{-1}).[102] However there is clearly a large experimental error as indicated by the difference

between the repeated measurements for BLG solution heated without irradiation. The difference for T_m is approximately 1 K and for determined enthalpies is 50 kJ mol^{-1}, both of which are significantly outside of the error quoted for the fit. Based on these results the minimum errors in measured T_m and ΔH_{vH} are ± 0.5 K and ± 25 kJ mol^{-1}, respectively. Although there is insufficient data to obtain a more accurate estimate of error, the results for samples irradiated with an absorbed microwave power of 0.5 mW (SAR = 0.14 W kg^{-1}) could not justifiably be said to differ significantly from samples not subjected to irradiation.

However, samples irradiated with higher microwave powers exhibit an elevation of T_m that is more significant. In addition, this elevation and the enthalpy determined for these samples both correlate with the absorbed power level and/or frequency. It is not possible to state whether the effect correlates specifically with the absorbed power level or with the frequency of the microwaves as both of these change. The intention was to only vary frequency and therefore the power level was maintained at 10 mW. However, these experiments were carried out before it was determined that the absorption varies as a function of frequency.

Nevertheless, the effect was contrary to that which was expected. The experimental regime was designed such that the heating rate was sufficient for the sample to be in thermal equilibrium but insufficient for the much slower denaturation process to be in equilibrium. Therefore if microwave irradiation increases the rate of the denaturation process, as has been previously reported,[16] samples irradiated during heating would be expected to undergo a transition at a lower temperature. As the effect observed is the direct opposite, the previously posited resonance models discussed in chapter 1 do not offer an obvious explanation. However, before discussing the possibility of microwaves influencing the unfolding of BLG by a *non-thermal* mechanism, the more probable *thermal* effects should first be discounted.

Fluoroptic probe measurements determined that the power of the microwaves used was insufficient to cause significant heating of the sample above the temperature set by and measured for the Peltier-holder. The sample and its environment are in thermal equilibrium as the sample, applicator and holder are all in good contact and the sample temperature is homogenised by magnetic agitation. Any heat generated due to absorbed microwaves is efficiently dissipated before thermal inhomogeneity occurs. In any case, in order to explain the observed elevation in

T_m, the thermal effect of microwaves would have to be to somehow lower the actual sample temperature relative to that observed. We can find no reason why this should be the case.

The large errors in determining the thermodynamic parameters of the irreversible unfolding of BLG make it difficult to conclude anything about the effect of microwaves on the transition. It was decided that the low temperature, reversible folding of BLG in urea solution should be probed. Because this process is reversible it is possible to probe the same sample repeatedly, thus reducing the opportunities for introducing error into the measurement. The results of probing this system with different irradiation conditions will be reported before discussing the apparent microwave-influenced retardation of the unfolding process in the conclusions section.

4.2.3.3 *In situ* analysis of the low temperature reversible unfolding of βLG with urea

The aim of these experiments was to probe the low temperature reversible folding transition for BLG denatured with urea. At certain urea concentrations the protein can be seen to go from a cold denatured state to a folded state at a higher temperature. The protein will then undergo irreversible thermal denaturation if it is further heated but will return to the cold denatured state if cooled.

This reversible transition has been utilised in the previously cited report of microwave-enhanced folding and unfolding of a BLG as measured by optical rotation.[16] In that study BLG was dissolved in a solution of potassium chloride and urea and the transition from unfolded to folded state was observed over the temperature range 4 to 48°C. The experimental section of the report states that the KCl/urea solution was prepared by mixing 3 ml 0.1 M KCl with 4 ml 4 M urea and adjusting to pH 2 with HCl. This would result in urea and KCl concentrations of 2.29 and 0.43 M respectively (although the addition of HCl will lower these concentrations further). However, in the results section of the report it is stated that the transition occurred in 4 M urea solution. Contact was made with the authors in order to clear up this disparity but no response was received.

The change in ellipticity of a solution of BLG in 2.29 M urea and 0.43 M KCl at pH 2 has been measured from 0 to 45°C.[111] The resulting profile exhibited no clear transition. Therefore these

conditions were not used. Instead a urea concentration of 3 M was chosen based on a titration curve determined for BLG against urea (both in sodium phosphate/sodium chloride buffer, pH 6.8) at 20° C.[111] A concentration of 3 M was at the onset of the transition from the native state to the denatured state, therefore cooling back to 0°C at this concentration should induce denaturation.

Figure 4.23 is the ellipticity profile recorded for the BLG in 3 M urea and phosphate buffer from 0 to 20°C in the absence of microwave irradiation. The protein can be seen to change from a denatured state at 0°C to the native state at temperatures above.T_m and ΔH_{vH} can be determined by fitting the differential plot to the van't Hoff model (figure 4.24). Table 4.4 provides a summary of the results obtained from profiles recorded with different irradiation conditions.

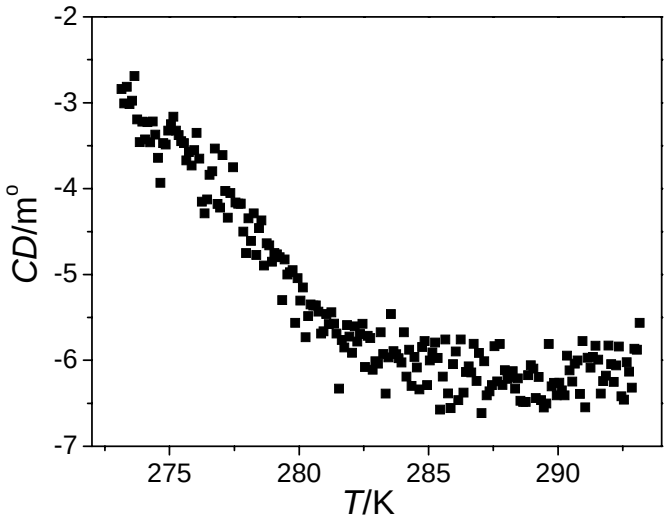

Figure 4.23: Thermal folding of BLG in 3 M urea, pH 6.72, sodium phosphate/sodium chloride buffer as shown by the change in *CD* as a function of temperature.

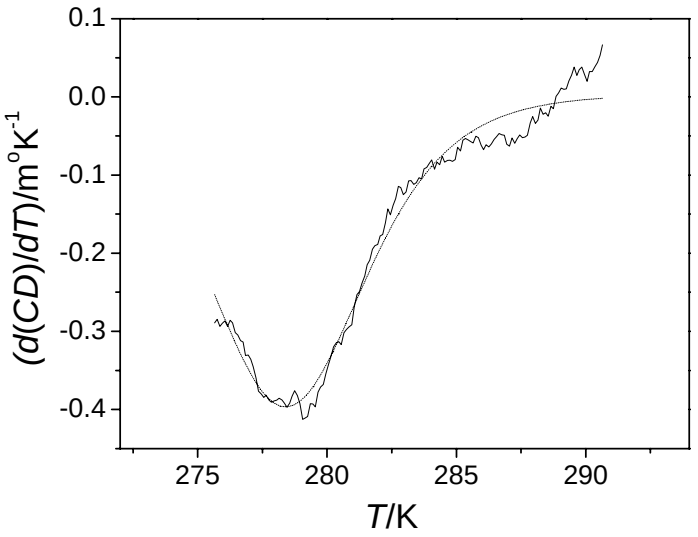

Figure 4.24: Smoothed differential plot (solid line) of the denaturation curve in figure 4.23. The broken line is a fit to the differential van't Hoff model: $f = 1/(1+(\exp((\Delta H*(T_m-x))/(T_m*8.314*x))))$; $y = (A_1*f*(1-f)*(x\text{^}2))+A_2$.

Table 4.4: Results of van't Hoff fits to low temperature folding profiles for BLG in solution with urea with different irradiation conditions.

Frequency/GHz	Absorbed Power/mW	T_m/K	ΔH_{vH}/kJ mol^{-1}
N/A	0	278.3 ± 0.08	289 ± 9
N/A	0	278.3 ± 0.05	319 ± 8
N/A	0	279.1 ± 0.07	371 ± 14
0.9	0.1	278.3 ± 0.03	391 ± 8
0.9	1.0	277.4 ± 0.17	160 ± 9
0.9	2.0	278.2 ± 0.12	240 ± 9
0.9	10.0	278.4 ± 0.05	307 ± 8
1.8	2.0	278.3 ± 0.12	240 ± 9
2.45	2.0	278.5 ± 0.11	252 ± 9

The standard deviations in T_m and ΔH_{vH} for the results of the three profiles for BLG solutions not subjected to microwaves are 0.46 K and 41 kJ mol^{-1} respectively. As 95% of results can be

expected to fall within 2 standard deviations, ± 0.9 and ± 82 are reasonable estimates of error for T_m and ΔH_{vH}. Assuming these large experimental uncertainties, T_m does not differ significantly regardless of the microwave irradiation conditions that the BLG is exposed to during heating. Variations in T_m of the order of those observed for the high temperature denaturation process were not observed and no correlation between T_m and microwave power or frequency could be discerned.

Only one of the results for ΔH_{vH} does not fall within the margins of error of the others. This is the result for BLG irradiated with 0.9 GHz microwaves at an absorbed power level of 1 mW. However results for the same frequency but with lower and higher power levels do not correlate with the result. The reasons for this anomalous result are unknown. However, it is highly improbable that the protein would couple, by some resonant mechanism, only with microwaves of a specific power level.

Together, the evidence shows that microwaves, even up to relatively high absorbed power levels (10 mW ≡ SAR = 2.9 W kg^{-1}), have no effect upon the thermally-induced folding of urea-denatured BLG.

4.2.4 Conclusions

An initial attempt to probe the effects of microwave exposure upon the irreversible denaturation of BLG was made by *post mortem*, *ex situ* measurement of treated protein solutions. Within the limits of the measurement precision it was not possible to discern any differences between the irreversible denaturation profiles resulting from heat treatment of treated protein solutions by conventional and microwave means. The main limitation on the method was the number of treated solutions that can feasibly be probed.

Therefore a technique for *in situ* measurement of the circular dichroism of protein during heating with simultaneous microwave irradiation was devised. This is the first example of *in situ* structural probing of protein in aqueous environment during microwave exposure. A bespoke microwave applicator based on square coaxial transmission line fits over the top of the sample cell, which is held in a Peltier-controlled cuvette holder allowing precise automated temperature control.

In situ measurement yielded well-defined thermal melting curves that were fitted to give precise values of two thermodynamic properties that describe the unfolding transition: the melting or mid-point temperature, T_m; and the van't Hoff enthalpy, ΔH_{vH}. The T_m of protein solutions irradiated with higher microwave power levels (≥ 2 mW) was elevated by as much as 3.5 K for the highest power level (8 mW, SAR = 2.3 W kg^{-1}). However, T_m elevation was not observed for the more reproducible lower-temperature transition from the urea-denatured state to the folded state of BLG at any of a range of power levels from 0.1 to 10 mW.

Thus there is some evidence that microwave irradiation affects the folding/unfolding; however the effect is to retard it. This directly contradicts the conclusions of a previous study in which it was determined that microwave irradiation increases the rate of protein folding/unfolding by two orders of magnitude.[16] In that study the SAR was also at least two orders of magnitude higher than the highest used here. Nevertheless, if their model is correct the rate constant ought to be proportional to the absorbed power level and therefore some increase in the rate would be expected.

4.3 Overall conclusions

In the absence of sufficiently powerful theoretical or computational approaches, the debate over the possibility of microwaves acting upon living entities by athermal mechanisms will only be resolved with rigorous experimental methods. Up until now studies have suffered from poor control of exposure conditions. Fundamentally important factors such as power absorbed by the system and the heating effect of exposure are not known or are poorly quantified. It is therefore impossible to rule out thermal effects as the real cause of any supposed athermal effects observed in systems.

The probing techniques described in this chapter are a significant improvement. For the first time structural changes in model biological systems have been probed *in vitro* and *in situ* during continuous controlled exposure to microwaves and with accurate thermometry. The techniques have been used to probe model systems that were likely to be sensitive to microwave irradiation, either because theoretically proposed mechanisms suggested that they were (lipids) or because

previous experimental evidence has concluded that they were (β-lactoglobulin). In neither case was any conclusive evidence for the existence of athermal microwave interaction found. No number of 'null' results will settle the debate, but arguments for or against will become clearer if poor experimental techniques are disregarded.

Bibliography

1. Stewart, W. Mobile Phones and Health: a report of the Independent Expert Group on Mobile Phones; National Radiation Protection Board: Chilton, 2000.
2. Gedye, Richard; Smith, Frank; Westaway, Kenneth; Ali, H.; Baldisera, L.; Laberge, L.; Rousell, J. *Tetrahedron Letters* **1986,** *27*, 279-282.
3. Bykov, Y. V.; Rybakov, K. I.; Semenov, V. E. *Journal of Physics D-Applied Physics* **2001,** *34*, R55-R75.
4. Baghurst, D. R.; Mingos, D. M. P. Journal of the Chemical Society-Chemical Communications **1988**, 829-830.
5. Mingos, D. M. P.; Whitakker, A. G. Microwave dielectric heating effects in chemical synthesis. In *Chemistry under extreme or non-classical conditions;* van Eldik, R.; Hubbard, C. D. Eds.; John Wiley & Sons, Inc: New York, 1997; pp. 479-514.
6. Benedict, R. P. *Fundamentals of temperature, pressure and flow measurements*, 3 ed.; John Wiley & Sons, Inc.: New York, 1984.
7. Naitoh, K.; Takizawa, T.; Matsuse, T. *Japanese Journal of Applied Physics Part 2-Letters* **1999,** *38*, L724-L726.
8. Allison, S. W.; Gillies, G. T. *Review of Scientific Instruments* **1997,** *68*, 2615-2650.
9. Klan, P.; Literak, J.; Relich, S. Journal of Photochemistry and Photobiology a-Chemistry **2001,** 143, 49-57.
10. Baghurst, D. R.; Mingos, D. M. P. *Journal of Organometallic Chemistry* **1990,** *384*, C57-C60.
11. Frohlich, H. *Physics Letters A* **1975,** *A 51*, 21-22.
12. Taylor, K. M.; van der Weide, D. W. *Ieee Transactions on Microwave Theory and Techniques* **2005,** *53*, 1576-1586.
13. Adair, R. K. *Biophysical Journal* **2002,** *82*, 1147-1152.
14. Adair, R. K. *Bioelectromagnetics* **2003,** *24*, 39-48.
15. Bohr, H.; Brunak, S.; Bohr, J. *Bioelectromagnetics* **1997,** *18*, 187-189.
16. Bohr, H.; Bohr, J. *Physical Review E* **2000,** *61*, 4310-4314.
17. de Pomerai, D.; Daniells, C.; David, H.; Allan, J.; Duce, I.; Mutwakil, M.; Thomas, D.; Sewell, P.; Tattersall, J.; Jones, D.; Candido, P. *Nature* **2000,** *405*, 417-418.
18. de Pomerai, D. I.; Dawe, A.; Djerbib, L.; Allan, J.; Brunt, G.; Daniells, C. *Enzyme and Microbial Technology* **2002,** *30*, 73-79.

19. Dawe, A. S.; Smith, B.; Thomas, D. W. P.; Greedy, S.; Vasic, N.; Gregory, A.; Loader, B.; de Pomerai, D. I. *Bioelectromagnetics* **2006,** *27*, 88-97.
20. Guven, R. G.; Guven, K.; Dawe, A.; Worthington, J.; Harvell, C.; Popple, A.; Smith, T.; Smith, B.; de Pomerai, D. I. *Enzyme and Microbial Technology* **2006,** *39*, 788-795.
21. Repacholi, M. H.; Basten, A.; Gebski, V.; Noonan, D.; Finnie, J.; Harris, A. W. *Radiation Research* **1997,** *147*, 631-640.
22. Utteridge, T. D.; Gebski, V.; Finnie, J. W.; Vernon-Roberts, B.; Kuchel, T. R. *Radiation Research* **2002,** *158*, 357-364.
23. Utteridge, T. *Radiation Research* **2003,** *159*, 835-836.
24. Metaxas, A. C.; Meredith, R. J. Industrial microwave heating; Peter Peregrinus Ltd: London, 1983; pp. 32-38.
25. Stuchly, M. A.; Stuchly, S. S. Ieee Transactions on Instrumentation and Measurement **1980,** 29, 177-183.
26. Roberts, S.; Von Hippel, A. R. *Journal of Applied Physics* **1946,** *17*, 610.
27. Bringhurst, S.; Iskander, M. F. Ieee Transactions on Microwave Theory and Techniques **1996,** 44, 926-935.
28. Bringhurst, S.; Iskander, M. F.; White, M. J. *Ieee Transactions on Microwave Theory and Techniques* **1997,** *45*, 2073-2083.
29. Gershon, D. L.; Calame, J. P.; Carmel, Y.; Antonsen, T. M.; Hutcheon, R. M. *Ieee Transactions on Microwave Theory and Techniques* **1999,** *47*, 1640-1648.
30. Colpitts, B. G. Ieee Transactions on Microwave Theory and Techniques **1993,** 41, 229-233.
31. Mack, N. R., The University of Edinburgh 2005.
32. Brown, B. A. VNA Cal Kit Manager Version 2.10, 2002.
33. Microsoft. Visual Basic 5.0; Microsoft Corporation, 1997.
34. MathSoft. Mathcad professional; MathSoft, Inc., 1997.
35. Gabriel, C.; Grant, E. H. Dielectric Properties of Standard Liquids.
36. Jordan, B. P.; Sheppard, R. J.; Szwarnowski, S. *Journal of Physics D-Applied Physics* **1978,** *11*, 695-701.
37. OriginLab. OriginPro 7.5; OriginLab Corporation, 2003.
38. Hoffmann, J.; Nuchter, M.; Ondruschka, B.; Wasserscheid, P. *Green Chemistry* **2003,** *5*, 296-299.
39. Leadbeater, N. E.; Torenius, H. M. *Journal of Organic Chemistry* **2002,** *67*, 3145-3148.

40. Leadbeater, N. E.; Torenius, H. M.; Tye, H. *Combinatorial Chemistry & High Throughput Screening* **2004,** *7*, 511-528.
41. Asaki, M. L. T.; Redondo, A.; Zawodzinski, T. A.; Taylor, A. J. *Journal of Chemical Physics* **2002,** *116*, 10377-10385.
42. Wilkes, J. S.; Levisky, J. A.; Wilson, R. A.; Hussey, C. L. *Inorganic Chemistry* **1982,** *21*, 1263-1264.
43. Gabriel, C.; Gabriel, S.; Grant, E. H.; Halstead, B. S. J.; Mingos, D. M. P. *Chemical Society Reviews* **1998,** *27*, 213-223.
44. Seddon, K. R.; Stark, A.; Torres, M. J. *Clean Solvents* **2002,** *819*, 34-49.
45. Lockwood, M. "Scale-up of Microwave Chemistry - An Engineer's Perspective"; "Microwaves in Chemistry", 2004, Imperial College, London.
46. Hodge, P.; Sherrington, D. C. *Polymer-supported Reactions in Organic Synthesis*; Wiley-Interscience: Chichester, 1980.
47. Fenniri *Combinatorial Chemistry: A Practical Approach*; Oxford University Press: Oxford, 2000.
48. Kirschning, A.; Monenschein, H.; Wittenberg, R. *Angew Chem Int Ed Engl 2001* **2001,** *40*, 650-679.
49. Merrifield, R. B. Journal of the American Chemical Society **1963,** 85, 2149-2154.
50. Vaino, A. R.; Janda, K. D. *Journal of Combinatorial Chemistry* **2000,** *2*, 579-596.
51. Delgado, M.; Janda, K. D. *Current Organic Chemistry* **2002,** *6*, 1031-1043.
52. Czarnik, A. W. *Biotechnology and Bioengineering* **1998,** *61*, 77-79.
53. Sherrington, D. C. *Chemical Communications* **1998**, 2275-2286.
54. Santini, R.; Griffith, M. C.; Qi, M. *Tetrahedron Letters* **1998,** *39*, 8951-8954.
55. Kappe, C. O. Current Opinion in Chemical Biology **2002,** 6, 314-320.
56. Kappe, C. O. *American Laboratory* **2001,** *33*, 13-+.
57. Lew, A.; Krutzik, P. O.; Hart, M. E.; Chamberlin, A. R. *Journal of Combinatorial Chemistry* **2002,** *4*, 95-105.
58. Yu, H. M.; Chen, S. T.; Wang, K. T. *Journal of Organic Chemistry* **1992,** *57*, 4781-4784.
59. Stadler, A.; Kappe, C. O. *Tetrahedron* **2001,** *57*, 3915-3920.
60. Strohmeier, G. A.; Kappe, C. O. *Journal of Combinatorial Chemistry* **2002,** *4*, 154-161.
61. Stadler, A.; Kappe, C. O. *European Journal of Organic Chemistry* **2001**, 919-925.
62. Brewster, R. E.; Kidd, M. J.; Schuh, M. D. *Chemical Communications* **2001**, 1134-1135.

63. Bur, A. J.; Vangel, M. G.; Roth, S. *Applied Spectroscopy* **2002,** *56*, 174-181.
64. Lavieille, P.; Lemoine, F.; Lavergne, G.; Virepinte, J. F.; Lebouche, M. *Experiments in Fluids* **2000,** *29*, 429-437.
65. Lavieille, P.; Lemoine, F.; Lavergne, G.; Lebouche, M. *Experiments in Fluids* **2001,** *31*, 45-55.
66. Lemoine, F.; Antoine, Y.; Wolff, M.; Lebouche, M. *Experiments in Fluids* **1999,** *26*, 315-323.
67. Finegan, T.; Laibinis, P. E.; Hatton, T. A. *Aiche Journal* **2006,** *52*, 2727-2735.
68. Lakowicz, J. R. *Principles of Fluorescence Spectroscopy*, 2 ed.; Kluwer Academic/Plenum Publishers: New York, 1999.
69. deMelo, J. S.; Becker, R. S.; Elisei, F.; Macanita, A. L. *Journal of Chemical Physics* **1997,** *107*, 6062-6069.
70. Acemioglu, B.; Arik, M.; Onganer, Y. *Journal of Luminescence* **2002,** *97*, 153-160.
71. Kumar, S.; Giri, R.; Mishra, S. C.; Machwe, M. K. *Spectrochimica Acta Part a-Molecular and Biomolecular Spectroscopy* **1995,** *51*, 1459-1467.
72. O'Connor, D. V. *Time-correlated single photon spectroscopy*; Academic Press Inc.: London, 1984.
73. Kitamura, N.; Hosoda, Y.; Iwasaki, C.; Ueno, K.; Kim, H. B. *Langmuir* **2003,** *19*, 8484-8489.
74. Farrer, R. A.; Copeland, G. T.; Previte, M. J. R.; Okamoto, M. M.; Miller, S. J.; Fourkas, J. T. *Journal of the American Chemical Society* **2002,** *124*, 1994-2003.
75. Annaka, M.; Tanaka, C.; Nakahira, T.; Sugiyama, M.; Aoyagi, T.; Okano, T. *Macromolecules* **2002,** *35*, 8173-8179.
76. Vaino, A. R.; Goodin, D. B.; Janda, K. D. *Journal of Combinatorial Chemistry* **2000,** *2*, 330-336.
77. Kress, J.; Zanaletti, R.; Rose, A.; Frey, J. G.; Brocklesby, W. S.; Ladlow, M.; Bradley, M. *Journal of Combinatorial Chemistry* **2003,** *5*, 28-32.
78. Karstens, T.; Kobs, K. *Journal of Physical Chemistry* **1980,** *84*, 1871-1872.
79. Microsoft. Microsoft Excel 97; Microsoft Corporation, 1997.
80. McAlpine, S. R.; Schreiber, S. L. *Chemistry-a European Journal* **1999,** *5*, 3528-3532.
81. Rademann, J.; Barth, M.; Brock, R.; Egelhaaf, H. J.; Jung, G. *Chemistry-a European Journal* **2001,** *7*, 3884-3889.
82. Mrkic, J.; Saunders, B. R. *Journal of Colloid and Interface Science* **2000,** *222*, 75-82.

83. Frohlich, H. Abstracts of Papers of the American Chemical Society **1980,** 179, 109-PHYS.
84. Bond, J. D.; Wyeth, N. C. *Journal of Chemical Physics* **1986,** *85*, 7377-9.
85. Saalman, E.; Norden, B.; Arvidsson, L.; Hamnerius, Y.; Hojevik, P.; Connell, K. E.; Kurucsev, T. *Biochimica et Biophysica Acta (BBA) - Biomembranes* **1991,** *1064*, 124-130.
86. Bergqvist, B.; Arvidsson, L.; Pettersson, E.; Galt, S.; Saalman, E.; Hamnerius, Y.; Norden, B. *Biochimica et Biophysica Acta (BBA) - General Subjects* **1994,** *1201*, 51-54.
87. Gaber, M. H.; El Halim, N. A.; Khalil, W. A. *Bioelectromagnetics* **2005,** *26*, 194-200.
88. Alekseev, S. I.; Ziskin, M. C. *Bioelectromagnetics* **1995,** *16*, 124-131.
89. Darkes, M. J. M.; Harroun, T. A.; Davies, S. M. A.; Bradshaw, J. P. *Biochimica Et Biophysica Acta-Biomembranes* **2002,** *1561*, 119-128.
90. Cherezov, V.; Siegel, D. P.; Shaw, W.; Burgess, S. W.; Caffrey, M. *Journal of Membrane Biology* **2003,** *195*, 165-182.
91. Gruner, S. M.; Tate, M. W.; Kirk, G. L.; So, P. T. C.; Turner, D. C.; Keane, D. T.; Tilcock, C. P. S.; Cullis, P. R. *Biochemistry* **1988,** *27*, 2853-2866.
92. King, S. M. Small Angle Neutron Scattering; ISIS Facility: Oxford, 2000.
93. Harrison, A. *Fractals in Chemistry*; Oxford University Press: Oxford, 1995; Vol. 22.
94. Gagne, J.; Stamatatos, L.; Diacovo, T.; Hui, S. W.; Yeagle, P. L.; Silvius, J. R. *Biochemistry* **1985,** *24*, 4400-4408.
95. de Pomerai, D. I.; Smith, B.; Dawe, A.; North, K.; Smith, T.; Archer, D. B.; Duce, I. R.; Jones, D.; Candido, P. M. *Febs Letters* **2003,** *543*, 93-97.
96. Bismuto, E.; Mancinelli, F.; d'Ambrosio, G.; Massa, R. *European Biophysics Journal with Biophysics Letters* **2003,** *32*, 628-634.
97. Porcelli, M.; Cacciapuoti, G.; Fusco, S.; Massa, R.; d'Ambrosio, G.; Bertoldo, C.; De Rosa, M.; Zappia, V. *FEBS Letters* **1997,** *402*, 102-106.
98. Bohr, H.; Bohr, J. *Bioelectromagnetics* **2000,** *21*, 68-72.
99. Weissenborn, R.; Diederichs, K.; Welte, W.; Maret, G.; Gisler, T. *Acta Crystallographica Section D-Biological Crystallography* **2005,** *61*, 163-172.
100. Flower, D. R. *Biochemical Journal* **1996,** *318*, 1-14.
101. Bhattacharjee, C.; Das, K. P. *European Journal of Biochemistry* **2000,** *267*, 3957-3964.
102. Fessas, D.; Iametti, S.; Schiraldi, A.; Bonomi, F. *European Journal of Biochemistry* **2001,** *268*, 5439-5448.

103. Manderson, G. A.; Creamer, L. K.; Hardman, M. J. *International Dairy Federation [Special Issue] S.I.* **1997,** *9702*, 217-223.

104. Mills, O. E. Biochimica et Biophysica Acta, Protein Structure **1976,** 434, 324-32.

105. Kuwata, K.; Hoshino, M.; Forge, V.; Era, S.; Batt, C. A.; Goto, Y. *Protein Science* **1999,** *8*, 2541-2545.

106. Kelly, S. M.; Price, N. C. *Current protein & peptide science FIELD Publication Date:2000* **2000,** *1*, 349-84. FIELD Reference Number:132 FIELD Journal Code:100960529 FIELD Call Number:.

107. Cavatorta, P.; Farruggia, G. *Bulletin of Molecular Biology and Medicine* **1993,** *18*, 179-98.

108. Lau, K. H. Iee Proceedings-H Microwaves Antennas and Propagation **1988,** 135, 207-209.

109. Marky, L. A.; Breslauer, K. J. *Biopolymers* **1987,** *26*, 1601-1620.

110. John, D. M.; Weeks, K. M. *Protein Science* **2000,** *9*, 1416-1419.

111. Rowe, J. Circular dichroism studies of non-thermal microwave effects upon β-lactoglobulin, The University of Edinburgh 2006.

Appendix